Investigation of monitoring strategies for the Zeelandbrug

Valerie Stoop

Delft University of Technology

TU Delft

Witteveen + Bos

Investigation of monitoring strategies for the Zeelandbrug

by

Valerie Stoop

to obtain the degree of Master of Science in Civil Engineering
at the Delft University of Technology

Student number: 5191394
Project duration: February, 2024 – September, 2024
Thesis committee: Dr. ir. Y. Yang, TU Delft
Dr. E. Lourens, TU Delft
Ir. F. Besseling, Witteveen+Bos

An electronic version of this thesis is available at http://repository.tudelft.nl/.

Cover: The Zeelandbrug [1]

TU Delft

Witteveen + Bos

Acknowledgements

This thesis marks the end of my studies at TU Delft. As I reflect on my academic journey, I am deeply grateful to those who have supported me along the way. First, I would like to thank my committee for their support throughout this thesis. I fondly recall our visit to the Zeelandbrug on March 19th, which provided a memorable and unique start to this project. I am grateful to my chair, Yuguang Yang, for his guidance and suggestions that always improved the quality of my work. I would like to thank my supervisor Floris Besseling for always making time to address my questions and engage in discussions that deepened my understanding. I am also very grateful to my supervisor Eliz-Mari for her pleasant support during this project and for always being able to see the bigger picture.

Special thanks goes to my friends who made my time at TU Delft so enjoyable and supported me through both good and challenging times. Above all, my deepest gratitude goes to my family, particularly to my parents, for their unwavering support. I have always been able to count on you.

Valerie Stoop
Delft, September 2024

Summary

The Zeelandbrug serves as an important connection between Noord-Beveland and Schouwen-Duiveland. The bridge completed construction in 1965 using the balanced cantilever method and has been in operation for nearly 60 years. After the passage of these years, the current status of the bridge's bearing capacity is unknown. Monitoring devices can be applied to obtain more information about the bridge's condition and to help extend its lifespan. Hence, this study aims to investigate the application of monitoring strategies for the Zeelandbrug. As part of the process of obtaining the monitoring plan, this research also aims to gain a better understanding of the bridge's structural behaviour. To achieve this, a linear Finite Element Model using one-dimensional beam elements was developed for the Zeelandbrug. This model was used to evaluate how the settlement of a support affects the magnitude of shear forces within the bridge's superstructure. A structural assessment on the bridge's superstructure was conducted, with in longitudinal direction incorporating the additional shear forces resulting from a support settlement. Through this assessment, failure modes were identified together with their associated physical parameters. Then, a brief investigation was performed on monitoring strategies that can be applied to monitor these parameters.

Two monitoring strategies have been developed, each tailored to a specific type of identified potential failure: a global or local failure. Possible failure modes corresponding to a global failure are the shear failure of the box girder's webs in longitudinal direction and the exceeded tensile force in the box girder's top slab due to the bending moment in the longitudinal direction. In-situ measurements on the Zeelandbrug could allow for the evaluation of the following physical parameters: the concrete compressive strength, the Young's modulus and the residual prestressing force. Furthermore, a monitoring technology that can be implemented is weigh-in-motion sensors to monitor the vehicle weights, while regular surveys can assess potential occurring settlements of the bridge's supports. To address the risk of global failure, the monitoring strategy (strategy I) should focus on utilising data from monitoring technologies to update the recalculations and Finite Element Model of the Zeelandbrug. With these updates, more accurate predictions can be made on the Zeelandbrug's overall bearing capacity and expected lifespan. If, after updating the model and recalculations, structural elements are still found to have an insufficient bearing capacity, their use should be re-evaluated. This re-evaluation can be done by developing a nonlinear Finite Element Model to enhance the accuracy of the structural assessment or by performing recalculations using the actual vehicle weights recorded by the weigh-in-motion sensors. Possible failure modes corresponding to a local failure are the shear force failures in transverse direction within the cantilever of the top slab, or at the section extending from the midspan towards the web in the top slab of the box girder. Additionally, local failure could be induced by the bending moment within the cantilever of the top slab in transverse direction. Another corresponding failure mode relates to the box girder's webs, which may fail in the transverse direction due to bending moments. These may cause concrete cracks to form on the outer surface of the webs. The most effective strategy (strategy II) for mitigating local failures is the implementation of monitoring technologies designed to detect these early signs of structural damage. This approach would allow for timely warnings and interventions.

Contents

List of Figures

List of Tables

Nomenclature

Abbreviations

Abbreviation	Definition
CC	Consequence Class
FEM	Finite Element Model
LM	Load Model
Loc.	Location
MP	Maintenance Platform
NAP	Normaal Amsterdams Peil
U.C.	Unity Check
UDL	Uniformly Distributed Load
ULS	Ultimate Limit State
V.O.S.B.	Voorschriften voor het Ontwerpen van Stalen Bruggen
WIM	Weigh-In-Motion

Symbols

Symbol	Definition
A_0	Area enclosed by the cell to the member centerlines used in the Prandtl membrane analogy to determine the torsional moment of inertia
A_p	Area of prestressing tendons
A_{sl}	Cross-sectional area of reinforcement
A_{sw}	Cross-sectional area of the shear reinforcement
$A_{s,tension}$	Cross-sectional area of reinforcement under tension
a	Distance
arm	Lever arm
b	Width
b'	Box girder's width of the bottom slab
b_w	Smallest width of the cross-section in the tensile area
c_d	Concrete cover to the reinforcement
D_{grain}	Maximum aggregate grain size in concrete
d	Effective depth of a cross-section
$d_{bottom\ slab}$	Thickness of box girder's bottom slab
d_{dg}	Shear crack roughness parameter
$d_{top\ slab}$	Thickness of box girder's top slab
$dist.$	Distribution length over which a load is spread
E	Design value of modulus of elasticity of concrete
E_{cm}	Secant modulus of elasticity of concrete
E_s	Design value of modulus of elasticity of reinforcing steel
e_p	Eccentricity of the prestressing tendons
F	Force
F_{Ed}	Design value of the normal force
F_p	Working prestress force
F_{top}	Superimposed, axial load in top slab of box girder
ΔF_{Ed}	Additional design normal force
f	Drape of the prestressing tendons

Symbol	Definition
f_{bd}	Design value of the ultimate bond stress between the reinforcing steel and concrete
f_{cd}	Design value of compressive strength of concrete
f_{ck}	Characteristic compressive strength of concrete
f_{ctd}	Design value of axial tensile strength of concrete
f_{pd}	Design value of tensile strength of prestressing steel
f_{pk}	Characteristic tensile strength of prestressing steel
f_{td}	Design value of working prestress
f_{yd}	Design value of yield strength of reinforcement
f_{yk}	Characteristic yield strength of reinforcement
f_{ywd}	Design yield strength of the shear reinforcement
h	Height
h'	Box girder's height from top of top slab to bottom of bottom slab
I_t	Torsional moment of inertia
k	Coefficient ; Factor
k_r	Rotational stiffness of a spring
k_t	Translational stiffness of a spring
L	Length
L_{eff}	Effective length
l_{bd}	Design anchorage length of the reinforcing steel
$l_{b,rqd}$	Basic required anchorage length of the reinforcing steel
l_i	Length of the ith member of the cell used in the Prandtl membrane analogy to determine the torsional moment of inertia
M	Moment
M_{Ed}	Design value of the applied internal bending moment
M_{MP}	Moment due to the weight of the Maintenance Platform
M_{Rd}	Design value of the bending moment capacity
M_{TS}	Moment due to a Tandem System
M_{UDL}	Moment due to a Uniformly Distributed Load
$M_{barrier}$	Moment due to the weight of the barrier
$M_{cantilever}$	Moment due to the self-weight of the cantilever
M_{curv-}	Moment due to negative curvature effect from prestressing tendons
M_{curv+}	Moment due to positive curvature effect from prestressing tendons
$M_{pavement}$	Moment due to the weight of the pavement
N_{Ed}	Design value of the applied axial force
$N_{Rd,c}$	Design axial compressive force resistance of the concrete
N_c	Design value of the normal force of concrete
$N_{s,tension}$	Design value of the normal force of the reinforcing steel under tension
n	Number
$\emptyset$	Diameter
P_m	Axial compressive force due to prestressing
p	Surface load
q	Line load or distributed load
q_p	Curvature pressure of prestressing tendons
s	Spacing of the stirrups
t_i	Thickness of the ith member of the cell used in the Prandtl membrane analogy to determine the torsional moment of inertia
u	Displacement
V	Shear force
V_{Ed}	Design value of the applied shear force
$V_{Ed,curv}$	Design value of the shear force due to curvature pressure of the prestressing tendons
$V_{Ed,tot}$	Design value of the total shear force
V_{Rd}	Design value of the shear force capacity
$V_{Rd,c}$	Design value of the shear force capacity of the concrete
$V_{Rd,curv}$	Design value of the shear resistance due to curvature pressure of the prestressing tendons

Symbol	Definition
$V_{Rd,s}$	Design value of the shear force that can be sustained by the yielding shear reinforcement
V_{TS}	Shear force due to a Tandem System
V_{UDL}	Shear force due to a Uniformly Distributed Load
ΔV_{Ed}	Additional design shear force
$\Delta V_{Ed;TS}$	Additional design shear force due to a Tandem System
$\Delta V_{Ed;UDL}$	Additional design shear force due to a Uniformly Distributed Load
$V_{barrier}$	Shear force due to the weight of the barrier
$V_{cantilever}$	Shear force due to the self-weight of the cantilever
V_{ccd}	Design value of the force in the compression area in the case of an inclined compression chord
$V_{pavement}$	Shear force due to the weight of the pavement
V_{sett}	Design value of shear force due to a support settlement
V_{td}	Design value of the shear component of the force in the tensile reinforcement in the case of an inclined tensile chord
w	Box girder's thickness of the webs
x	Height of the concrete compressive zone
z	Lever arm of internal forces
α	Angle ; Ratio
α_L	Distance of shift in moment curve
γ	Specific weight
γ_c	Partial factor for concrete
$\gamma_{F,perm}$	Partial factor for permanent loads
$\gamma_{F,var}$	Partial factor for variable loads
θ	Angle between concrete compressive strut and the beam axis perpendicular to the shear force
ρ	Density
ρ_l	Flexural reinforcement ratio
σ_{cp}	Compressive stress in the concrete from axial load or prestressing
σ_{sd}	Design stress of the reinforcing steel
υ	Poisson's ratio
υ_1	Strength reduction factor for concrete cracked in shear
ϕ	Rotation

1

Introduction

In this chapter, the context of the research topic is given together with the identified research problem. To solve this problem, objectives have been created. A description is given of the scope of the research which leads to the main research question. Lastly, this chapter contains the research method that will be employed and describes the structure of this thesis.

1.1. Context

The Zeelandbrug in the Netherlands is located on the N256 and serves as a connection between Noord-Beveland and Schouwen-Duiveland. The bridge is frequently used by residents and visitors. Every day, about 12,000 vehicles drive over the Zeelandbrug [2]. The bridge opens almost 4,000 times per year, accommodating around 20,000 boats [3]. Hence, the Zeelandbrug is an important bridge and keeping the bridge operational is important for the province of Zeeland. The Zeelandbrug completed construction in 1965 and has been in operation for nearly 60 years [2]. After the passage of these years, the current status of the bridge's bearing capacity is unknown. Additionally, there has been a notable surge in the intensity of traffic on bridges over the past few decades. This reflects the broader trends of modernisation and population growth. With the Westerscheldetunnel expected to become toll-free around 2025, a further increase in traffic intensity is expected on the Zeelandbrug [4]. The uncertain current bearing capacity of the bridge, combined with the increased loading levels, has raised safety concerns, necessitating structural safety assessments of the bridge.

1.2. Research problem

On behalf of the Province of Zeeland, Iv-Infra has evaluated the structural safety of the Zeelandbrug [5]. The assessment report contains a visual inspection and a recalculation of the concrete structure, indicating that the concrete structure is sufficient for the bridge's actual current usage [5]. An exception to this are the shear force dowels, for which it is recommended to further examine the load effect on these elements [5]. Following the report of Iv-Infra, TNO was commissioned to review the recalculation of the Zeelandbrug [6]. Some of the remarks in TNO's review concern specific values used for material properties and comments regarding certain calculations. Based on this review, a visual inspection and a document review, TNO has identified which structural elements they consider to be critical or soon to become critical. Nevertheless, it is currently unknown how incorporating these remarks into the assessment calculations by Iv-Infra would influence the identification of critical structural elements. Furthermore, it is unclear whether the Zeelandbrug experiences differential settlement and what impact these settlements might have on the shear forces within the bridge's superstructure. Looking ahead, the potential failure modes and associated physical parameters of the bridge are not yet known, nor are the most effective strategies for monitoring these parameters.

1.3. Research objectives

The aim of this research project is to investigate monitoring strategies that are applicable to the Zeelandbrug to improve its safety. This research is structured around three primary objectives. The first

objective is to gain a better understanding of the magnitude of shear loads that can be expected within the bridge's cantilever caused by differential settlements. The second objective is to assess the structural elements of the Zeelandbrug that have their resistance exceeded by the applied loading and to identify the uncertainties in the bridge's performance. Then, to improve the Zeelandbrug's safety and minimise these uncertainties, the final objective is to develop a monitoring plan. This monitoring plan will contain strategies for effectively monitoring the physical parameters associated with the identified failure modes of the Zeelandbrug.

1.4. The scope

This research adopts a case study approach focused specifically on the Zeelandbrug. The bridge is a prestressed concrete box girder bridge constructed using the balanced cantilever method. At a global level, a Finite Element Model of the Zeelandbrug will be developed with one-dimensional structural elements. This model contains the south part of the bascule bridge within the Zeelandbrug. The Finite Element Analysis will assess the shear loads within the bridge's cantilevers resulting from hypothetical differential settlement scenarios. The Finite Element Analysis involves several material simplifications. Furthermore, this research will focus on identifying the potential risks associated solely with the superstructure of the Zeelandbrug. The spans extending from the bridge to the abutments and the bascule bridge are beyond the scope of this research. The potential risks identified can be a global or local phenomenon. Based on the output from the Ultimate Limit State (ULS), physical parameters associated with the identified failure modes will be examined. To be able to address these failure modes, this research will develop monitoring strategies aimed at enhancing the safety of the Zeelandbrug. For these strategies, monitoring technologies and methods for using the collected data will be explored. The monitoring technologies to be investigated will be based on the specific physical parameters intended for monitoring.

1.5. Research questions

The focus of this project results in the following main research question:

"What monitoring strategies could be applied to improve the safety of the Zeelandbrug?"

To answer this main research question, the following sub-questions have been formulated:

- How can a physical model contribute to the understanding of the Zeelandbrug's behaviour, and in which detail level does the model need to be?
- What is known about the current status of the bearing capacity of the Zeelandbrug?
- What are important uncertainties involved in determining the safety of the Zeelandbrug's structure?
- What are the critical failure modes of the Zeelandbrug and its associated physical parameters?
- What kind of technologies can be used to monitor these parameters and reduce the identified uncertainties?

1.6. Research method

Understanding the behaviour specific to the Zeelandbrug requires a physical model. A global Finite Element Model with one-dimensional structural elements will be developed. This model aims to investigate the shear forces in the bridge's cantilevers induced by hypothetical differential settlement scenarios. To further obtain a better understanding of the behaviour of the Zeelandbrug, the focus will be on the previously conducted calculations of the bridge's bearing capacity. The calculations from Iv-Infra will be revisited to incorporate the remarks from TNO and identify critical structural elements of the Zeelandbrug. Following the identification of the failure modes and associated physical parameters of the bridge, there will be looked into monitoring strategies for these parameters. Finally, this will result in the development of a monitoring plan for the Zeelandbrug.

1.7. Thesis structure

The structure of the thesis will be as followed. Following the introductory chapter, chapter 2 presents the Zeelandbrug, including the geometry and material properties. The Finite Element Model is introduced in chapter 3, which details the settlement scenarios, model considerations and results. Then,

chapter 4 focuses on the assessment of the current status of the Zeelandbrug, presenting a review of previous recalculations and a reassessment of the bridge along with the identified uncertainties. Moreover, chapter 5 discusses potential monitoring strategies aimed at improving the safety of the Zeelandbrug. Lastly, chapter 6 presents the final conclusions of this thesis along with several recommendations.

2

The Zeelandbrug

This chapter describes the main characteristics of the Zeelandbrug. First, a general introduction is given to the bridge in section 2.1. This is followed by section 2.2 and 2.3 which explain the geometry and material properties of the Zeelandbrug, respectively. Lastly, section 2.4 briefly describes the construction of the bridge.

2.1. Introduction

The Zeelandbrug is a box girder prestressed concrete bridge located in the Province of Zeeland (the Netherlands). Figure 2.1 depicts notable landmarks in Zeeland, such as the Zeelandbrug, the Westerscheldetunnel and the Oosterscheldekering, a series of dams and storm surge barriers. The Zeelandbrug crosses the Oosterschelde and connects Noord-Beveland with Schouwen-Duiveland as part of the national road N256. The province of Zeeland owns and maintains the bridge [2]. The Zeelandbrug was constructed using the balanced cantilever method between 1963 and 1965 [7]. Regular maintenance has been carried out on the bridge over time. Figure 2.2 displays the Zeelandbrug.

Figure 2.1: Zeeland. A indicates the Zeelandbrug, B the Westerscheldetunnel and C the Oosterscheldekering. Adapted from [8]

Figure 2.2: The Zeelandbrug [9]

The design of the Zeelandbrug was initially based on class B of the V.O.S.B. 1938, a former standard for steel bridge design [10]. During the design process of the Zeelandbrug, the V.O.S.B. 1963 was released. As a result, the bridge was also tested to ensure compliance with class 60 of this updated standard [10].

2.2. Geometry

This section contains the general geometry of the Zeelandbrug, as well as its longitudinal and transverse profile. Moreover, this section describes the functionality of the Zeelandbrug's main system of coupling elements and the reinforcement applied in the bridge's superstructure.

2.2.1. General

The Zeelandbrug is a prestressed concrete box girder bridge. The total length of the bridge is approximately 5020 m, including the abutments [10]. The bridge has a fixed and a movable part (bascule bridge). The fixed part is made up of 50 T-frames, each spanning 95 m. The bascule bridge is 40 m long [10]. The prefabricated concrete elements of a single T-frame are shown in Figure 2.3. One T-frame contains three concrete hollow piles. These concrete piles are made up of 6 m long prefabricated disks that have been constructed separately [11]. The disks are assembled with 40 cm thick joints [11]. The number of assembled disks ranges from five to eight. The length of the piles thus ranges between 30 and 48 m depending on the location's water depth and the load-bearing capacity of the soil layers [11]. The three piles are connected by a prefabricated concrete caisson. The hollow caisson has internal partition walls creating compartments where the pile heads fit. Openings in the caisson's bottom, around 35 cm larger than the pile heads, allow for some tolerance [10]. The space between the caisson and piles is filled with concrete in-situ.

A pillar stands on top of the caisson. Concrete is poured in the joint between the caisson and the pillar. The pillar consists of two prefabricated concrete halves which are identical and have a supporting surface for the superstructure. The superstructure is formed by seven prefabricated concrete segments, with there being four types of segments: A, B, C, and D. The middle segment (type A) or hammerhead rests on the pillar and is connected in such a manner that it can transfer bending forces [5]. The segments of one T-frame connect to one another through longitudinal prestressing. Between the segments of a T-frame are 40 cm thick joints which have been filled with concrete [10]. These joints are known as construction joints. The transitions between the different T-frames are referred to as expansion joints. In Table 2.1 the total number of prefabricated elements are depicted for the bridge. Finally, the Zeelandbrug has a 7.6 m wide roadway and a 2.75 m wide bike lane [10].

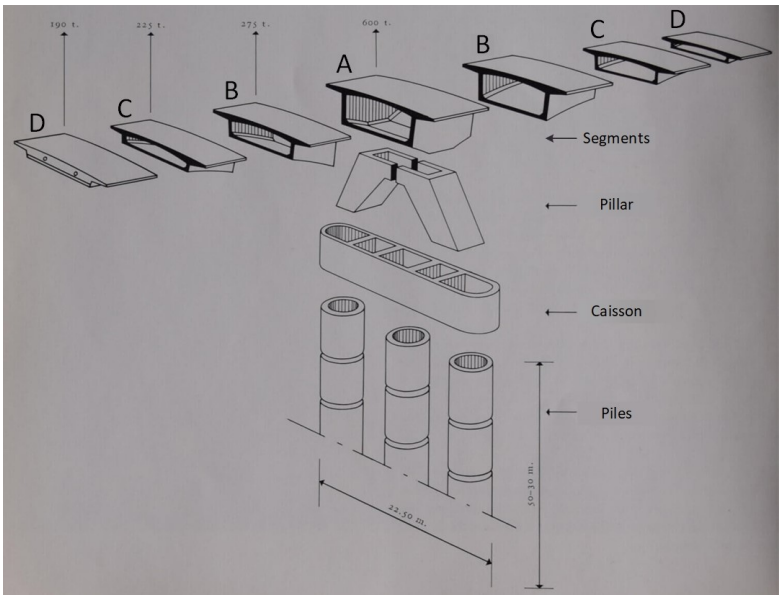

Figure 2.3: Prefabricated concrete elements of the Zeelandbrug. Adapted from [7]

Table 2.1: Number of prefabricated concrete elements [7]

Concrete elements
162 hollow concrete piles of varying lengths. Made up of a total of 1100 disks.
54 caissons
50 pillars
50 segments of type A
102 segments of type B
102 segments of type C
102 segments of type D

2.2.2. Longitudinal profile

The Zeelandbrug is around 5 km long, with 95 m spans making up the majority of its length (Figure 2.4). The bascule bridge is located around 400 m from the embankment of Shouwen-Duiveland and has a passage width of 40 m [10]. The top of the deck is situated at + 17 m NAP. This drops to around + 11 m NAP at the bridge's ends, see Figure 2.5. The water depth at the locations of the piles ranges from 3 to 35 m [5]. It should be noted that during the design of the Zeelandbrug, the initial objective was to close the Oosterschelde with the construction of a permanent dam [10]. It was planned to fill the deep channel south of the bascule bridge after 1978 with sand to -15 m NAP at the piles' locations [10]. However, this did not happen since a permeable barrier was built in the Oosterschelde estuary rather than a permanent dam.

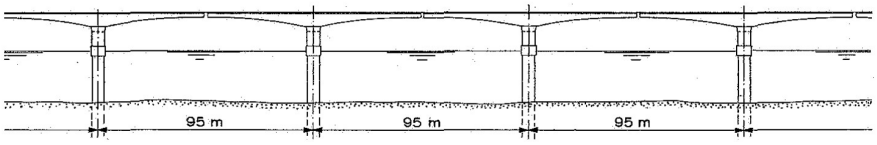

Figure 2.4: Longitudinal profile of a few spans of the Zeelandbrug [10]

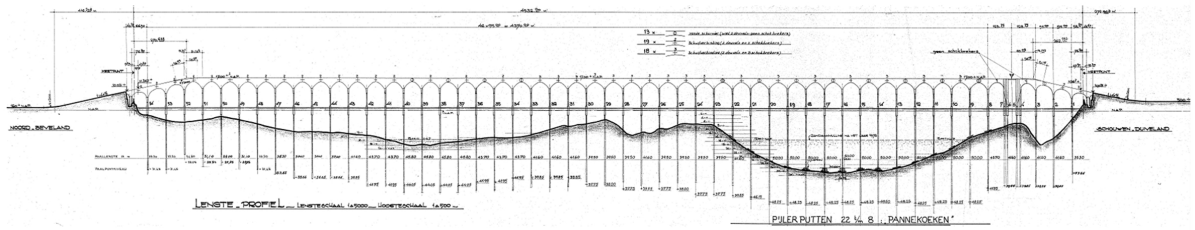

Figure 2.5: Longitudinal profile Zeelandbrug [6]

2.2.3. Transverse profile

The superstructure of the Zeelandbrug consists of prefabricated concrete segments. The cross-section is a single-cell box girder with a total width of 11.60 m, see Figure 2.6. The height of the box girders changes along the length of the bridge and ranges from 1.90 m to 5.39 m. The thickness of the top slab in the field is constant and equal to 200 mm. Near the webs, the thickness of the top slab increases to 480 mm. The cantilever part of the deck has a length of 2.25 m and a variable thickness between 315 mm on the web and 200 mm at the end. The webs vary in thickness from 322 mm to 670 mm. Finally, the bottom slab ranges in thickness between 153 mm and 530 mm. Although the bridge includes a bike lane, both the design and recalculation consider the theoretical use of the bridge. This means that the full width of the bridge is used to divide into road lanes.

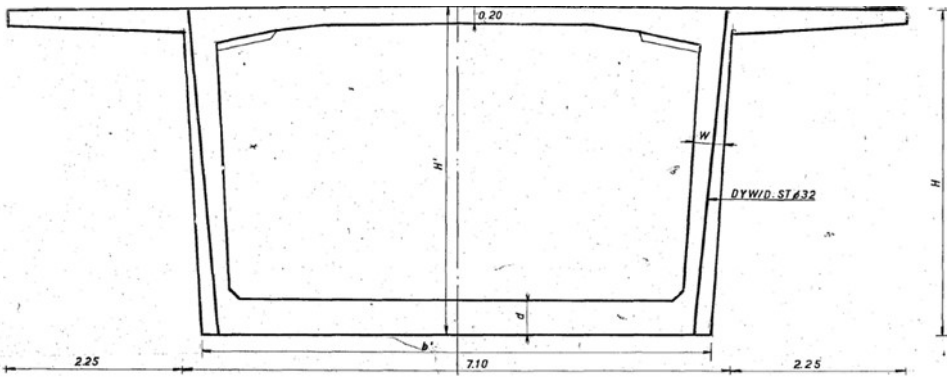

Figure 2.6: Transverse profile Zeelandbrug. Adapted from [6]

2.2.4. The main system

The T-frames of the Zeelandbrug are clamped into the ground, each capable of independently supporting their own weight and traffic loads. However, due to traffic loads, the variations in deflections between adjacent cantilevers could become unacceptable large [10]. For instance, this occurs when one cantilever is fully loaded with a uniformly distributed load combined with two 60-ton load systems from the V.O.S.B. 1963 class 60 [10]. Under these conditions, the loaded cantilever may deflect by approximately 25 cm at an average water depth of 15 m and 40 cm at the deepest water depth of 33 m, while the adjacent cantilever remains in place [10]. To address this issue, a coupling element between adjacent cantilevers is necessary. This element should prevent vertical movements between the cantilevers by transferring shear forces. It should also allow for variations in the joint width due to temperature changes, concrete shrinkage, and creep. Furthermore, it should facilitate angular rotations of the cantilevers relative to each other without transferring bending moments. For all these reasons, shear force dowels have been applied between the cantilevers [10].

By applying shear force dowels, the differential deflections have been minimised to zero, with the absolute deflection at midspan now approximately 14 cm at a 15 m water depth and 21 cm at a 30 m water depth [10]. This last value exceeds 1/600 of the span, so that extra measures had to be applied at these critical locations [10]. Consequently, three hinges have been installed at these locations at every other span to comply with the criteria. This fixed hinge connection was feasible because the long free-standing piles could absorb the bending moments resulting from changes in the superstructure's length caused by temperature variations, for example [10]. As the free-standing length of the piles increases, the bending moments within the piles decrease [10].

Despite the coupling elements applied, concerns remained regarding the potential for significant movement under the passage of heavy vehicles across multiple spans [10]. The solution was found in the installation of two or three shock absorbers. These elements are designed to restrict movement under short-term loads while allowing gradual adjustments to accommodate length changes of the concrete over time [10]. Each expansion joint with shock absorbers will function as a sliding joint under traffic loads, while still permitting movement due to temperature variations, concrete shrinkage and creep.

Hence, an expansion joint may have one of the following three coupling element configurations:

- Fixed hinge (2 shear force dowels, 3 hinges, no shock absorbers)
- Sliding joint (2 shear force dowels, 2 shock absorbers)
- Sliding joint (2 shear force dowels, 3 shock absorbers)

Each expansion joint contains two shear force dowels. A detail of the shear force dowel is shown in Figure 2.7. In addition, the expansion joint may contain either two or three shock absorbers or three hinges. A detail of the shock absorber and hinge can be found in Figures 2.8 and 2.9, respectively.

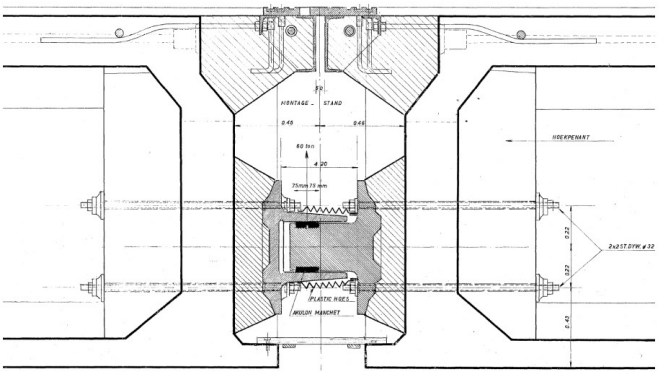

Figure 2.7: Detail shear force dowel

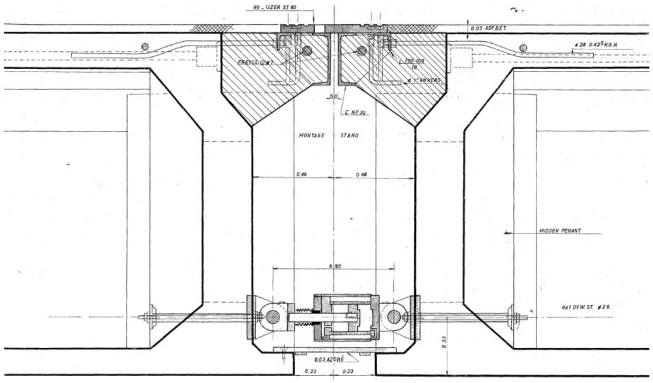

Figure 2.8: Detail shock absorber

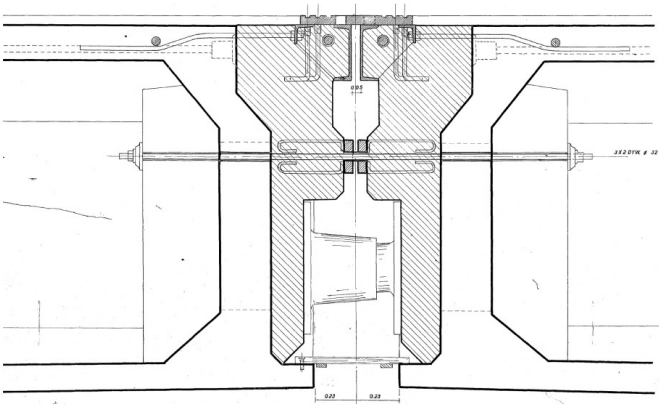

Figure 2.9: Detail hinge

2.2.5. Reinforcement

Only the reinforcement in the superstructure of the Zeelandbrug has been examined.

Reinforcement in longitudinal direction

The mild steel reinforcement that is present in the longitudinal direction varies per location and is in the order of Ø10-200. At the construction joints the mild steel reinforcement has a limited anchorage length. The contribution of the mild steel reinforcement to the moment capacity is neglected. Hence, further details of the mild steel reinforcement will not be discussed as it is not included any further in the report. Prestressing has been implemented in the longitudinal direction in the top slab, see Figure 2.10. The number of longitudinal prestress tendons changes over the different segments. In addition, segment D contains seven prestressing tendons in its bottom slab. The prestressing tendons used are Freyssinet 12Ø17.

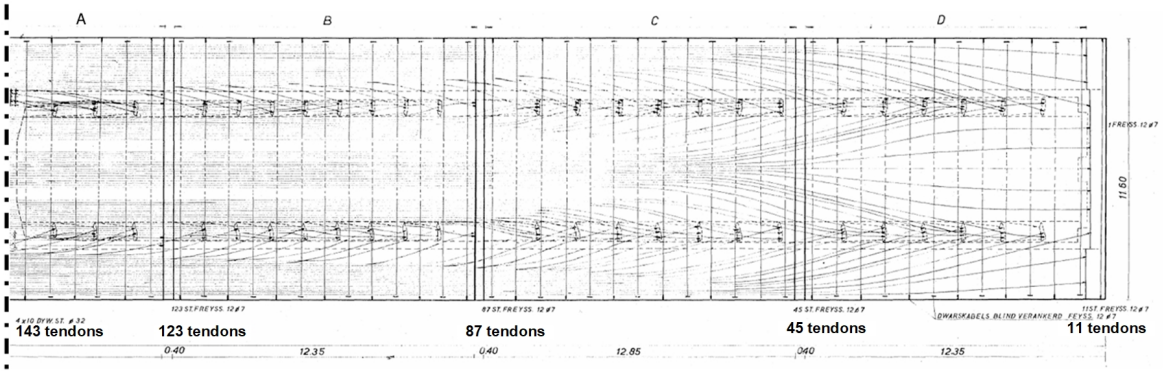

Figure 2.10: Longitudinal prestressing [5]

Reinforcement in transverse direction

Conventional reinforcement has been applied in the box girder's webs, bottom slab and top slab. Over a span of the bridge, the reinforcement in the webs and bottom slab changes. Figure 2.11 illustrates the reinforcement that has been applied at a cross-section in segment type B. The reinforcement in the top slab remains unchanged in the longitudinal direction. A possible exception to this is the additional reinforcement 5Ø22 near the joints.

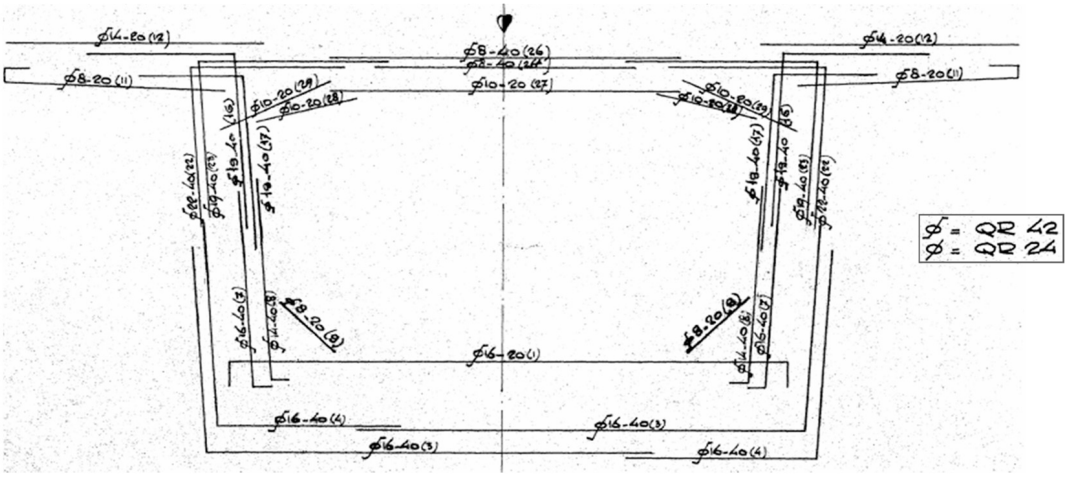

Figure 2.11: Reinforcement in transverse direction in segment B, cross-section 5 [5]

The webs have been reinforced to withstand shear forces using Dywidag bars Ø32. The layout of the Dywidag bars in the webs is depicted in Figure 2.12.

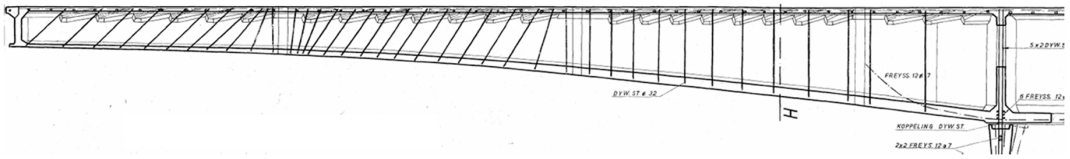

Figure 2.12: Layout of the Dywidag bars in the webs [5]

Also, prestressing has been implemented in the transverse direction (Freyssinet 12Ø7). The course of the transverse prestressing tendons is slightly curved, see Figure 2.13. The transverse prestressing is alternately applied on one side. Regarding five T-frames, external prestressing has been applied at the location of segment D. This is due to a possible deviation of the position of the transverse prestressing. Used are four wires Ø7 with a center to center distance of 0.90 m.

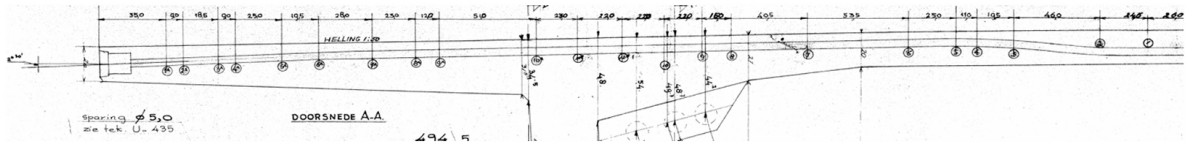

Figure 2.13: Transverse prestressing [5]

Additionally, segment type A has transverse prestressing at the bottom (Figure 2.14). Details on the additional transverse presstressing at the bottom of segment type A have been omitted since they are not utilised in the calculations nor the Finite Element Model.

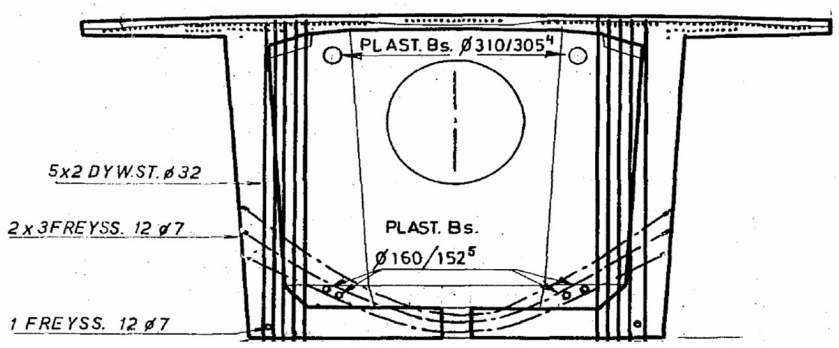

Figure 2.14: Additional transverse prestressing at the bottom of segment A [5]

Concrete cover

The theoretical concrete cover of the box girder segments are given in Table 2.2. As is visible, the cover to the outer reinforcement at the upper side of the top slab is only 20 mm thick. Though, the pavement on the top slab gives a layer of protection against the influence of environmental factors.

Table 2.2: Concrete cover of the box girder segments [5]

Description	Concrete cover
Upper side of the top slab	20 mm
Inside the box girder	25 mm
Underside of the cantilever	30 mm
Underside of the bottom slab	30 mm
Outside the webs	30 mm

2.3. Material properties

The Zeelandbrug is primarily constructed using prefabricated concrete elements. Only connections between different elements of the Zeelandbrug have been realised by pouring concrete cast in-situ. There is only focused on the material properties of the superstructure. The prestressed concrete of the box girder segments have a cube compressive strength of 425 kg/cm^2, which corresponds to a characteristic compressive strength f_{ck} of 30 N/mm^2 [5]. Table 2.3 presents the relevant material properties of the segments' prestressed concrete. The same material properties have been assumed for the construction joints which were cast in-situ.

Table 2.3: Prestressed concrete properties of the box girder segments [5]

Material property	**Value**
Concrete strength	C30/37
Partial factor for concrete γ_c [-]	1.5
Characteristic compressive strength (28 days) f_{ck} [N/mm^2]	30
Design value of compressive strength f_{cd} [N/mm^2]	20
Design value axial tensile strength f_{ctd} [N/mm^2]	1.35
Secant modulus of elasticity E_{cm} [N/mm^2]	33000

The properties of the reinforcing steel that have been used are displayed in Table 2.4. As is visible, the characteristic yield strength f_{yk} ranges from 240 to 420 N/mm^2.

Table 2.4: Reinforcing steel properties [5]

Material property	Type of reinforcing steel	
	QR24	**QRn42**
Surface texture	plain steel	ribbed
Characteristic yield strength f_{yk} [N/mm^2]	240	420
Design yield strength f_{yd} [N/mm^2]	209	300
Design value of modulus of elasticity E_s [N/mm^2]	200000	200000

The prestressing steel has material properties as described in Table 2.5. In these values and in the original design, a 15% prestress loss has been accounted for in the tensile strength of the prestressing steel. However, according to a research into existing creep models conducted by TNO, the influence of creep can be underestimated [6]. This can lead to several percent extra prestress loss. In this context, TNO recommends to incorporate a 5% extra prestress loss in longitudinal direction of the Zeelandbrug [6]. In the longitudinal direction, Freyssinet cables have been applied. The design tensile strength $f_{pd,20\%}$ of the Freyssinet cables in the longitudinal direction, considering a 20% prestress loss, is then 1231 N/mm^2. In the transverse direction, a prestress loss of 15% has been assumed, consistent with the prestress loss considered in the original design and the properties listed in Table 2.3.

Table 2.5: Prestressing steel properties with 15% prestress loss considered [5, 6]

Material property	Type of prestressing steel	
	Dywidag	**Freyssinet**
Characteristic tensile strength f_{pk} [N/mm^2]	1050	1700
Design tensile strength f_{pd} [N/mm^2]	713	1308
Design working prestress f_{td} [N/mm^2]	576	935

2.4. Construction

In Figure 2.3 the prefabricated elements of the Zeelandbrug are illustrated. As mentioned before, prefabrication played a big role in the construction of the bridge. The Zeelandbrug is located in the middle of the Oosterschelde, heavily exposed to weather and water influences. Hence, if the construction of the bridge primarily took place on site, many unworkable days would have to be accounted for. Additionally, the transportation of personnel and materials would be a significant concern [10]. These considerations, coupled with the aim of a very short construction time and the repetitive nature of the bridge design, led to the decision to use mainly large prefabricated elements [10]. A site of approximately 7 hectares near the village of Kats at Noord-Beveland was made available for the prefabrication of these elements [10]. On site, the assembly of the elements started with the installation of the three piles, followed by the caisson and pillar, and then the hammerhead. After the installation of several hammerheads, the progress schedule for the installation of the concrete segments for two spans is shown in Figure 2.15. Following this, the launching gantry is repositioned for the installation of the next segments.

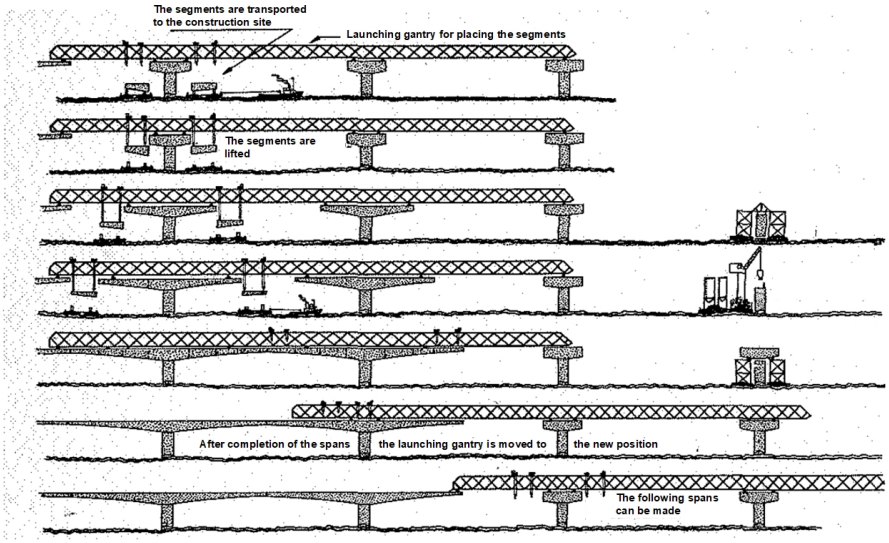

Figure 2.15: Progress schedule of the Zeelandbrug's construction. Adapted from [12]

3

Finite Element Model

In section 3.1, this chapter covers the development of hypothetical differential settlement scenarios by examining the geotechnical subsoil underneath the Zeelandbrug. Subsequently, section 3.2 includes the model considerations for the Finite Element Model of the Zeelandbrug. The analyses conducted and their corresponding results are detailed in section 3.3 and section 3.4 respectively. Finally, section 3.5 outlines the next steps to be taken in this research after obtaining the results from the Finite Element Model.

3.1. Differential settlements

This section describes the relevance of understanding the effect of differential settlements on the load effect within a structure. Additionally, this section outlines hypothetical settlement scenarios for the Zeelandbrug.

3.1.1. Relevance

The load of a structure during and after construction may cause the soil to compress in a downward vertical movement. This is known as settlement [13]. Uniform settlement does not particularly cause damage to a structure, as it does not create differential stresses. Non-uniform settlement, however, induces differential stresses within a structure and may cause structural damage. This type of non-uniform settlement is referred to as differential settlement. Differential settlement occurs when the foundation of a structure settles in one area more than the other. There are various causes to differential settlement, including variations in soil properties, changes in moisture content, loading conditions and construction practices.

In the case of the Zeelandbrug, it is uncertain whether significant differential settlements can be expected and what their impact would be. TNO has made two remarks regarding the settlement of the Zeelandbrug in their assessment report. Firstly, if the bridge possesses sufficient rotational capacity, the additional moments resulting from differential settlement will be redistributed [6]. Secondly, with respect to shear forces, TNO states that the additional shear force caused by differential settlement should be considered in the bridge's evaluation, particularly in the webs of the box girder and the shear force dowels [6]. However, in both Iv-Infra's recalculation and TNO's subsequent review, the influence of settlements was omitted from any of the loading cases of the Zeelandbrug [5, 6]. Therefore, the impact of differential settlements on the superstructure's load effect remains unclear. A gap in knowledge is identified. Hence, this chapter aims to investigate the impact of a pier settlement on the increase in the superstructure's internal shear forces. For this purpose, the increase in shear forces is examined near the support, at the construction joints and at the expansion joint.

3.1.2. Anticipated settlements and scenarios

As stated before, the magnitude of the settlement that the Zeelandbrug may experience is currently unknown. Therefore, different scenarios will be analysed. These scenarios include varying degrees of settlements of a support. By examining these different scenarios, insights can be gained into how

different levels of settlement influence the degree of shear forces in the superstructure. Typically, it can be expected that the settlement of a structure's foundation is in the range of 0-10 cm. Despite the uncertainty regarding the occurrence of support settlements for the Zeelandbrug, an effort is made to predict the potential location and magnitudes of a pier's settlement. This was realised by examining the geological profiles along the Zeelandbrug, as illustrated in Figures 3.1 and 3.2.

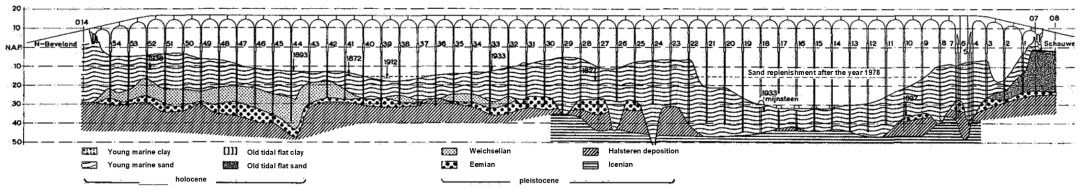

Figure 3.1: Geological profile along the Zeelandbrug. Adapted from [10].
(left to right: South to North)

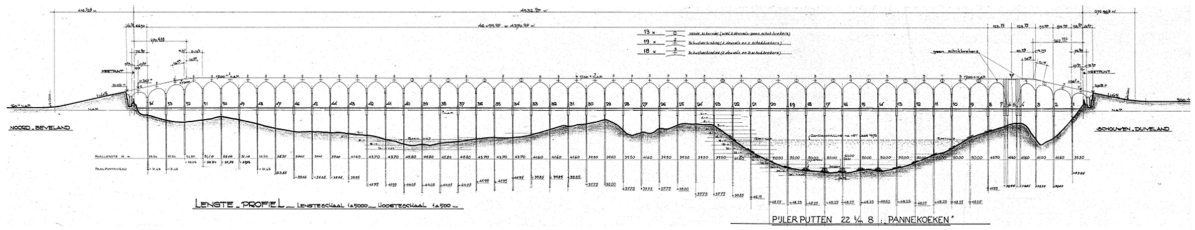

(a) Longitudinal profile Zeelandbrug [6]

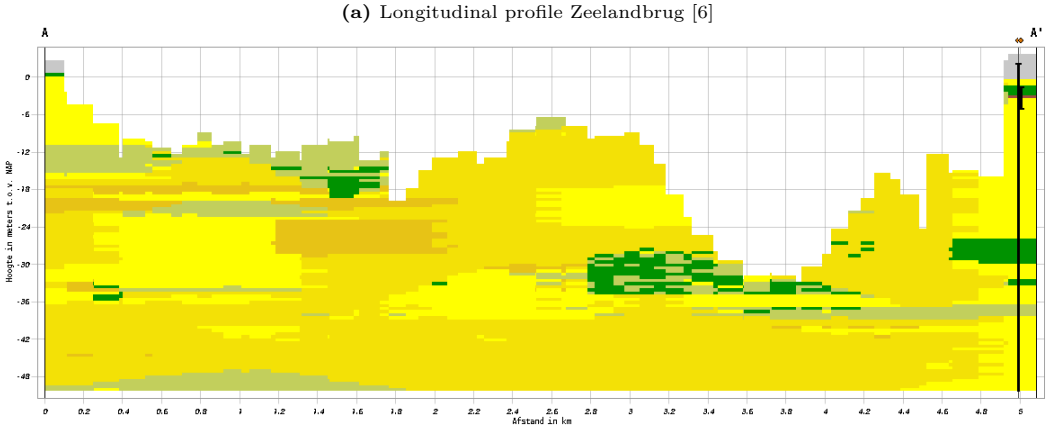

(b) Geotechnical subsoil cross-section along the Zeelandbrug

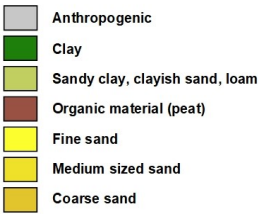

(c) Legend for the geotechnical subsoil cross-section

Figure 3.2: Longitudinal profile and geotechnical subsoil cross-section of the Zeelandbrug
(left to right: South to North)

Based on the geological profiles, it becomes apparent that the soil profile of the Oosterschelde primarily consists of sand layers. The geological profile in Figure 3.1 reveals that the soil profile contains a layer of young sea sand belonging to the Holocene, reaching a depth varying from approximately 20 to 45 meters below NAP [10]. Beneath this lies the Pleistocene sand. Due to the significantly higher cone penetration values in the Pleistocene sand compared to the Holocene sand, the foundation of the Zeelandbrug was established on or within the Pleistocene [10]. Additionally, the geotechnical subsoil cross-section in

Figure 3.2b reveals certain layers consisting of sandy clay and clay. Lastly, the geological profiles show a deep water channel characterised by a steep slope on its southern side.

If settlement of a pier were to occur then this is anticipated to happen at the location of the steep slope beneath the Zeelandbrug. The steep slope of the soil causes the lengths of the piles embedded in the soil to differ, resulting in varying stiffness. This variation in stiffness may cause the piers to settle by different amounts, which could potentially lead to differential settlement. Consequently, pier 20 (located at the steep slope) has been assigned specific hypothetical settlement values, as indicated in Table 3.1. The assigned hypothetical vertical settlement ranges from 10 mm to 200 mm, covering a broad spectrum of settlement values. It is also possible that the pier itself can settle unevenly, as covered in scenario 2. This scenario is meant to evaluate the possible lateral fixation of a pier. In this test, one side of the pier will vertically settle by either 5 or 10 mm, while the other side remains level.

Table 3.1: Settlement scenarios

Scenario	**Pier**	**Settlement [mm]**
Scenario 1a	20	5
Scenario 1b	20	10
Scenario 1c	20	50
Scenario 1d	20	100
Scenario 1e	20	150
Scenario 1f	20	200
Scenario 2a	20	0 - 5
Scenario 2b	20	0 - 10

3.2. Model considerations

Finite element modelling is a tool used to simulate the behaviour of complicated structures. DIANA is a finite element program that uses a range of finite element techniques, including linear and nonlinear analyses and static and dynamic analyses. For this research, the software DIANA FEA version 10.8 will be used to model the Zeelandbrug. This section contains the model considerations, such as the modelling assumptions, geometry, material properties, connections, applied loads, mesh distribution, boundary conditions, and model verifications.

3.2.1. Modelling assumptions

The Finite Element Model of the Zeelandbrug is a three-dimensional model, in which the bridge is modelled as one-dimensional beam elements. Only the bridge's section south of the bascule bridge has been modelled, as it represents the majority of the structure. This approach was chosen because the load effects of interest are effectively captured by modelling the number of spans south of the bascule bridge. Additionally, it is assumed that the bascule bridge is fixed at this end due to its stiff foundations. Solely the superstructure of the Zeelandbrug is modelled, while the pillars, caisson and piles are represented as supports.

Since it is currently not possible in DIANA to vary the height of a cross-section along its longitudinal axis, the Zeelandbrug has been divided into several segments along its longitudinal direction. Within these segments, the box girder's geometric dimensions have been simplified. The segments of the Zeelandbrug have been modelled as beams. These beam elements are based on the Euler-Bernoulli theory. This means that shear deformation is neglected and assumes that plane cross-sections remain plane and perpendicular to the neutral axis. This implies that the beam's depth should be small compared to its length. Namely, this ensures that the change of angle between cross-sections during bending is negligible. Additionally, when a beam is long relative to its depth, shear deformations are minor compared to bending deformations, validating the assumption that plane sections remain perpendicular to the neutral axis. Hence, it is recommended to have a height-to-length ratio between 0.33 and 0.5.

However, achieving an accurate geometry representation and weight estimation of the Zeelandbrug requires a careful balance. At the support, where the box girder's height reaches almost 6 m, a length of 12 m would excessively overestimate the bridge's geometric properties and bearing capacity. Closer to midspan, the box girder's height decreases, making it easier to implement a smaller height-to-length ratio. To balance these factors, the bridge has been divided into segments with a maximum height-to-length ratio of 1.45 adjacent to the support, reducing to 0.43 closer to midspan.

Regarding the material properties, concrete is represented as a linear elastic isotropic material. The non-linear behaviour of the concrete due to cracking has been neglected, making the modelling of the reinforcement unnecessary. Instead, the impact of reinforcement and prestressing is accounted for in the Young's modulus under the assumption that the concrete remains uncracked.

3.2.2. Geometry

To model the Zeelandbrug, the bridge has been discretised into segments along the longitudinal axis (x-axis). In the original drawing of the Zeelandbrug (NZC-78), one cantilever has specific cross-sections labelled 0, 1', 2', 2 to 14, for which the geometric properties are known (Figure 3.3). Regarding the segmentation, each segment begins at the midpoint (point 1) between the previous cross-section and the current cross-section and extends to the midpoint (point 2) between the current cross-section and the next cross-section. At the ends of the cantilever, the boundary segments end. This segmentation approach is consistent for all cross-sections, except for the second segment, where cross-sections 1' and 2 were omitted and the last segment where cross-section 14 was omitted because of the recommended height-to-length ratio.

The segments have been modelled as beam elements. The element class used is the Class-I Beams 3D, which consists of two-node straight elements. Class-I beam elements are applicable in both linear and geometric nonlinear analyses. Following analysis, the beam elements can describe the axial force, the shear force and the bending moment. In the three-dimensional Finite Element Model, all beam elements have y-coordinates of zero. Due to the varying height of the box girders along the span, the height of the elements in the Finite Element Model changes along the vertical axis (z-axis). This height change can be determined in the following manner. The height at the centroid of the cross-section at the support is set to zero. With all geometric properties of the cross-sections known, the positions of their centroids relative to the centroid of the support's cross-section are established with AutoCAD 2025. To calculate the height change at the midpoint between adjacent cross-sections, linear interpolation can be used. Appendix B contains the geometric properties of the modelled segments along with their height-to-length ratio.

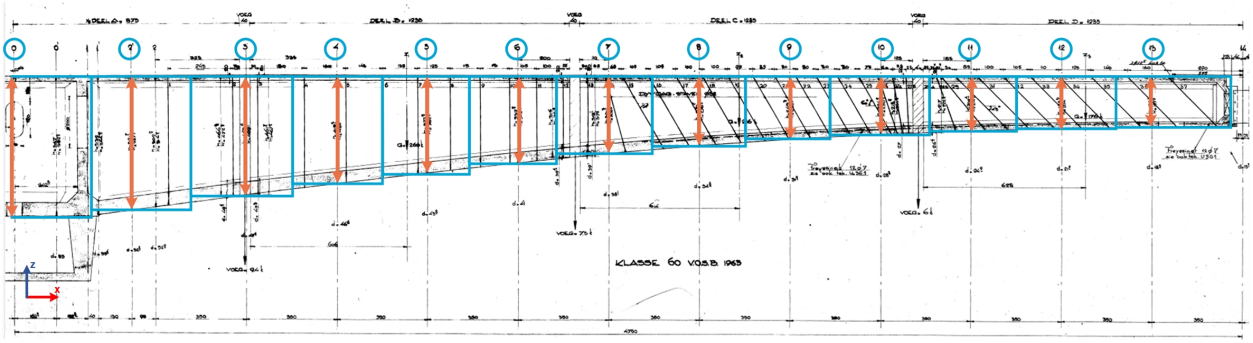

Figure 3.3: Modelled segments in the longitudinal section of the Zeelandbrug. Modified [NZC-78].

Element geometries

The element geometric properties of each segment of the Zeelandbrug correspond to those of its respective cross-section. The dimensions of the box girder at the different cross-sections were obtained from the original drawing of the bridge NZC-78. In Figure 3.4, the dimensions of the box girder are illustrated by presenting cross-section 8. In the figure, h' represents the height from the top of the top slab to the bottom of the bottom slab. Furthermore, w denotes the width of the web, d indicates the

thickness of the bottom slab and b' denotes the actual width of the bottom slab. These parameters of the box girder vary along the longitudinal axis of the bridge.

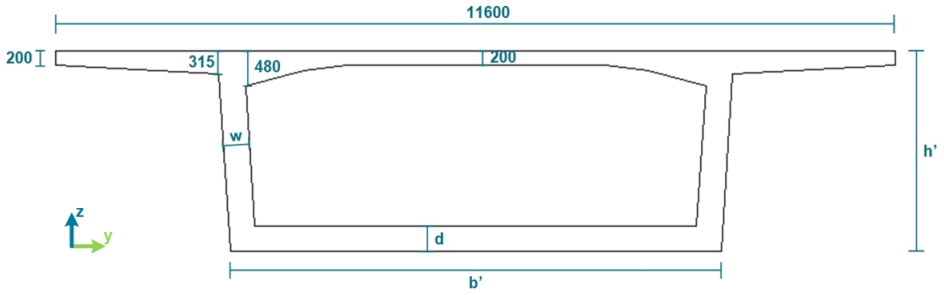

Figure 3.4: Dimensions of the modelled box girder

Each segment or beam element was assigned an element geometry. In the element geometry, an arbitrary shape was defined for which the cross-sectional area and moments of inertia had to be determined. These geometric properties were acquired by modelling the cross-sections using AutoCAD 2025. AutoCAD facilitates the determination of a profile's area, centroid, and principal moments of inertia about the centroid in both y and z directions.

Slight simplifications were made to the dimensions of the modelled cross-sections, as already depicted in Figure 3.4. Figure 3.5 further illustrates this simplification, showing a modelled cross-section in AutoCAD on the left and the actual cross-section on the right. Differences include simplified corners, omission of the bottom slab vault, and flattening of the slope on the top slab. Appendix B presents the figures displaying the modelled cross-sections in AutoCAD labelled 0, 1', 2', 2 to 14. Appendix B also presents the provided cross-sectional area and the principal moments of inertia about both the y and z axes. The moment of inertia about the yz plane is zero, due to the symmetrical nature of the box girder about the z-axis. This symmetry ensures that the mass distribution is balanced.

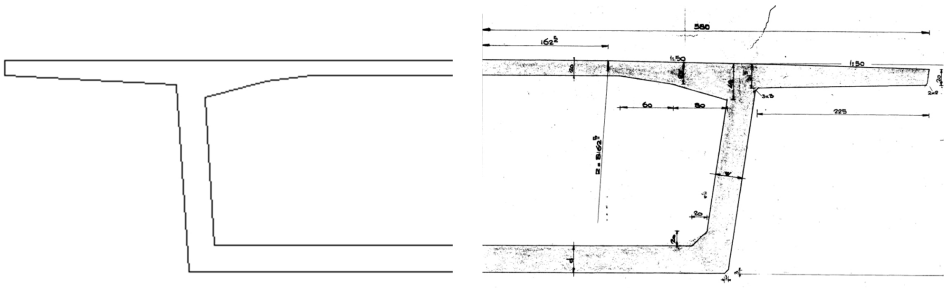

Figure 3.5: Comparison modelled (left) and actual (right) cross-section

Furthermore, the torsional moments of inertia of the cross-sections were determined. The torsional moment of inertia is important as it signifies the cross-section's resistance to torsional deformation and contributes to the structural stiffness against torsional loads. To compute the torsional moments of inertia, the cross-sections were further simplified as illustrated in Figure 3.6. The contribution of the cantilevers of the box girder to the overall torsional stiffness can be neglected. Then, the calculation of the torsional moments of inertia can performed using Equation 3.1. The derivation of this equation can be found in Appendix C. The calculated torsional moments of inertia for the cross-sections are provided in Appendix B.

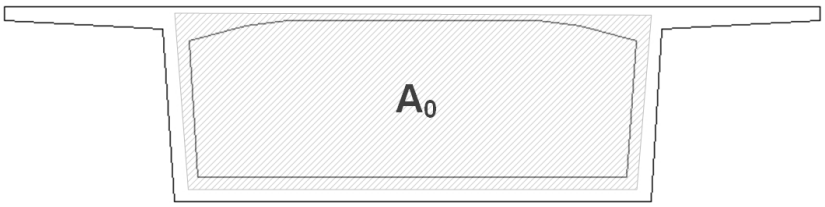

(a) Enclosed cell area to the member centerlines

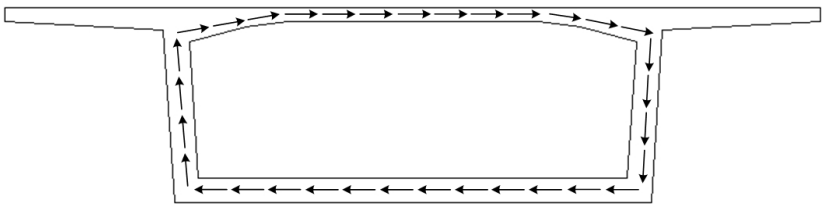

(b) Shear flow around enclosed cell

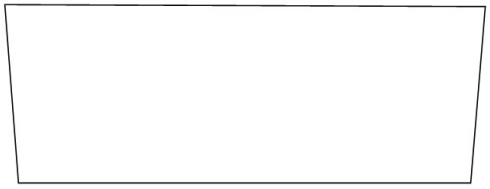

(c) Cell-definition along member centerlines

Figure 3.6: Cell-definition, enclosed cell area and shear flows

$$I_t = \frac{4 \cdot A_0^2}{\sum_i \frac{l_i}{t_i}} \tag{3.1}$$

where:
I_t is the torsional moment of inertia in [m^4].
A_0 is the enclosed cell area to the member centerlines in [m^2].
l_i is the length of the ith member in the cell in [m].
t_i is the thickness of the ith member in the cell in [m].

3.2.3. Material properties

The superstructure of the Zeelandbrug consists mainly of prefabricated concrete elements. Only the construction joints were created by pouring concrete on site. For these construction joints, the concrete properties were assumed to be the same as for the precast concrete, similar to the modelling assumptions by Iv-Infra [5]. Consequently, a single material model was specified for the concrete. The material specified falls under the class concrete and masonry. Due to the reinforcement and prestressing, it is assumed that the concrete remains uncracked. Therefore, the Young's modulus was set to 30 GPa. Furthermore, the Poisson's ratio and density of the concrete in the Zeelandbrug's superstructure have been estimated and are visible in Table 3.2. The material model used is linear elastic isotropic. This implies the following material properties of the concrete. An isotropic material has material properties that are the same in all directions. Given that the model contains one-dimensional beam elements and considers the behaviour of the bridge along a single axis, it was assumed that the concrete could be simplified as isotropic. A linear elastic material has an elastic deformation that is linear in response to the applied loads. Thus, the relationship between stress and strain is linear and Hooke's law applies.

Table 3.2: Modelled material properties of the precast and cast in-situ concrete

Material properties in DIANA	Value
Young's modulus E [N/m^2]	3*10^{10}
Poisson's ratio υ [-]	0.25
Density ρ [kg/m^3]	2400

3.2.4. Connections

The expansion joints between the T-frames have different coupling element configurations, as described in subsection 2.2.4. The presence of the shear force dowels and hinges were modelled by applying connections between the T-frames. Since there is an open space in the expansion joints, the connections are considered to be open. Each connection is classified by its element class, material, and geometric properties. The shear force dowels were modelled as connections using translational springs. The element class assigned to these connections is discrete translational spring/dashpot. The specification of the spring's material requires its spring behaviour and stiffness. The translational spring was assumed to behave as a linear elastic spring. The stiffness of the shear force dowels was derived from detailed Finite Element Model simulations of the dowels under vertical loading. The stiffness of the shear force dowels was estimated to be equal to 1.64*10^8 N/m. The geometry of the translational spring is specified using the shape type points, indicating its working direction in transferring shear forces along the z-axis of the bridge. Additionally, it is assumed that the hinges present in some of the expansion joints may transfer a small amount of bending moment. Therefore, hinges in these expansion joints were modelled as rotational springs. The element class for these connections is discrete rotational spring/dashpot. The material behaviour of the hinges is assumed to be linear elastic. The stiffness of the hinges was estimated to be 4817 Nm/rad. Furthermore, the element geometry of the rotational springs was defined using points as shape type, reflecting the hinges' working direction in rotating around the y-axis.

3.2.5. Loads

The applied loads are static. The aim is to investigate the influence of settlements on the shear forces in the bridge. Thus, the loading includes only the self-weight of the bridge and the prescribed support deformations to simulate the anticipated settlements. As stated before, the prestressing has been taken into account by assuming that the concrete remains uncracked and therefore using a corresponding Young's modulus.

Self-weight

The self-weight is defined as a global load. The mass density of the concrete was defined in the material properties in subsection 3.2.3 and has a value of 2400 kg/m^3.

Prescribed deformations

Settlements have been incorporated in the model as prescribed deformations of the supports. The translation is specified in the negative z direction, simulating downward movement. By prescribing these deformations, the model can effectively capture the resulting changes in the deformation and moment and shear force distributions. The prescribed deformations of the designated supports have been defined in subsection 3.1.2, which outlines the various settlement scenarios considered.

3.2.6. Mesh distribution

After all of the properties are assigned to the structure, the mesh can be generated. The mesh is automatically generated. The mesh type used is quadratic/hexagonal and the mesh order applied is linear. The segments with element class Class-I Beams 3D have element type L12BE. This represents a two-node straight element. The basic variables of an element are the translations and rotations in the x, y and z directions in the nodes. Within the element, the displacement field is approximated through linear interpolation polynomials. The default in DIANA is to use a 2-point Gauss integration scheme for the beam element along its bar axis.

3.2.7. Boundary conditions

Two models have been developed. Each model contains different boundary conditions to simulate the support of the substructure. Both models are described below.

Model with supports

In Figure 3.7 a T-frame of the Zeelandbrug depicts how the superstructure is supported by a pillar at two locations along the centered longitudinal section. Supports have been applied at these locations in the first model, as illustrated in Figure 3.8. These supports restrict translation only in the z-direction. In the model, supports that restrict translation in the x-direction are placed at the ends of the bridge to simulate the abutments and maintain stability of the bridge.

Model with springs

On a global scale, the Zeelandbrug south of the bascule bridge comprises 48 spans, each measuring 95 m. Given the significant scale of these cantilever spans compared to the supports, it could be argued that the supports can be modelled as springs that provide support to the superstructure at a single location, see Figure 3.9. This model includes two translational boundary springs, which restrict movement in the z- and x-directions, as well as a rotational boundary spring that restricts rotation around the y-axis.

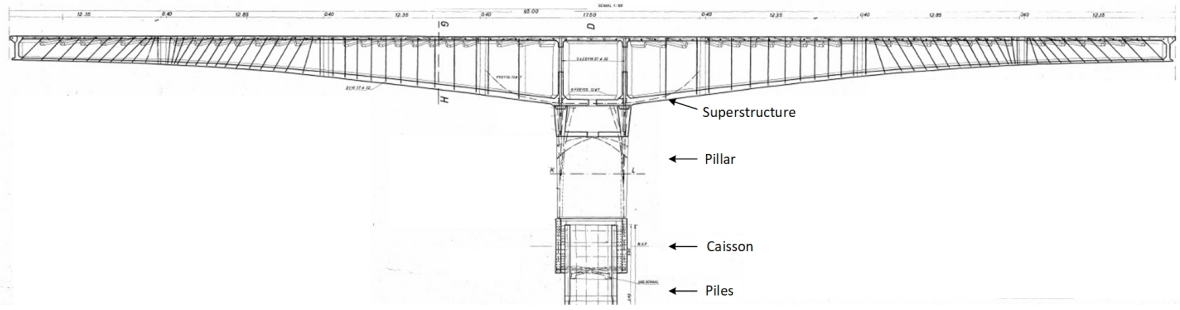

Figure 3.7: T-frame of the Zeelandbrug

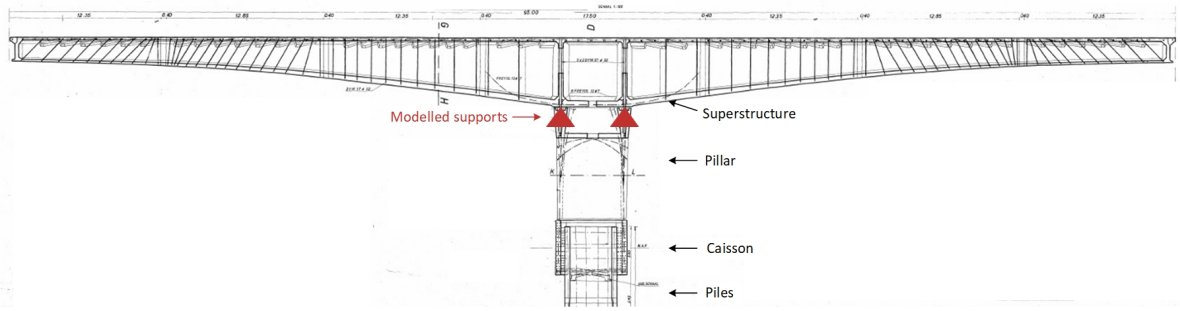

Figure 3.8: Illustration of the modelled supports for a T-frame of the Zeelandbrug

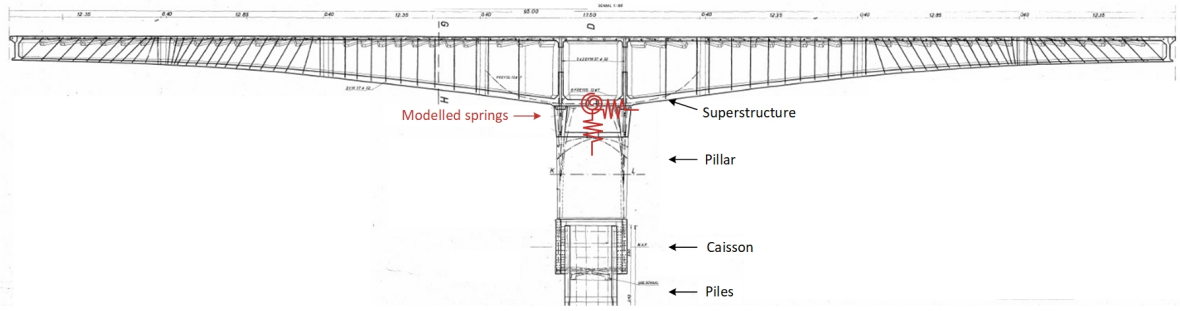

Figure 3.9: Illustration of the modelled springs for a T-frame of the Zeelandbrug

The stiffnesses of the boundary springs need to be determined. A Finite Element Model of the Zeelandbrug's substructure was used to compute the translational spring's stiffnesses (Figure 3.10). Deformations were applied at the top of the substructure. The forces resulting from these applied deformations

could be obtained in the model. To apply a deformation at the top of the substructure, a prescribed deformation was assigned to the node at the center of the top of the substructure. Master and slave nodes were then used to define the connection between this center node and the other nodes at the top of the substructure. A deformation of 0.1 m was applied in separate load cases in the x- and z-direction (Figures 3.11, 3.12 and 3.14). The resultant force in x- and z-direction were captured within the model (Figures 3.13 and 3.15). The stiffnesses of the translational springs in the x- and z-directions were then determined using Hooke's law, described by Equation 3.2. This results in an estimated stiffness of the translational spring in the x-direction of $1.27*10^8$ N/m and in the z-direction of $4.58*10^9$ N/m.

$$k_t = \frac{F}{u} \tag{3.2}$$

where:
k_t is the translational stiffness of the spring in [N/m].
F is the restoring force in [N].
u is the displacement of the spring from its equilibrium position in [m].

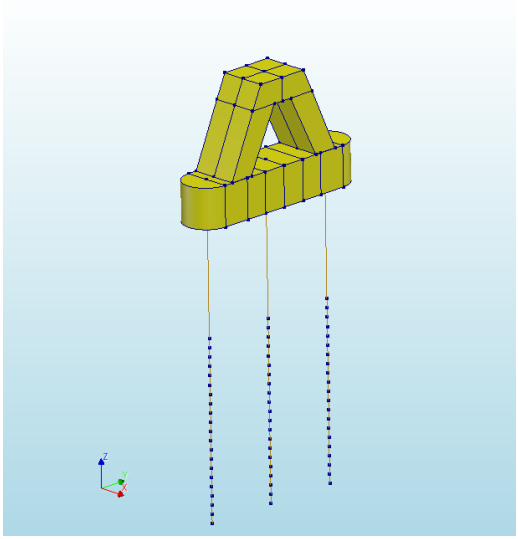

Figure 3.10: FEM substructure: substructure

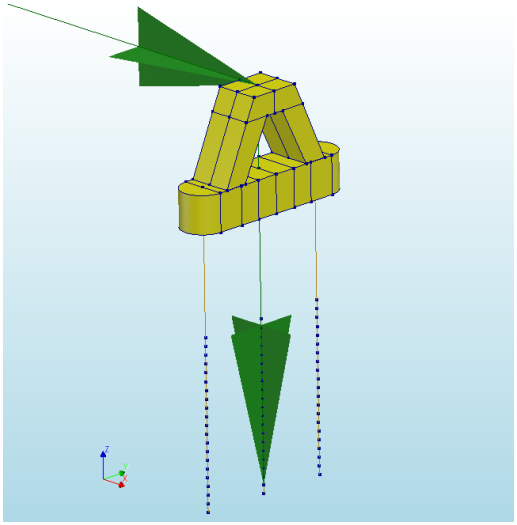

Figure 3.11: FEM substructure: prescribed deformations

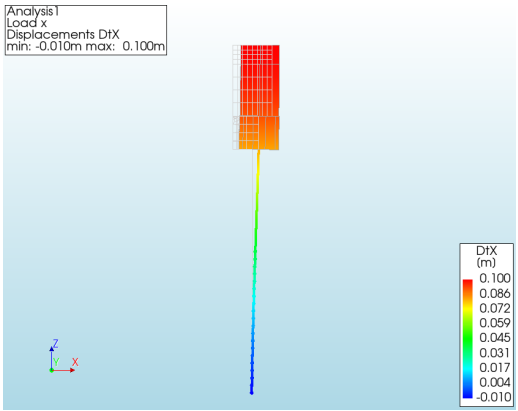

Figure 3.12: FEM substructure: deformation in x

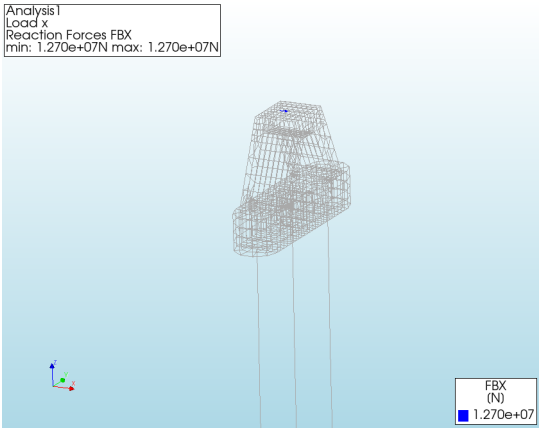

Figure 3.13: FEM substructure: resulting force in x due to the deformation in x

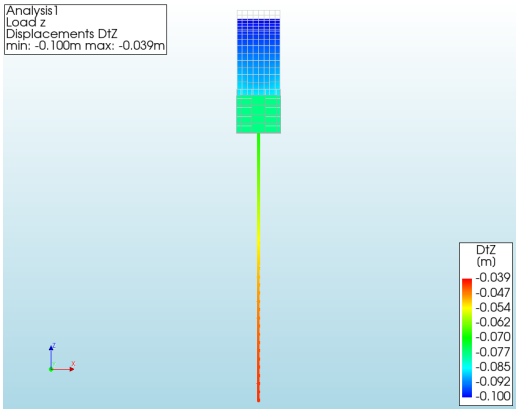

Figure 3.14: FEM substructure: deformation in z

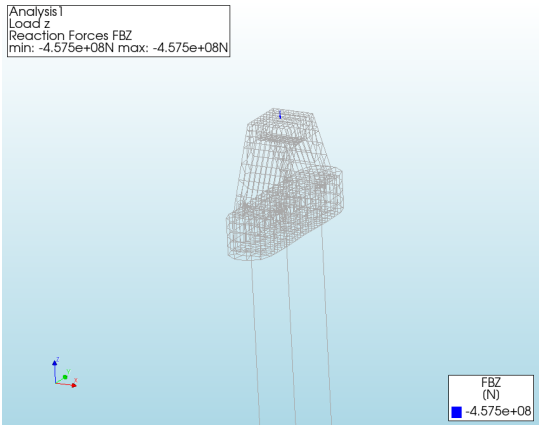

Figure 3.15: FEM substructure: resulting force in z due to the deformation in z

The stiffness of the rotational spring was roughly estimated using the applied deformation and resulting force in the x-direction. It was approximated that the substructure deforms as a straight line, as illustrated in Figure 3.16. The rotation point, around which the substructure rotates under the applied deformation, can be seen in Figure 3.12. This rotation point is roughly 5 m from the bottom of the piles. Knowing the length from the top of the substructure to the rotation point (41.8 m), the moment could be calculated by multiplying the resulting force due to the applied deformation by this length. The rotation of the substructure was calculated by dividing the applied deformation by the length to the rotation point. Using the moment and rotation, the stiffness of the rotational spring about the y-axis could be determined using the rotational analog of Hooke's law, as described in Equation 3.3. This results in an estimated stiffness of the rotational spring about the y-axis of $2.22{*}10^{11}$ Nm/rad.

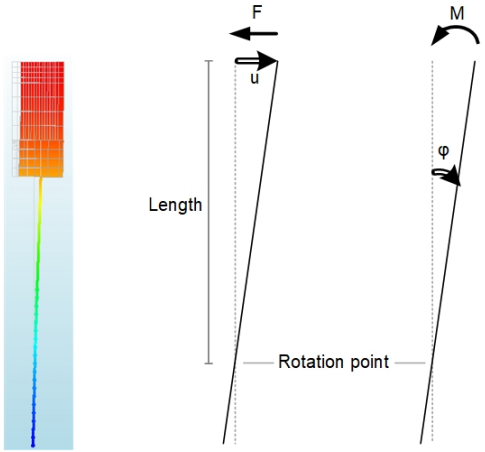

Figure 3.16: Illustration of the rotation resulting from a deformation in x (exaggerated)

$$k_r = \frac{M}{\varphi} \tag{3.3}$$

where:
k_r is the rotational stiffness of the spring in [Nm/rad].
M is the restoring moment in [Nm].
φ is the rotation of the spring from its equilibrium position in [rad].

3.2.8. Model verifications

The complete model with supports is presented in Figure 3.17a. A close-up of the model is shown in Figure 3.17b. Additionally, Figure 3.17c presents the complete model with springs and Figure 3.17d a close-up of this model. Accordingly, the modelled Zeelandbrug south of the bascule bridge consists of 48 spans, each span measuring 95 m.

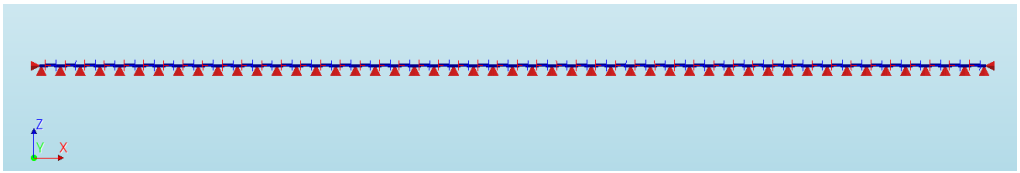

(a) Model with supports

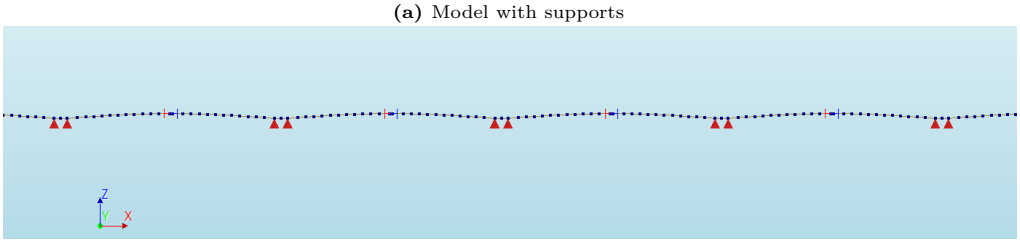

(b) Close-up of the model with supports

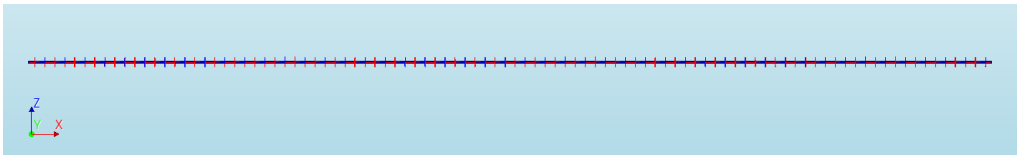

(c) Model with springs

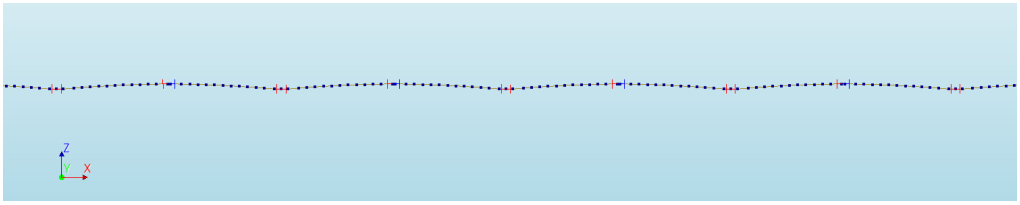

(d) Close-up of the model with springs

Figure 3.17: The global Finite Element Model of the Zeelandbrug

To perform the model verifications, a model was developed of only a single span of the Zeelandbrug, see Figure 3.18. The supports were modelled as boundary conditions. Subsequently, structural linear static analyses were performed to perform the model verifications, considering only the effect of the self-weight on the bridge.

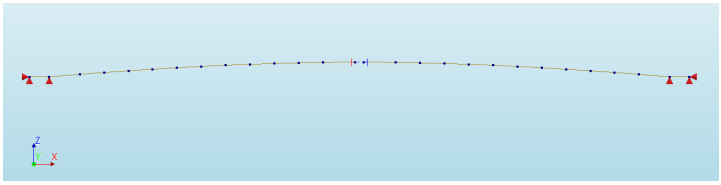

Figure 3.18: Finite Element Model of a single span of the Zeelandbrug

Weight of the superstructure

To check the Finite Element Model, the first step involves comparing the self-weight of one span of the modelled Zeelandbrug with the estimated actual self-weight of one span of the bridge. The self-weights of the segment types and the joints of the bridge can be found on the original drawing NZC-78. An exception is the self-weight of segment type A, which is according to Hoving et al. [10]. The total self-weight of the superstructure has been calculated for one T-frame, see below. Hence, the actual self-weight of the superstructure was estimated to be $1.95*10^6$ kg. DIANA calculates the total self-weight

of the superstructure to be 1.68*10^6 kg. The difference is 13%. This difference could be attributed to the fact that the model includes simplified elements. The segments of the bridge have been simplified in terms of geometry and material properties. Additionally, the model omits secondary elements that might have been considered in the weight of the segments and joints, such as the inner partition walls at the ends of the bridge's cantilevers.

Estimated actual self-weight of the Zeelandbrug's superstructure for one T-frame:

Segment type A:	600	ton	*	1	=	600	ton
Joint A-B:	9.4	ton	*	2	=	18.8	ton
Segment type B:	260	ton	*	2	=	520	ton
Joint B-C:	7.5	ton	*	2	=	15	ton
Segment type C:	216	ton	*	2	=	432	ton
Joint C-D:	6	ton	*	2	=	12	ton
Segment type D:	176	ton	*	2	=	352	ton
						1950	ton

Finite Element Model with curved shell elements

The second step in checking the Finite Element Model involves comparing the vertical deflection of one span with that of a Finite Element Model with curved shell elements. DIANA calculated the self-weight of the model with curved shell elements to be 1.81*10^6 kg. As previously mentioned, the model with one-dimensional beam elements weighs 1.68*10^6 kg. As depicted in Figure 3.19c, the vertical displacement of the model with beam elements is -0.101 m due to the bridge's self-weight. Similarly, the model with curved shell elements has a deflection of -0.116 m (Figure 3.19d). The deflection has increased 13%.

Both models have used different simplifications to simulate the same bridge's behaviour. Therefore, the difference in deflection response should be minimal and should be explainable by understanding why one model shows greater deflection than the other. The difference in deflection can be attributed firstly to the difference in self-weight between the two models, with the model using curved shell elements being 7% heavier. Even though the increased weight causes an increased stiffness of the bridge, it will simultaneously result in an extra load. Secondly, the difference can be explained by the models using different classes of elements and types. Curved shell elements take into account shear deformation within the shell's thickness according to the Mindlin-Reissner theory. Conversely, the Euler-Bernoulli theory assumes shear deformation to be negligible, focusing primarily on bending effects along the beam's length. Thus, it can be expected that incorporating shear deformation leads to an increased deflection. Lastly, the difference in deflection can be a simple cause of reducing a structure in dimension and omitting any secondary elements in the model with one-dimensional beam elements.

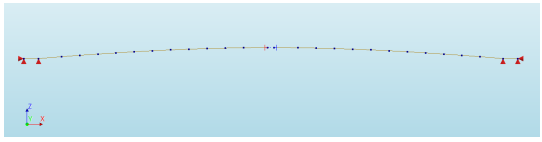

(a) FEM with 1D beam elements of the superstructure

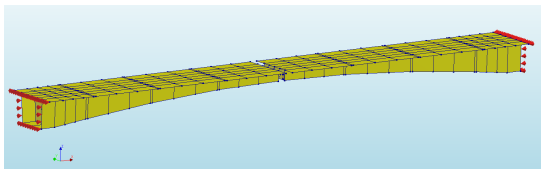

(b) FEM with curved shell elements of the superstructure

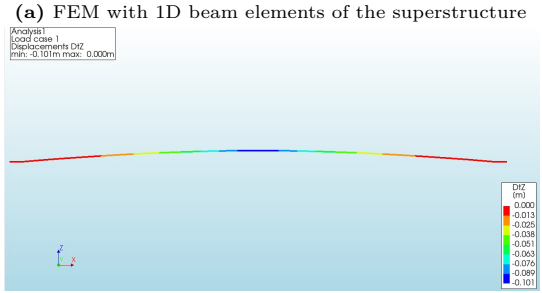

(c) Displacement of the FEM with 1D beam elements

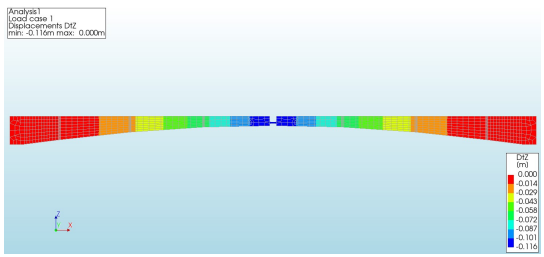

(d) Displacement of the FEM with curved shell elements

Figure 3.19: Comparison of Finite Element Models of a single span of the Zeelandbrug

Model with supports versus model with springs
Following the check of the DIANA model with one-dimensional beam elements, a comparison can be made in the application of different boundary conditions. This comparison is important, because it helps understand the differences in structural response when the piers of the bridge are modelled as supports with translational restrictions or as springs with translational and rotational stiffnesses. Figures 3.20a and 3.20b illustrate the displacement due to the self-weight of the bridge. The deflection is greater in the model with springs because the boundary condition at the support applies stiffness in the z-direction, rather than restricting the displacement in the z-direction.

Figures 3.20c and 3.20d show the shear forces due to the self-weight of the bridge. Note that the legend in Figure 3.20c shows very high shear forces. These occur at the boundaries of the bridge. The model with supports, which represents the pier as two adjacent supports, shows large shear forces between these supports to balance the resulting moments. The shear forces over the cantilever are comparable between both models.

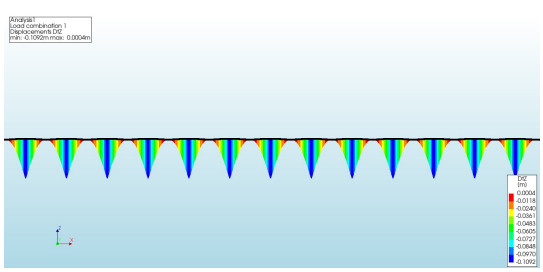

(a) Model with supports: displacement due to self-weight

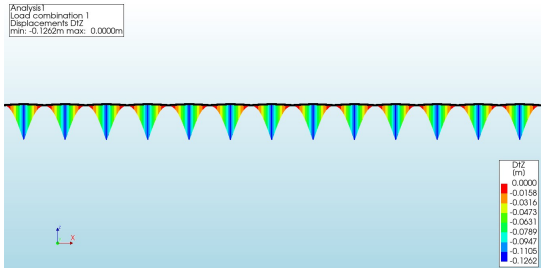

(b) Model with springs: displacement due to self-weight

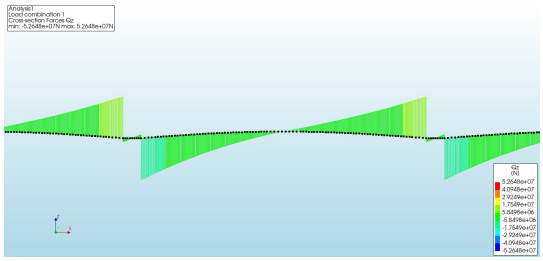

(c) Model with supports: shear forces due to self-weight

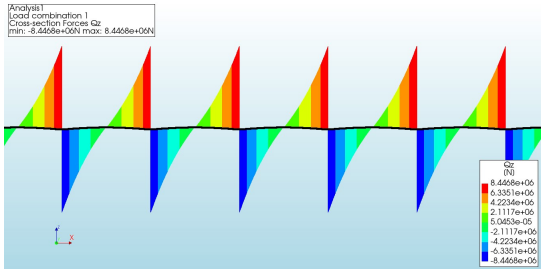

(d) Model with springs: shear forces due to self-weight

Figure 3.20: Comparison between the model with supports and the model with springs

3.3. Analysis

The analyses performed to record the Zeelandbrug's structural response to the different settlement scenarios were structural linear static. This suggests that the material's response is assumed to be linear elastic, conforming to Hooke's law. Another implication of a structural linear static analysis is that the loads are applied gradually and remain constant over time. When the deformations of the structure are assumed to be small, the assumption of linear elastic material behaviour is justified. Given that the prescribed deformations are not small, a non-linear analysis is generally recommended to accurately capture the structure's response. However, in this study, the material properties were assumed to be linear elastic. The results will therefore indicate no difference in the structural response of the bridge when comparing non-linear and linear analyses. Consequently, the analyses performed were structural linear static.

3.4. Results

After conducting the analyses, the results of the different settlement scenarios were obtained. This section contains the results corresponding to each scenario.

3.4.1. Scenario 1

Scenario 1 comprises the possible vertical settlements of pier 20 of the Zeelandbrug. The defined hypothetical settlements were 5, 10, 50, 100, 150 and 200 mm. In Figure 3.21, scenario 1b is shown for both the model with supports and the model with springs. A deformation of 10 mm was applied to pier 20. As a result, the figures include diagrams of displacement and shear forces, reflecting the effects of self-weight and settlement.

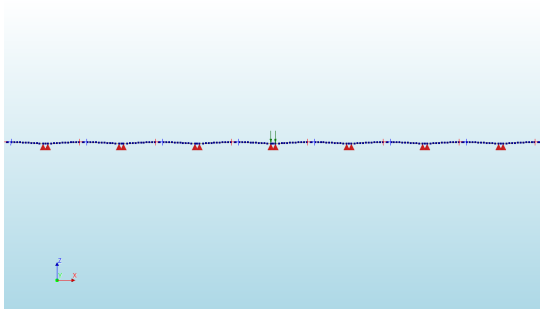

(a) Model with supports: prescribed deformation

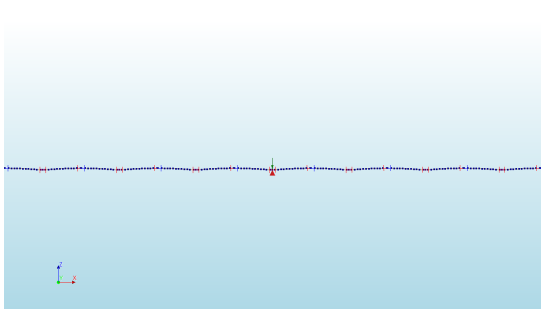

(b) Model with springs: prescribed deformation

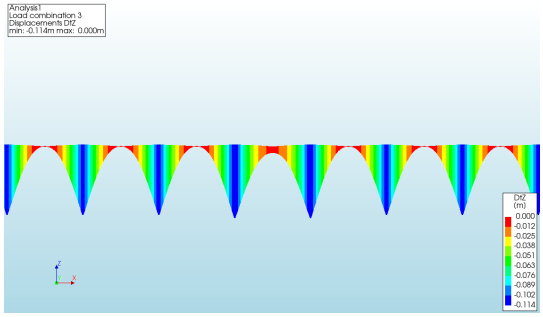

(c) Model with supports: displacement due to self-weight and settlement

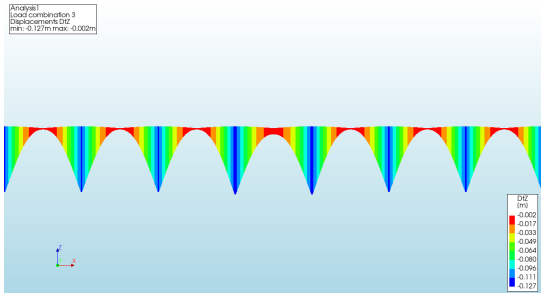

(d) Model with springs: displacement due to self-weight and settlement

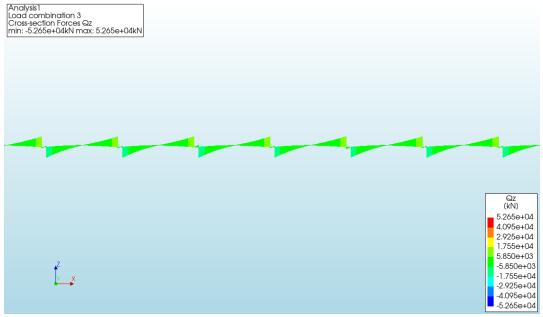

(e) Model with supports: shear due to self-weight and settlement

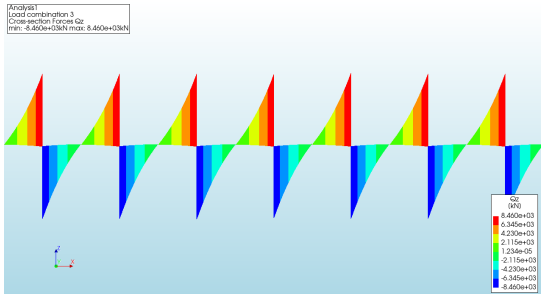

(f) Model with springs: shear due to self-weight and settlement

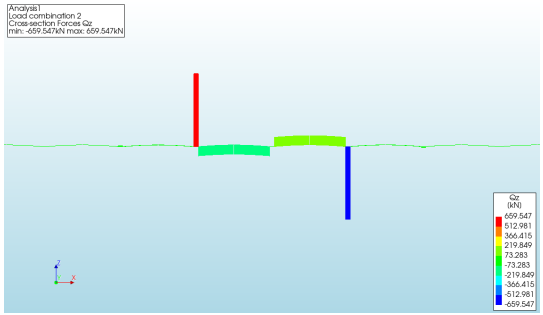

(g) Model with supports: shear due to settlement

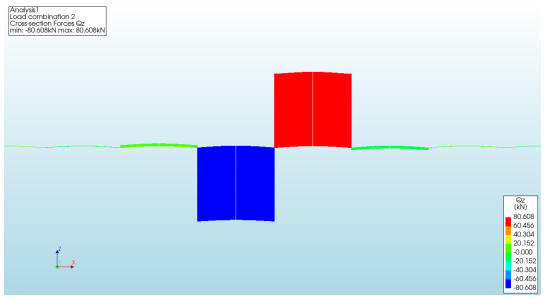

(h) Model with springs: shear due to settlement

Figure 3.21: Structural response of Finite Element Model with a settlement of 10 mm

Table 3.3 displays the shear forces in the bridge's cantilever, as obtained from the model with supports, in response to the potential settlement of pier 20. Similarly, Table 3.4 presents these shear forces for the model with springs. As previously observed, the model with supports exhibits higher shear forces across the bridge's cantilever compared to the model with springs due to the increased stiffness of the supports, which attract greater forces. As noted before, each shear force dowel has a capacity of 650 kN. With two dowels at each midspan joint, the total capacity is 1.3 MN. Consequently, for large hypothetical settlements of 150 mm or less, the shear force at the midspan joint remains within this capacity.

Table 3.3: Resulting shear forces of the model with supports due to scenario 1

Additional shear force [kN]					
Settlement 5 mm	Settlement 10 mm	Settlement 50 mm	Settlement 100 mm	Settlement 150 mm	Settlement 200 mm
42.19	84.40	422.01	844.03	1266.04	1688.05

Table 3.4: Resulting shear forces of the model with springs due to scenario 1

Additional shear force [kN]					
Settlement 5 mm	Settlement 10 mm	Settlement 50 mm	Settlement 100 mm	Settlement 150 mm	Settlement 200 mm
40.25	80.46	402.04	804.92	1207.37	1609.83

Tables 3.5 and 3.6 display the shear forces within the bridge's cantilever due to a hypothetical settlement of 100 mm and a varying Young's modulus of the concrete. Visibly, a reduction in the Young's modulus results in decreased shear forces in the bridge.

Table 3.5: Shear forces from 100 mm settlement with varying Young's modulus in the model with supports

Additional shear force [kN]		
Settlement 100 mm E=30 GPa	Settlement 100 mm E=25 GPa	Settlement 100 mm E=20 GPa
844.03	709.45	572.52

Table 3.6: Shear forces from 100 mm settlement with varying Young's modulus in the model with springs

Additional shear force [kN]		
Settlement 100 mm E=30 GPa	Settlement 100 mm E=25 GPa	Settlement 100 mm E=20 GPa
804.92	679.95	551.55

3.4.2. Scenario 2

Scenario 2 comprises the uneven hypothetical vertical settlement of the supports representing pier 20 of the Zeelandbrug. Scenario 2a is presented in Figure 3.22, where a pier is modelled as two supports. In this scenario, one of the supports of pier 20 is subjected to a deformation of 5 mm. The resulting diagrams illustrate the displacement and shear forces caused by the self-weight and settlement.

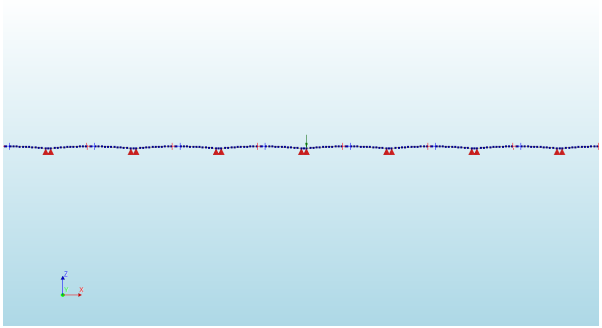

(a) Model with supports: prescribed deformation

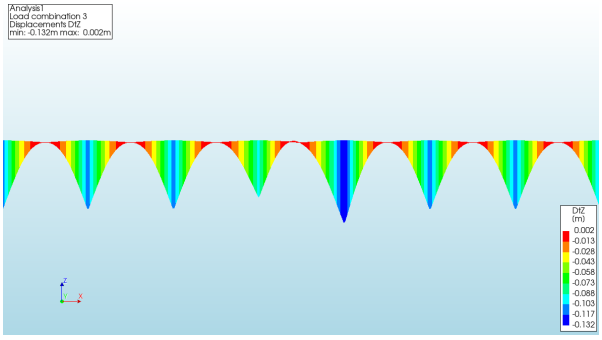

(b) Model with supports: displacement due to self-weight and settlement

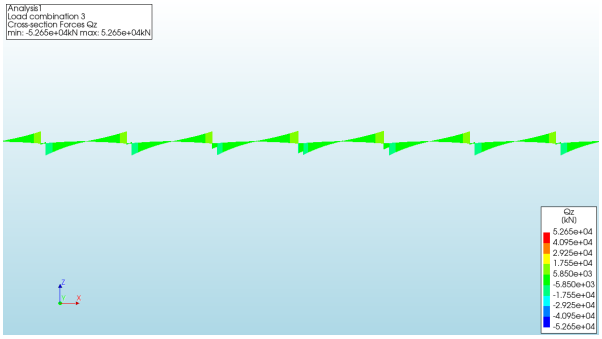

(c) Model with supports: shear due to self-weight and settlement

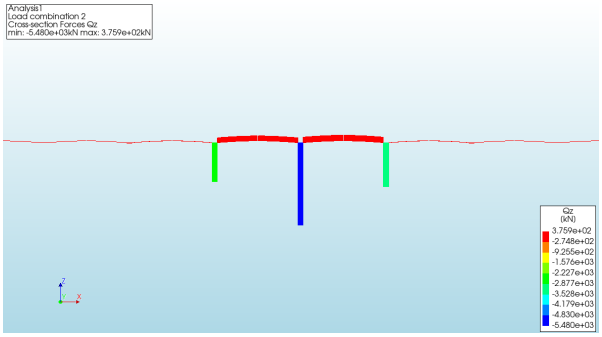

(d) Model with supports: shear due to settlement

Figure 3.22: Structural response of Finite Element Model with an uneven settlement of 5 mm

Table 3.7 demonstrates the shear forces within the bridge's cantilever due to the uneven hypothetical settlement of pier 20. It is evident that the occurrence of minor uneven settlements of a pier could lead to significant shear forces.

Table 3.7: Resulting shear forces of the model with supports due to scenario 2

Additional shear force [kN]	
Uneven settlement 5 mm	Uneven settlement 10 mm
333.15	666.31

3.5. Next steps

By obtaining the Finite Element Model (FEM) results, the shear forces within the bridge's cantilevers were determined for different settlement scenarios. The next step involves integrating these findings into the recalculation of the bridge's structure. For this, the results of the model with supports for scenario 1d (100 mm settlement) were selected. This is because the geological profiles beneath the Zeelandbrug revealed mostly sand layers, suggesting that large settlements are not expected, but this choice still maintains a conservative approach. A lower and upper bound of 5 and 200 mm support settlement will also be integrated in the recalculation of the bridge's structure to include a range of expected outcomes. Hence, the additional shear forces due to a support settlement of 5, 100 and 200 mm will be incorporated into the moment and shear force capacity checks in the longitudinal direction. Subsequently, the FEM results will be assessed for their reliability and analysed to interpret the implications of the additional shear force magnitudes on the overall bridge structure and its capacity.

4

Assessment of the current status

First, this chapter contains an overview of the loads that the Zeelandbrug experiences in section 4.1. In section 4.2, a revision is performed of the recalculations on the Zeelandbrug's concrete structure. Taking this revision into account, recalculations on the Zeelandbrug are conducted with in longitudinal direction incorporating the additional shear forces resulting from a support settlement. With the final objective to identify critical failure modes, the recalculations are detailed in section 4.3. This section also analyses the Finite Element Model results and their impact when incorporated into the recalculations. Lastly, section 4.4 discusses the identified uncertainties that were found while performing the recalculations.

4.1. Loads

The various types of loads that the Zeelandbrug experiences have been split into permanent loads, variable loads, horizontal loads and other loads. The Zeelandbrug has Consequence Class 3 (CC3) and is assumed to have a remaining service life of 30 years. The load combinations were performed according to NEN-EN 1990+A1+A1/C2:2011, and the load factors were selected based on the serviceability requirements specified in NEN8700:2011.

4.1.1. Permanent loads

The permanent loads consist of the self-weight of the bridge's segments, the weight of the pavement and the weight of the barrier.

Self-weight

In subsection 3.2.8 the actual self-weight of the superstructure for one T-frame was estimated to be $1.95*10^6$ kg. The self-weights of the segments and joints were found listed on the original drawing NZC-78, whereas segment type A is according to Hoving et al. [10].

Pavement

The initial, future-proof assumption of the pavement's design load is according to the Richtlijn Ontwerp Kunstwerken (ROK), which are guidelines for the design of structures. In Table 4.1, the thickness, weight per unit volume and the load of the pavement are depicted. The pavement's actual thickness, and hence its load, is smaller.

Table 4.1: Self-weight of the pavement [5, 6]

	Thickness [m]	γ [kN/m^3]	p [kN/m^2]
Pavement conform ROK 1.2, used by Iv-Infra [5]	0.140	23	3.220
Pavement conform ROK 2.0, recommended by TNO [6]	0.156	23	3.588

Barrier

At the edges, the bridge has a barrier on the east side and a guard rail for the bike lane on the west side. The loads of the barriers and guard rails are shown in Table 4.2. When considering theoretical road

lanes on the bridge, it is assumed that the road traffic spans the entire width of the bridge. Therefore, it is assumed that there are barriers on both edges of the bridge.

Table 4.2: Self-weight of the barriers and guard rail [5]

	q [kN/m]
Edge barrier (east side)	9.88
Barrier to seperate bike lane	7.80
Guard rail, including kerb (west side, assumption)	1.00

4.1.2. Variable loads

The variable loads consist of traffic loads and the load from the maintenance platform.

Traffic loads

The actual lane configuration of the Zeelandbrug is depicted in Figure 4.1. A dedicated bike lane is situated on the west side, separated from two road lanes in opposing directions on the east side. Figure 4.2 illustrates the theoretical lane distribution based on Eurocode Load Model 1. In this scenario, the barriers are installed along both edges of the bridge. According to Load Model 1, a bridge's width is divided into notional lanes of 3 m each, with any remaining area allocated accordingly. For the Zeelandbrug, this results in three notional lanes and a remaining area of 1.85 m wide. Figure 4.2 also presents the distribution of uniformly distributed loads and Tandem Systems across the notional lanes as per Load Model 1.

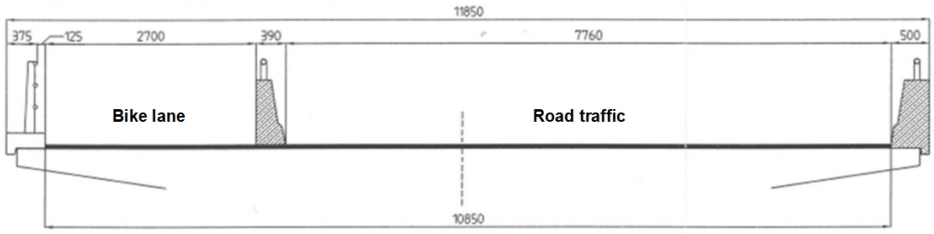

Figure 4.1: Actual road lane division. Modified [NZC-1881].

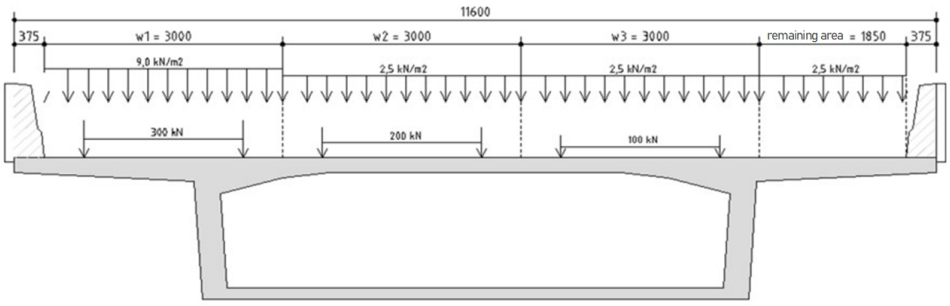

Figure 4.2: Theoretical road lane division based on Eurocode LM1. Adapted from [5]

In the recalculations, Eurocode Load Model 2 is also taken into account. Load Model 2 may significantly impact the cantilever of the box girders [5]. The model contains two wheel loads of 200 kN each. The single axle load should be applied at any location on the carriageway that could be perceived as critical.

Maintenance platform

To perform maintenance activities on the Zeelandbrug, a self-propelled maintenance platform is used. The driving portal for this platform is positioned on the bridge's bike lane, as depicted in Figure 4.3. The maintenance platform itself is visible in Figure 4.4. It is important to consider the additional

loads imposed by the maintenance platform in the recalculations. The self-weight of the maintenance platform is specified as 125 kN [5]. In addition, an additional variable load of 10 kN is accounted for, representing personnel and added equipment on the platform [5]. Due to the presence of the maintenance platform, other traffic cannot access this lane in theoretical scenarios. Therefore, the load imposed by the maintenance platform is critical only for local assessments in transverse directions [5].

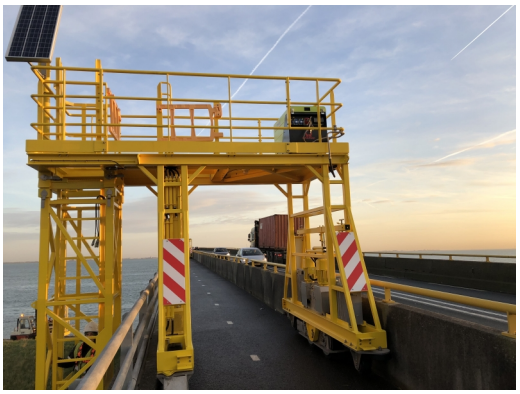

Figure 4.3: Maintenance platform on the bike lane [14]

Figure 4.4: Full-view of the maintenance platform at site [14]

4.1.3. Horizontal loads

The original design incorporated an ice load of 10,000 kN per pier, which included a 1,000 kN wind load [10]. This substantial ice load was justified by the anticipation that a permanent dam would be constructed, thereby closing off the Oosterschelde from the sea and converting it to fresh water [10]. However, this plan was never realised. Given that the ice load has not increased, it is not further considered in the recalculation of Iv-Infra [5]. In the original design, a wind load of 1.105 kN/m^2, acting perpendicular to the structure, was used. Nowadays, a wind load of 1.5 kN/m^2 is typically used for standard constructions [5]. However, considering the Zeelandbrug's elevated position and exposure in the sea area, Iv-Infra accounted for a wind load of 2.0 kN/m^2 [5]. Lastly, the horizontal braking force incorporated by Iv-Infra over two T-frames is 875 kN [5].

4.1.4. Other loads

Potential collisions of ships with the pillars and/or the superstructure are not considered. The recalculation by Iv-Infra, and hence this study, excludes factors such as temperature variations, concrete shrinkage, and creep, as these are not expected to cause structural collapse [5]. However, Iv-Infra did indirectly account for creep through the modulus of elasticity [5]. The impact of settlements is also excluded in the recalculation by Iv-Infra [5]. The original design considered differential settlements of the pillars relative to each other by assuming a maximum differential settlement of 6 cm between two adjacent pillars [10]. In comparison, this study includes the impact of a support settlement of 5, 100 and 200 mm on the load effects in longitudinal direction within the bridge's cantilevers.

4.2. Revision recalculations of the Zeelandbrug

On behalf of the Province of Zeeland, the structural safety of the Zeelandbrug has been assessed by Iv-Infra [5]. For this assessment, Iv-Infra examined some of the original design documents to obtain information about the geometry, the reinforcement configuration, material properties and certain design assumptions. The concrete structure of the Zeelandbrug has been assessed based on a recalculation assuming a remaining service life of 30 years and CC3. The recalculation is in accordance with the norms RBK 1.1, NEN8700 and NEN8701. Two loading scenarios are the basis for the recalculation. In the first loading scenario, the bridge's whole width is divided into three theoretical lanes of traffic, each having a maximum theoretical thickness of the pavement. If this scenario does not comply with the standards there will be looked at the second loading scenario. This scenario is based on the actual pavement thickness and the actual road lane configuration, which consists of two road lanes and one bike lane. To determine the load effect in the bridge, Iv-Infra developed a model of the bridge [5]. Furthermore, Iv-Infra had carried out a visual inspection on the bridge. From this inspection it followed

that no structural damage was observed that indicates overload or that has to be taken into account in the recalculation [5].

Important findings of the recalculation by Iv-Infra that could prove to be critical to the safety of the Zeelandbrug have been summarised [5]. Critical conditions have been defined to occur when the applied loading on a structural element exceeds its resistance. Firstly, the shear force capacity of the field of the box girder's top slab was found to be critical in relation to the applied shear force in the transverse direction. The model was used to determine the occurring shear force in top slab of the box girder. In transverse direction, the box girder was modelled based on the dimensions of the center of a type D box girder. Different load cases have been implemented in the model in which the Tandem System shifts positions on the bridge. In this manner, the highest occurring shear force in the box girder's top slab has been determined through the model. The shear force resistance of the concrete was calculated. It appeared that the shear force occurring in the top slab slightly exceeds the capacity (unity check of 1.06) [5]. Nevertheless, based on the actual usage of the bridge, the assessment would prove to be just acceptable (unity check of 0.99) [5].

Secondly, the shear force capacity of the box girder's webs in longitudinal direction was proven to be critical to withstand the applied shear force [5]. The shear force capacity of the webs have been determined by combining the shear resistance due to prestressing and a changing height, as well as the shear resistance of the concrete. Furthermore, the capacity of the concrete compression diagonal was determined. The actual shear force capacity of the web is determined by the lowest of the two previously mentioned capacities. The webs were tested on shear force capacity at the construction joints and adjacent to the support. The highest occurring shear force in the webs was determined by using the model of five T-frames of the Zeelandbrug and implementing different load cases. In these load cases, both the position of the uniformly distributed traffic load and the Tandem System changes. Furthermore, torsion induces tension and compression in the webs. These forces have been added to the occurring shear force. It was found that particularly the construction joint between segments B and C does not suffice (unity check of 1.06) [5]. The capacity of the concrete compression diagonal appeared to be governing. Due to a remaining service life of 30 years, reduction factors may be considered conform NEN8701:2011. These reduction factors concern a reduction in traffic loading trends and a reduction in the size of vertical traffic loading. In longitudinal direction, these reduction factors are 0.95 and 0.98 respectively. Taking these reduction factors into account would result in a unity check of 1.03 for the construction joint between segments B and C [5].

Thirdly, the capacity of the shear force dowels has been assessed and was found to be exceeded [5]. In each expansion joint, two shear force dowels are present. One shear force dowel has a capacity of 650 kN. The occurring shear force in the expansion joint was determined using the model. Furthermore, the additional shear force due to torsion has been incorporated in the total occurring shear force in the expansion joint. The most critical position of the Tandem System was found to be just above the expansion joint [5]. The total occurring shear force exceeds the shear force capacity of the dowels with a unity check of 1.68 [5]. A possible reason is given by Burggraaf and Borsje from TNO as to why the unity check is so high. Namely, it is speculated that uncertainties in the loads have been incorporated in the shear force resistance of the dowels during the design [6].

Fourthly, fatigue of the steel reinforcement has been initially found to be critical in the box girder's cantilever in transverse direction [5]. The occurring and allowable stress range were determined of the soft steel reinforcement. It was found that based on fatigue Load Model 1, the assessment on fatigue could be critical [5]. However, based on fatigue Load Model 4, it follows that the number of occurring stress variations is sufficiently acceptable compared to the number of allowable stress variations [5].

Overall, it can be concluded that the capacity of a few structural elements do not suffice based on the first loading scenario (theoretical usage of the bridge). However, considering the actual usage of the bridge, the capacity of the structural elements of the Zeelandbrug do suffice with the exception of the shear force dowels [5].

Following the report of Iv-Infra, the Province of Zeeland has commissioned TNO to review the recalculation of the Zeelandbrug. Based on this review, a visual inspection and a document review, TNO has identified which structural elements they consider to be critical or soon to become critical. Some of the remarks in TNO's review concern an overestimated yielding strength of the Dywidag bars and an underestimated prestress loss in longitudinal direction [6]. Through the recalculation of Iv-Infra and its subsequent review by TNO, it can be assumed which structural elements of the Zeelandbrug's superstructure may be or become critical. Structural elements have been defined as critical when their resistance is exceeded by the applied loading. The potentially critical structural elements are listed below.

In transverse direction:

- The moment and shear force capacity of the cantilever of the box girder.
- The moment and shear force capacity of the top slab of the box girder.
- The moment capacity of the webs when tension occurs on the outer side of the webs.

In longitudinal direction:

- As a result of the longitudinal moment; tension in the top slab and compression in the bottom slab of the box girder.
- The shear force capacity of the box girder's webs.

Coupling elements:

- Shear force dowels
- Shock absorbers
- Hinges

4.3. Recalculation of the Zeelandbrug

Structural elements of the Zeelandbrug's box girders have been recalculated once more. This recalculation was done for the structural elements that were previously identified to be potentially critical. In this recalculation, remarks made by TNO have been taken into account. A 30-year remaining service life of the Zeelandbrug has been assumed. The bridge has Consequence Class 3 and the bridge's recalculation complies with the norms RBK 1.1, NEN8700 and NEN8701.

4.3.1. Checks in transverse direction

Initially, the focus is directed towards examining potential critical structural elements in the transverse direction.

Check 1: Moment capacity cantilever

The first calculation is the assessment of the moment capacity of the cantilever. This evaluation is conducted for all of the segment types when looking in the longitudinal direction. This is because the dimensions of the cantilever are the same for all of the segments. Figure 4.5 provides an illustrative depiction of the box girder, highlighting the location of this assessment.

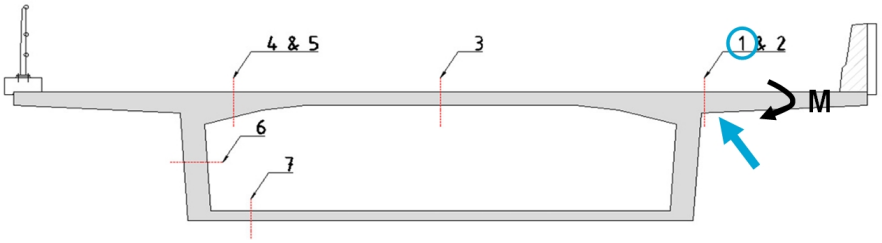

Figure 4.5: Check 1: Moment capacity of the cantilever. Adapted from [5]

The cantilever will experience a bending moment due to the applied load, which includes both permanent loads and variable loads (traffic loads). Figure 4.6 depicts the most critical position of the traffic loads. Considered are Eurocode Load Model 1 (LM1) and Load Model 2 (LM2). Figure 4.6 also illustrates the distribution of the traffic loads over the cantilever in general, assuming an angle of 45 degrees for this distribution.

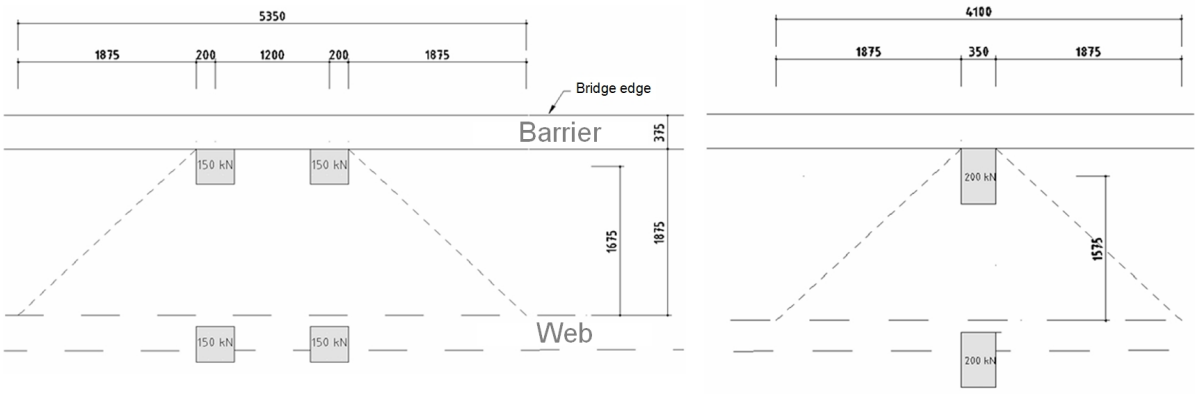

Figure 4.6: Top view of the traffic loads on the cantilever with LM1 (left) and LM2 (right). Adapted from [5]

The weight of the maintenance platform has also been considered for the bending moment capacity of the cantilever. The east tower of the maintenance platform rests on wheel sets, with the driving portal positioned on the bridge's bike lane. The maintenance platform weighs 125 kN, and an additional variable load on the platform has been assumed of 10 kN. This totals 135 kN. It has been conservatively assumed that the entire load will be on the outer wheel. Figure 4.7 illustrates how the load of the maintenance platform is applied and distributed over the cantilever, assuming an angle of 45 degrees.

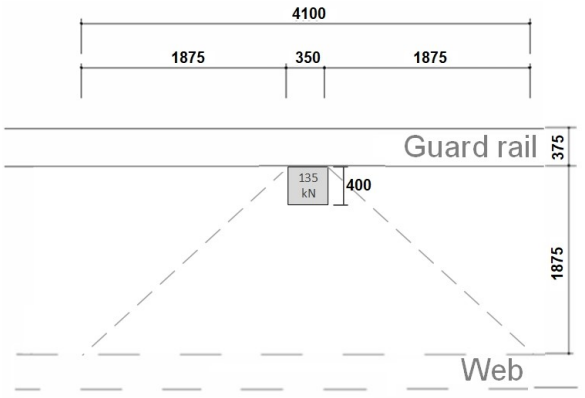

Figure 4.7: Top view of the load from the maintenance platform on the cantilever. Adapted from [5]

Figure 4.8 and Table 4.3 show the reinforcement in the cantilever. Except at location A at the hammerhead, the reinforcement is the same for all segments. Near the joints, additional reinforcement of 5Ø22 has been applied locally. This is because near the joints, load distribution is only possible in one direction. Due to the varying thickness of the cantilever and reinforcement, the most critical location on the cantilever is unknown. Therefore, the moment capacity of the cantilever will be checked at three locations (see Figure 4.8).

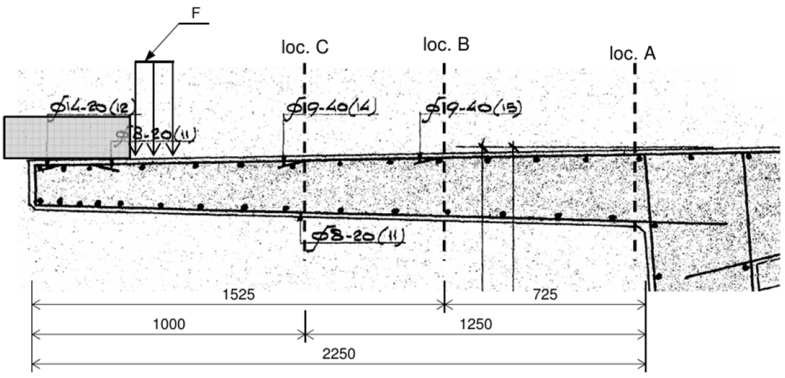

Figure 4.8: Reinforcement in the cantilever [5]

Table 4.3: Reinforcement applied in the cantilever

	Reinforcement QR42	
	General	Near joints
Loc. A	Ø19-400 + Ø19-400 + Ø14-200	+ 5Ø22
Loc. B	Ø19-400 + Ø14-200	+ 5Ø22
Loc. C	Ø14-200	+ 5Ø22

Applied bending moment

The bending moment due to a uniformly distributed load on the cantilever can be calculated as follows.

$$M = q \cdot arm \tag{4.1}$$

where:
M is the bending moment in [kNm/m].
q is the uniformly distributed load in [kN/m].
arm is the arm or distance in [m] from the centroid of the distributed load segment to the point where the bending moment is being calculated.

The bending moment due to a concentrated load on the cantilever can be calculated as follows.

$$M = F \cdot arm \ / \ dist. \tag{4.2}$$

where:
M is the bending moment in [kNm/m].
F is the concentrated load in [kN].
arm is the arm or distance in [m] between the concentrated load and the point where the bending moment is being calculated.
dist. is the distribution length in [m], which represents the length over which the concentrated load is assumed to be spread or distributed at the point where the bending moment is being calculated.

Appendix A provides a detailed description of the calculation for determining the applied bending moments due to both the distributed and concentrated loads on the cantilever at location A. Table 4.4 presents the calculated bending moments at the three different locations on the cantilever. These bending moments occur due to the self-weight of the cantilever, the weight of the barrier and pavement, as well as the uniformly distributed traffic load. For this, Equation 4.1 was used.

Table 4.4: Characteristic value of the bending moment due to a distributed load

	Self weight cantilever			Pavement			Barrier			UDL		
	q [kN/m]	arm [m]	M [kNm/m]	q [kN/m]	arm [m]	M [kNm/m]	q [kN/m]	arm [m]	M [kNm/m]	q [kN/m]	arm [m]	M [kNm/m]
Loc. A	14.5	1.125	16	6.7	0.938	6	9.88	2.25	22	16.9	0.938	16
Loc. B	9.8	0.763	7	4.1	0.575	2	9.88	1.525	15	10.4	0.575	6
Loc. C	6.4	0.5	3	2.2	0.313	1	9.88	1.0	10	5.6	0.313	2

Equation 4.2 has been used to calculate the bending moments that occur due to Load Model 1, Load Model 2 and the maintenance platform, see also Table 4.5. Among these, the highest occurring moments for each location have been highlighted. These will be used to calculate the total applied bending moment and check the cantilever's moment capacity. Near the joints, the distribution length is different. This is because load distribution is only possible in one direction. Hence, the bending moment is checked in general with a normal load distribution as visible in Figure 4.6 and near the joints with a load distribution in one direction.

Table 4.5: Characteristic value of the bending moment due to a concentrated load

		LM1				LM2				Maintenance Platform (MP)			
		F [kN]	arm [m]	dist. [m]	M [kNm/m]	F [kN]	arm [m]	dist. [m]	M [kNm/m]	F [kN]	arm [m]	dist. [m]	M [kNm/m]
General	Loc. A	300	1.675	5.35	**94**	200	1.575	4.1	77	135	1.675	4.1	55
	Loc. B	300	0.95	3.90	**73**	200	0.85	2.65	64	135	0.95	2.65	48
	Loc. C	300	0.425	2.85	**45**	200	0.325	1.6	41	135	0.425	1.6	36
Near joints	Loc. A	300	1.675	3.475	**145**	200	1.575	2.225	142	135	1.675	2.225	102
	Loc. B	300	0.95	2.75	104	200	0.85	1.5	**113**	135	0.95	1.5	86
	Loc. C	300	0.425	2.225	57	200	0.325	0.975	**67**	135	0.425	0.975	59

The design value of the total bending moment (M_{Ed}) is the summation of the individual moments multiplied by their respective load factors, see Equation 4.3. In Table 4.6 the total bending moments are presented that occur in the cantilever at locations A, B and C in general and near the joints as a result of the loading. The Zeelandbrug was built in 1965 and has Consequence Class 3. Then, according to NEN 8700:2011, the following partial load factors are applicable: $\gamma_{F,perm}$ of 1.15 and $\gamma_{F,var}$ of 1.25.

$$M_{Ed} = (M_{cantilever} + M_{pavement} + M_{barrier}) \cdot \gamma_{F,perm} + (M_{UDL} + \max(M_{TS}; M_{MP})) \cdot \gamma_{F,var} \tag{4.3}$$

Table 4.6: Total design bending moment

		M_{Ed} [kNm/m]
General	Loc. A	188
	Loc. B	127
	Loc. C	74
Near joints	Loc. A	252
	Loc. B	177
	Loc. C	101

Bending moment resistance
Having calculated the applied bending moments, the bending moment resistance should now be determined to verify the capacity. In Figure 4.9 the strain and stress diagrams are illustrated. Furthermore, a free body diagram shows the forces acting on the cantilever. Due to the bending moment, there is tension at the top.

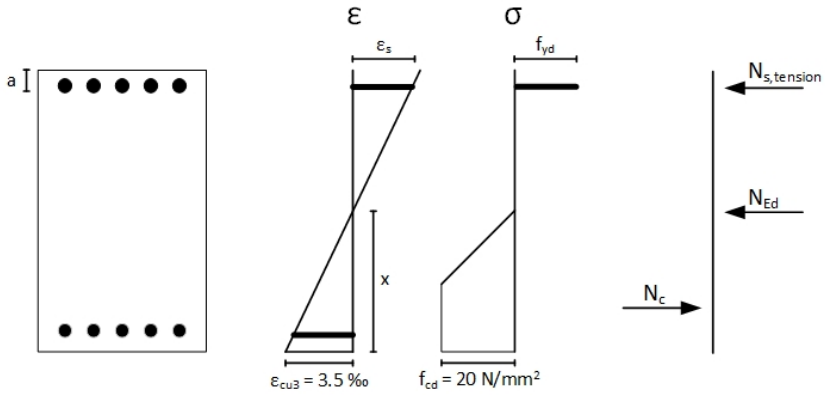

Figure 4.9: Strain and stress diagram with tension at the top and ϵ_c is 3.50 ‰ as moment of failure

The height of the concrete compressive zone can be calculated by ensuring that the sum of the horizontal forces equals zero (see Equation 4.4).

$$\sum H = 0 \tag{4.4}$$

$$N_c - N_{s,tension} - N_{Ed} = 0$$
$$\tfrac{3}{4} \cdot b \cdot x \cdot f_{cd} - A_{s,tension} \cdot f_{yd} - N_{Ed} = 0$$
$$x = \tfrac{N_{Ed} + A_{s,tension} \cdot f_{yd}}{\frac{3}{4} \cdot b \cdot f_{cd}}$$

Subsequently, the moment resistance can be determined by summing the moments around the center (see Equation 4.5).

$$\sum M_{|center} \tag{4.5}$$

$$M_{Rd} = N_c \cdot (\tfrac{1}{2}h - \tfrac{7}{18}x) + N_{s,tension} \cdot (\tfrac{1}{2}h - a)$$

The abbreviations shown represent the following:
M_{Rd} is the design value of the bending moment capacity in [Nmm/mm].
h is the height in [mm].
b is the width in [mm].
x is the height of the concrete compressive zone in [mm].
a is the length from the top surface of the tension zone to the center of gravity of the tensile reinforcement in [mm]. $a = h - d$
d is the effective depth of the reinforced concrete section, which is measured from the top surface of the compression zone to the center of gravity of the tensile reinforcement in [mm].

f_{cd} is the design value of the compressive strength of the concrete in [N/mm^2].
f_{yd} is the design yield strength of the reinforcement in [N/mm^2].
f_{td} is the design working prestress in [N/mm^2].
N_{Ed} is the design normal force due to transverse prestressing in [N]. $N_{Ed} = f_{td} \cdot A_p$
A_p is the area of the prestressing tendons applied in [mm^2].
N_c is the design normal force of the concrete in [N].
$N_{s,tension}$ is the design normal force of the reinforcing steel under tension in [N].
$A_{s,tension}$ is the area of the reinforcement under tension in [mm^2].

For the calculation of the bending moment resistance, certain simplifications have been applied. Firstly, the vertical component of the prestressing force has been neglected. Secondly, the area of the prestressing tendons has not been incorporated into the area of reinforcement under tension, due to the relatively large center-to-center distance of the prestressing tendons.

For the calculation of the moment resistance, a width of 1 m is considered. From the material properties in section 2.3, the following are known:
- $f_{cd} = 20\ N/mm^2$
- $f_{yd} = 300\ N/mm^2$
- $N_{Ed} = f_{td} \cdot A_p = 462 \cdot 935 = 431796\ N/m = 432\ kN/m$
- $f_{td} = 935\ N/mm^2$
- $A_p = 12 \cdot \pi \cdot (Ø/2)^2 = 12 \cdot \pi \cdot (7/2)^2 = 462\ mm^2$

Furthermore, according to remarks made by TNO, the following should be taken into account: a shifted moment line and the anchorage length of the reinforcement. These factors will ultimately result in a decreased area of reinforcement for locations A and B, because the length of the reinforcement at these locations is limited. According to NEN-EN 1992-1-1, the following holds true for the anchorage length of the reinforcement.
$f_{bd} = 2.25 \cdot \eta_1 \cdot \eta_2 \cdot f_{ctd} = 2.25 \cdot 0.7 \cdot 1.0 \cdot 2.0/1.5 = 2.10\ N/mm^2$
$l_{b,rqd} = (Ø/4)(\sigma_{sd}/f_{bd}) = (19/4)(300/2.10) = 679\ mm$
$l_{bd} = \alpha_1\alpha_2\alpha_3\alpha_4\alpha_5 l_{b,rqd} = 1.0 \cdot 0.99 \cdot 1.0 \cdot 1.0 \cdot 1.0 \cdot 679 = 672\ mm$
$\alpha_2 = 1 - 0.15 \cdot (c_d - Ø)/Ø = 1 - 0.15 \cdot (20 - 19)/19 = 0.99-$
where:
f_{bd} is the ultimate bond stress in [N/mm^2] with η's the coefficients related to the reinforcement.
f_{ctd} is the design value of the concrete tensile strength in [N/mm^2].
$l_{b,rqd}$ is the basic required anchorage length in [mm].
σ_{sd} is the design stress of the bar in [N/mm^2] at the position from where the anchorage is measured from.
l_{bd} is the design anchorage length in [mm] with α's and c_d the coefficients related to the reinforcement.

If a shift in the moment line is taken into account, then a lower anchorage length remains. This has been calculated as follows.
Loc. A: $l - (h - c_d - Ø/2) = 725 - (315 - 20 - 19/2) = 439\ mm$
Loc. B: $l - (h - c_d - Ø/2) = (1525 - 1000) - (278 - 20 - 19/2) = 276\ mm$
where:
l is the length of the reinforcement in [mm].
h is the height of the cantilever in [mm].
c_d is the concrete cover to the reinforcement in [mm].
Ø is the diameter of the main reinforcement in [mm].

The decreased anchorage length will result in a lower area of the reinforcement. For locations A and B in general, the area of reinforcement are as follows.
Loc. A: $A_{s,tension} = \frac{\pi \cdot (19/2)^2 \cdot 1000}{400} + \frac{\pi \cdot (14/2)^2 \cdot 1000}{200} + \frac{\pi \cdot (19/2)^2 \cdot 1000}{400} \cdot 439/672 = 1941\ mm^2$
Loc. B: $A_{s,tension} = \frac{\pi \cdot (14/2)^2 \cdot 1000}{200} + \frac{\pi \cdot (19/2)^2 \cdot 1000}{400} \cdot 276/672 = 1061\ mm^2$
Near the joints, additional reinforcement has been applied of 5Ø22, supplementing the existing reinforcement. Substitution of the aforementioned values into Equations 4.4 and 4.5 will yield the height of the concrete compressive zone and subsequently the bending moment resistance.

Unity check
Finally, to evaluate the bending moment capacity, the unity check (U.C.) is calculated through Equation 4.6.

$$U.C. = \frac{M_{Ed}}{M_{Rd}} \tag{4.6}$$

The results are presented in Table 4.7, showing the applied bending moment, moment resistance, and unity check for each location at the box girder's cantilever. Since the hammerhead has less reinforcement at location A, the moment capacity for this segment has been assessed separately, and the results are shown in Table 4.8.

Table 4.7: Unity check moment capacity cantilever

		M_{Ed} [kNm/m]	$A_{s,tension}$ [mm^2]	h [mm]	d [mm]	x [mm]	M_{Rd} [kNm/m]	$U.C.$
General	Loc. A*	192	1941	315	287	65.41	204.98	0.92
	Loc. B	129	1061	278	250	47.81	121.54	1.04
	Loc. C	75	770	251	224	41.98	91.50	0.81
Near joints	Loc. A	255	3842	315	287	103.42	330.67	0.76
	Loc. B	179	2962	278	250	85.82	234.20	0.76
	Loc. C	102	2670	251	224	80.00	192.17	0.53

Table 4.8: *Unity check moment capacity cantilever (segment A, Loc. A)

		M_{Ed} [kNm/m]	$A_{s,tension}$ [mm^2]	h [mm]	d [mm]	x [mm]	M_{Rd} [kNm/m]	$U.C.$
General	Loc. A	192	1851	315	287	63.61	198.59	0.95
Near joints	Loc. A	255	3752	315	287	101.62	325.59	0.77

Conclusion
Hence, in this section calculations were performed to assess the bending moment capacity of the cantilever. The following were taken into account:

- The weight of the pavement.
- For locations A and B, the reduced area of reinforcement steel due to the shifted moment line and anchorage length.
- Less area of reinforcement at location A at the hammerhead.

From the results, it can be found that only location B with a general load distribution has a unity check above 1. This is due to the fact that the area of reinforcement at location B was significantly decreased due to a shifted moment line and anchorage length. On another note, near the joints the bending moment capacity of the cantilever seems very sufficient due to the additional applied reinforcement at these locations.

Check 2: Shear force capacity cantilever
The next step involves evaluating the shear force capacity of the cantilever. This analysis is performed for every segment type along the longitudinal direction because all segments have the same cantilever dimensions. Figure 4.10 illustrates the box girder, indicating the specific location of this assessment.

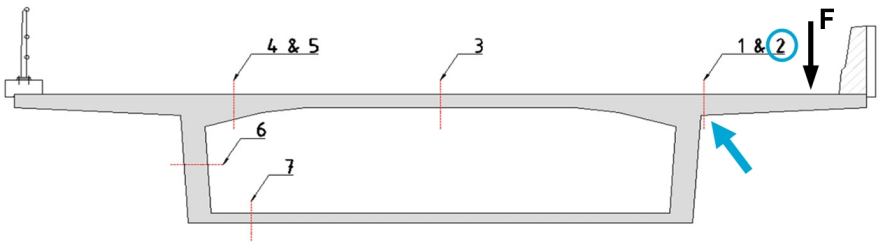

Figure 4.10: Check 2: Shear force capacity of the cantilever. Adapted from [5]

As a result of self-weight and applied traffic loading, the cantilever is subjected to a shear force. Figure 4.11 provides a visual representation of the critical position of the traffic loading [5]. Hence, location A will be assessed for the shear force capacity. Both Eurocode Load Model 1 and Load Model 2 have been considered. A 45-degree angle has been assumed again for the load distribution.

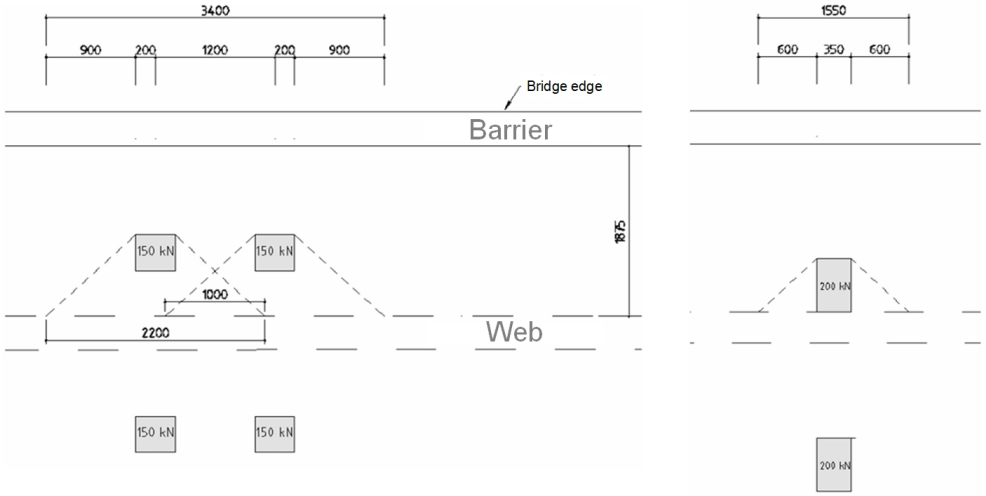

Figure 4.11: Top view of the traffic loads on the cantilever with LM1 (left) and LM2 (right). Adapted from [5]

Applied shear force
The occurring shear force is equal to the self-weight of the cantilever, the weight of the barrier and pavement, as well as the uniformly distributed traffic load. For this, Table 4.4 can be used. Furthermore, the occurring shear force due to traffic can be calculated through Equation 4.7. This is equal to the concentrated traffic load divided by its load distribution. In Table 4.9 the resulting shear force due to Eurocode Load Model 1 and Load Model 2 are presented.

$$V = F \ / \ dist. \tag{4.7}$$

where:
V is the shear force in [kN/m].
F is the concentrated load in [kN].
dist. is the distribution length in [m], which represents the length over which the concentrated load is assumed to be spread or distributed at the point where the shear force is being calculated.

Table 4.9: Characteristic value of the shear force

	LM1			LM2		
	F [kN]	dist. [m]	V [kN/m]	F [kN]	dist. [m]	V [kN/m]
General	150 | 150	2.2 | 2.2	**136**	200	1.55	129
Near joints	150 | 150	2.2 | 1.30	**184**	200	1.14	175

The design value of the total occurring shear force (V_{Ed}) is the summation of the individual forces multiplied by their respective load factors, see Equation 4.8. In Table 4.10 the total shear forces are presented that occur in the cantilever at location A in general and near the joints.

$$V_{Ed} = (V_{cantilever} + V_{pavement} + V_{barrier}) \cdot \gamma_{F,perm} + (V_{UDL} + \max(V_{TS})) \cdot \gamma_{F,var} \tag{4.8}$$

Table 4.10: Total design shear force

	V_{Ed} [kN/m]
General	227
Near joints	286

Shear force resistance
With the occurring shear forces calculated, the next step is to calculate the shear force resistance in order to check the capacity. The shear force resistance can be calculated according to RBK 1.2.1. The formula is given in Equation 4.9.

$$V_{Rd,c} = [0.12 \cdot k_{cap} \cdot k \cdot (100 \cdot \rho_l \cdot fck)^{(1/3)} + 0.15 \cdot \sigma_{cp}] \cdot b_w \cdot d \geq [v_{min} + 0.15 \cdot \sigma_{cp}] \cdot b_w \cdot d \tag{4.9}$$

where:
$V_{Rd,c}$ is the design shear capacity of the concrete in [N].
k_{cap} is 1.0 -.
k is the size effect factor, with d in [mm]. $k = 1 + \sqrt{\frac{200}{d}} \leq 2.0$.
d is the effective depth to the main flexural reinforcement in [mm].
ρ_l is the flexural reinforcement ratio. $\rho_l = \frac{A_{sl}}{b_w \cdot d}$.
A_{sl} is the area of reinforcement in [mm^2].
f_{ck} is the characteristic cylinder compressive strength of the concrete in [N/mm^2].
F_p is the working prestress force in [N].
σ_{cp} is the compressive stress in the concrete from axial load or prestressing [N/mm^2]. $\sigma_{cp} = \frac{F_p}{b_w \cdot h}$.
b_w is the smallest width of the cross-section in the tensile area in [mm].
v_{min} is $0.035 \cdot k_b \cdot k_h \cdot k_{cap}^{\frac{3}{2}} \cdot f_{ck}^{\frac{1}{2}}$.
k_b is 1.25 for smooth steel and 1.00 for ribbed steel.
k_h is $4.2 \cdot e^{-d/800} \leq 3.4$.

For the calculation of the shear force resistance, a width of 1 m is considered. From the material properties in section 2.3, the following are known:
- $d = h - c_d - \emptyset/2 = 315 - 20 - 19/2 = 285.5\ mm$
- $k = 1 + \sqrt{\frac{200}{285.5}} = 1.84-$
- General: $A_{sl} = 2 \cdot \frac{\pi \cdot (19/2)^2 \cdot 1000}{400} + \frac{\pi \cdot (14/2)^2 \cdot 1000}{200} = 2187\ mm^2$
- Near joints: $A_{sl} = 2187 + 5 \cdot \pi \cdot (22/2)^2 = 4088\ mm^2$
- General: $\rho_l = \frac{2187}{1000 \cdot 285.5} = 0.0077-$
- Near joints: $\rho_l = \frac{4088}{1000 \cdot 285.5} = 0.014-$
- $f_{ck} = 30 N/mm^2$

- $F_p = 432\ kN/m$
- $\sigma_{cp} = \frac{432 \cdot 10^3}{1000 \cdot 315} = 1.37\ N/mm^2$
- $v_{min} = 0.035 \cdot 1.0 \cdot 4.2 \cdot e^{-285.5/800} \cdot 1.0 \cdot 30^{1/2} = 0.56\ N/mm^2$

Substitution of the values obtained into Equation 4.9 yields the shear force resistance.

Unity check

To assess the shear force capacity, the unity check (U.C.) is calculated through Equation 4.10.

$$U.C. = \frac{V_{Ed}}{V_{Rd}} \tag{4.10}$$

Finally, in Table 4.11 the applied shear force, shear force resistance and unity check are presented for the cantilever of the box girders.

Table 4.11: Unity check shear force capacity cantilever

	V_{Ed} [kN/m]	V_{Rd} [kN/m]	$U.C.$
General	229	238	0.96
Near joints	288	279	1.03

Conclusion

For the evaluation of the cantilever's shear force capacity the weight of the pavement was also taken into account. It can be observed that the applied shear force near the joints exceeds the shear force resistance. However, this is only a slight surpassing.

Check 3: Moment capacity top slab at midspan
The third calculation is the assessment of the moment capacity of the box girder's midspan. This evaluation is conducted for segment type D when looking in the longitudinal direction. Figure 4.12 highlights the position of this assessment of the box girder.

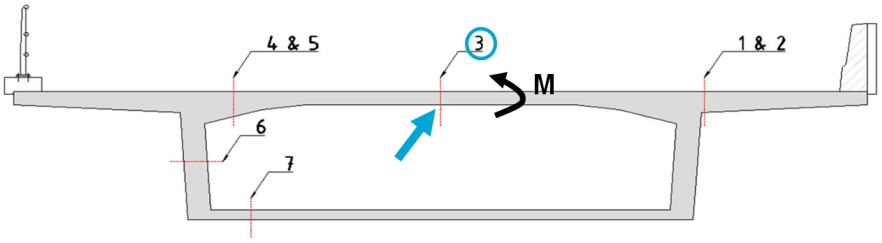

Figure 4.12: Check 3: Moment capacity of the box girder's top slab at midspan. Adapted from [5]

Applied bending moment
The applied bending moment induces tension at the bottom and compression at the top of the box girder's top slab. To determine the specific bending moment experienced by the top slab of the box girder at midspan, the outcomes of the model by Iv-Infra were utilised [5]. In transverse direction, the box girder was modelled based on the dimensions characteristic of a segment type D box girder center. Various load cases were integrated into the model. These include the self-weight of the cantilever, the load exerted by the pavement and the uniformly distributed traffic load. Moreover, the bending moment resulting from the load imposed by the Tandem System of Eurocode Load Model 1 was determined. Through summation, the total applied bending moment in the box girder's top slab at midspan could be calculated. The total bending moment was found to be equal to 69 kNm/m [5].

Bending moment resistance
To assess the moment capacity, the bending moment resistance should also be determined. In Figure 4.13 the relevant strain, stress and free body diagrams are illustrated.

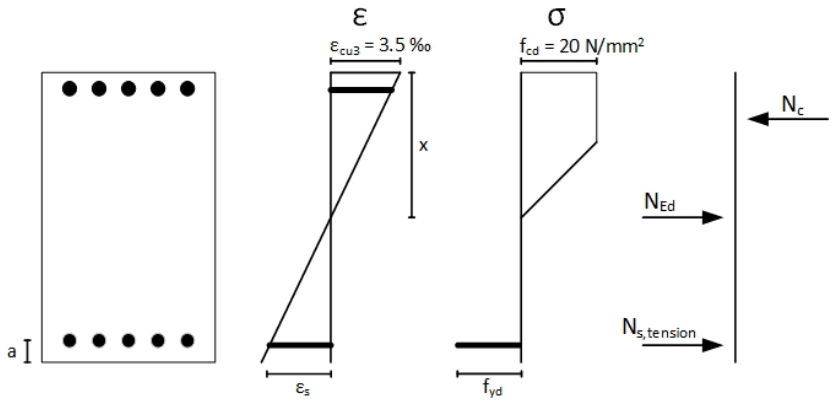

Figure 4.13: Strain and stress diagram with tension at the bottom and ϵ_c is 3.50 ‰ as moment of failure

As previously described, the height of the concrete compressive zone and the bending moment resistance can be calculated by the summation of the horizontal forces and moments.

$$\sum H = 0$$
$$N_c - N_{s,tension} - N_{Ed} = 0$$
$$\frac{3}{4} \cdot b \cdot x \cdot f_{cd} - A_{s,tension} \cdot f_{yd} - N_{Ed} = 0$$
$$x = \frac{N_{Ed} + A_{s,tension} \cdot f_{yd}}{\frac{3}{4} \cdot b \cdot f_{cd}}$$

$$\sum M_{|center}$$
$$M_{Rd} = N_c \cdot (\tfrac{1}{2}h - \tfrac{7}{18}x) + N_{s,tension} \cdot (\tfrac{1}{2}h - a)$$

The abbreviations shown represent the following:
h is the height in [mm].
b is the width in [mm].
x is the height of the concrete compressive zone in [mm].
a is the length from the top surface of the tension zone to the center of gravity of the tensile reinforcement in [mm]. $a = h - d$
d is the effective depth of the reinforced concrete section, which is measured from the top surface of the compression zone to the center of gravity of the tensile reinforcement in [mm].
f_{cd} is the design value of the compressive strength of the concrete in [N/mm^2].
f_{yd} is the design yield strength of the reinforcement in [N/mm^2].
f_{td} is the design working prestress in [N/mm^2].
N_{Ed} is the design normal force due to transverse prestressing in [N]. $N_{Ed} = f_{td} \cdot A_p$
A_p is the area of the prestressing tendons applied in [mm^2/m].
N_c is the design normal force of the concrete in [N].
$N_{s,tension}$ is the design normal force of the reinforcing steel under tension in [N].
$A_{s,tension}$ is the area of the reinforcement under tension in [mm^2].

For the calculation of the moment resistance, a width of 1 m is considered. From the material properties in section 2.3, the following are known:
- $h = 200\ mm$
- $d = 152\ mm$
- $a = 200 - 152 = 48\ mm$
- $f_{cd} = 20\ N/mm^2$
- $f_{yd} = 300\ N/mm^2$
- $N_{Ed} = f_{td} \cdot A_p = 462 \cdot 935 = 431796\ N/m = 432\ kN/m$
- $f_{td} = 935\ N/mm^2$
- $A_p = 12 \cdot \pi \cdot (Ø/2)^2 = 12 \cdot \pi \cdot (7/2)^2 = 462\ mm^2$

The area of the prestressing tendons can be combined with the area of the reinforcement subjected to tension. The Freyssinet prestressing is applied as 12Ø7, resulting in a prestressing area of 462 mm^2. To account for this in the reinforcement area, the prestressing has been converted to a reinforcement configuration of Ø24.2-1000.
- $A_{s,tension} = \frac{\pi \cdot (10/2)^2 \cdot 1000}{200} + \frac{\pi \cdot (24.2/2)^2 \cdot 1000}{1000} = 853\ mm^2$

Substitution of the values obtained into Equations 4.4 and 4.5 yields the bending moment resistance.

As described in subsection 2.2.5, which outlines the reinforcement details, it is noted that there is an exception regarding five T-frames. Specifically, these five T-frames have external prestressing applied at segment type D. This is due to a possible variation in the positioning of the transverse prestressing. TNO describes the way to predict the effect of this on the bending moment capacity [6].

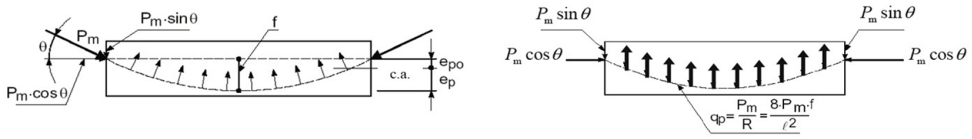

Figure 4.14: Curvature pressure due to curved tendons [15]

where:
q_p is the curvature pressure which is a uniformly distributed load in [kN/m]. $q_p = \frac{8 \cdot P_m \cdot f}{L^2}$
P_m is the axial compressive force due to prestressing in [kN].
f is the drape of the tendons in [m].
L is the slab length in [m].
e_p is the eccentricity of the prestressing tendons at midspan to the centroidal axis of the concrete section in [m].

In Figure 4.14 the curvature pressure and compressive force resulting from the application of prestressing are visualised. The axial compressive force P_m due to the external prestressing applied can be

calculated as follows.
$P_m = A_p \cdot f_{td} = 4 \cdot \pi \cdot (7/2)^2 \cdot 935/0.9/1000 = 159.92\ kN/m$
For these five T-frames where external prestressing is applied, the transverse prestressing has deviant positions. Namely, from the original design it was found that the distance between the center of the transverse prestressing and the underside of the deck is locally 122.8 mm. This positioning, along with the additional external prestressing applied, results in a moment resistance of 70.81 kNm/m. Additionally, the moment due to the negative curvature pressure from the transverse prestressing can be taken into account.
$M_{curv-} = -P_m \cdot e_p = -A_p \cdot f_{td} \cdot e_p = -462 \cdot 935 \cdot (122.8 - 100) \cdot 10^{-6} = -9.85\ kNm/m$
Similarly, the moment due to the positive curvature pressure from the external prestressing can be taken into account.
$M_{curv+} = P_m \cdot e_p = 159.92 \cdot 0.1 = 15.99\ kN/m$
The total moment resistance is the bending moment resistance adjusted for the negative curvature pressure from the transverse prestressing and increased by the positive curvature pressure from the external prestressing.
$M_{Rd} = 70.81 + M_{curv-} + M_{curv+} = 70.81 - 9.85 + 15.99 = 76.95\ kNm/m$

Unity check
The unity check (U.C.) is calculated through Equation 4.6 to evaluate the bending moment capacity.

$$U.C. = \frac{M_{Ed}}{M_{Rd}}$$

Ultimately, Table 4.12 shows the applied bending moment, the moment resistance and the unity check for the top slab of the box girder at midspan.

Table 4.12: Unity check moment capacity of box girder's top slab at midspan

	M_{Ed} [kNm/m]	$A_{s,tension}$ [mm^2]	h [mm]	x [mm]	M_{Rd} [kNm/m]	$U.C.$
Standard	69	853	200	45.85	69.81	0.99
With external prestressing	69	853	200	55.70	76.95	0.96

Conclusion
Thus, in evaluating the bending moment at midspan at the top slab, consideration has been given to five T-frames with incorrectly positioned transverse prestressing and their negative curvature effect. Consequently, the applied external prestressing intended to correct this has also been taken into account, along with their positive curvature effect. In conclusion, Table 4.12 shows that both the standard T-frames and those with external prestressing have a marginal bending moment resistance to withstand the applied bending moments.

Check 4: Shear force capacity top slab
The fourth check is the evaluation of the top slab of the box girder's shear force capacity. In longitudinal direction, this evaluation is conducted for segment type D. Figure 4.12 highlights where the evaluation of the box girder is located in transverse direction.

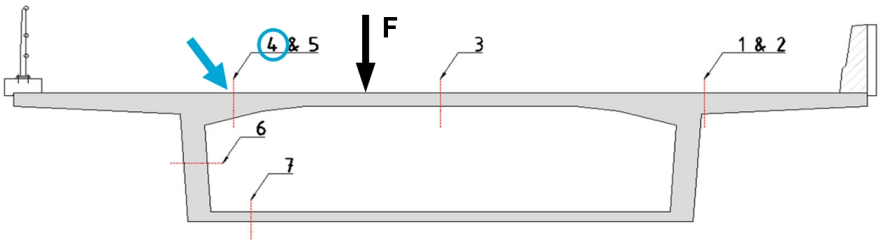

Figure 4.15: Check 4: Shear force capacity of the box girder's top slab. Adapted from [5]

To check the shear force capacity of the top slab, two locations (A and B) will be assessed. Figure 4.16 illustrates these locations.

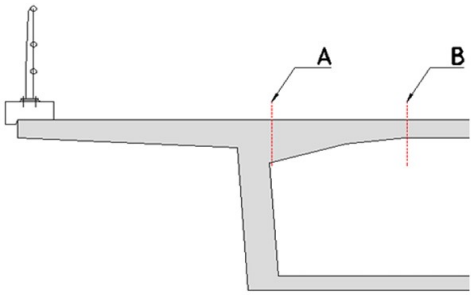

Figure 4.16: Check 4: Locations A and B on the box girder's top slab [5]

Based on the reinforcement properties detailed in subsection 2.2.5, the reinforcement applied in locations A and B is known, see Table 4.13.

Table 4.13: Reinforcement applied in the box girder's top slab at locations A and B

	Reinforcement QR42
Loc. A	Ø19-400 + Ø16-400 + Ø14-200
Loc. B	Ø16-400 + Ø8-400

Applied shear force
The outcomes of the model by Iv-Infra based on the box girder segment type D were used [5]. The applied shear force was found by including the cantilever's self-weight, the pavement and the uniformly distributed traffic load. Moreover, the highest applied shear force resulting from the Tandem System of Eurocode Load Model 1 was found. This was done by shifting the position of the Tandem System on the bridge. Through summation, the total applied shear force in the box girder's top slab could be calculated. At location A this is equal to 258 kN/m and at location B to 169 kN/m [5].

Shear force resistance
To verify the capacity, the shear force resistance should be computed. RBK 1.2.1 can be used again to compute the shear force resistance through Equation 4.9.

$$V_{Rd,c} = [0.12 \cdot k_{cap} \cdot k \cdot (100 \cdot \rho_l \cdot fck)^{(1/3)} + 0.15 \cdot \sigma_{cp}] \cdot b_w \cdot d \geq [v_{min} + 0.15 \cdot \sigma_{cp}] \cdot b_w \cdot d$$

where:
$V_{Rd,c}$ is the design shear capacity of the concrete in [N].
k_{cap} is 1.0 -.

k is the size effect factor, with d in [mm]. $k = 1 + \sqrt{\frac{200}{d}} \leq 2.0$.
d is the effective depth to the main flexural reinforcement in [mm].
ρ_l is the flexural reinforcement ratio. $\rho_l = \frac{A_{sl}}{b_w \cdot d}$.
A_{sl} is the area of reinforcement in [mm^2].
f_{ck} is the characteristic cylinder compressive strength of the concrete in [N/mm^2].
F_p is the working prestress force in [N].
F_{top} is the superimposed, axial load in the top slab in [N].
σ_{cp} is the compressive stress in the concrete from axial load or prestressing [N/mm^2]. $\sigma_{cp} = \frac{F_p + F_{top}}{b_w \cdot h}$.
b_w is the smallest width of the cross-section in the tensile area in [mm].
v_{min} is $0.035 \cdot k_b \cdot k_h \cdot k_{cap}^{\frac{3}{2}} \cdot f_{ck}^{\frac{1}{2}}$.
k_b is 1.25 for smooth steel and 1.00 for ribbed steel.
k_h is $4.2 \cdot e^{-d/800} \leq 3.4$.

For the calculation of the shear force resistance, a width of 1 m is considered. From the material properties in section 2.3, the following are known:
Location A:
- $d = h - c_d - Ø/2 = 480 - 20 - 10 = 450\ mm$
- $k = 1 + \sqrt{\frac{200}{450}} = 1.67-$
- $A_{sl} = \frac{\pi \cdot (19/2)^2 \cdot 1000}{400} + \frac{\pi \cdot (16/2)^2 \cdot 1000}{400} + \frac{\pi \cdot (14/2)^2 \cdot 1000}{200} = 1981\ mm^2$
- $\rho_l = \frac{1981}{1000 \cdot 450} = 0.0044-$
- $f_{ck} = 30\ N/mm^2$
- $F_p = 432\ kN/m$
- $F_{top} = 99\ kN/m$ according to Iv-Infra [5].
- $\sigma_{cp} = \frac{432 \cdot 10^3 + 99 \cdot 10^3}{1000 \cdot 480} = 1.1\ N/mm^2$
- $v_{min} = 0.035 \cdot 1.0 \cdot 4.2 \cdot e^{-450/800} \cdot 1.0 \cdot 30^{1/2} = 0.46\ N/mm^2$

Location B:
- $d = h - c_d - Ø/2 = 200 - 20 - 10 = 170\ mm$
- $k = 1 + \sqrt{\frac{200}{170}} = 2.08- \ \rightarrow k = 2.0-$
- $A_{sl} = \frac{\pi \cdot (16/2)^2 \cdot 1000}{400} + \frac{\pi \cdot (8/2)^2 \cdot 1000}{400} = 628\ mm^2$
- $\rho_l = \frac{628}{1000 \cdot 170} = 0.0037-$
- $f_{ck} = 30\ N/mm^2$
- $F_p = 432\ kN/m$
- $F_{top} = 99\ kN/m$ according to Iv-Infra [5].
- $\sigma_{cp} = \frac{432 \cdot 10^3 + 99 \cdot 10^3}{1000 \cdot 200} = 2.7\ N/mm^2$
- $v_{min} = 0.035 \cdot 1.0 \cdot 4.2 \cdot e^{-170/800} \cdot 1.0 \cdot 30^{1/2} = 0.65\ N/mm^2$

Substitution of the values obtained into Equation 4.9 yields the shear force resistance.

In Figure 4.14, the curvature pressure resulting from the tendon curvature is illustrated. This illustration hypothesises the external prestressing that was applied in five T-frames. The curvature pressure introduces an additional shear force at location B. TNO describes a method to predict its impact on the shear force capacity [6]. The additional shear force can be calculated as follows.
$V_{Ed,curv} = 0.5 \cdot q_p \cdot L = 0.5 \cdot (8 \cdot P_m \cdot f/L^2) \cdot L = 0.5 \cdot (8 \cdot 160 \cdot 0.1/3.48^2)/3.48 = 18.4\ kN$
The applied shear force is increased by the addition of this supplementary force to the existing shear force. Similarly, the shear force resistance can be increased by incorporating an additional resistance found due to the applied external prestressing.
$V_{Rd,curv} = 0.15 \cdot (P_m/(b \cdot h)) \cdot b \cdot d = 0.15 \cdot (160/(200 \cdot 1000)) \cdot 170 \cdot 1000 = 20.4\ kN$

Unity check
The shear force capacity is assessed by calculating the unity check (U.C.) through Equation 4.10.

$$U.C. = \frac{V_{Ed}}{V_{Rd}}$$

The applied shear force, shear force resistance and unity check are presented in Table 4.14 for the box girder's top slab.

Table 4.14: Unity check shear force capacity of box girder's top slab

		V_{Ed} [kN/m]	V_{Rd} [kN/m]	$U.C.$
Standard	Loc. A	258	287	0.90
	Loc. B	169	159	1.07
With external prestressing	Loc. B	187	179	1.05

Conclusion
For the box girder's top slab, similar to the evaluation of the bending moment capacity, the evaluation of the shear force capacity also considers the five T-frames with external prestressing. Namely, the external prestressing increases the shear force resistance but also introduces an additional shear force at location B. As indicated by the results, all T-frames have a unity check at location B that exceeds 1. One possible explanation is the critical nature of location B, as depicted in Figure 4.16, which shows its proximity to the web despite its small thickness of 200 mm.

Check 6: Moment capacity webs (tension outer side)
Check number 6 involves assessing the moment capacity of the box girder's webs under applied moments inducing tension on the outer side of the webs. Figure 4.17 illustrates the location of this assessment in the transverse direction of the box girder. In the longitudinal direction, this evaluation is conducted at cross-sections 5 and 11, located in segment types B and D, respectively (see Figure 4.18).

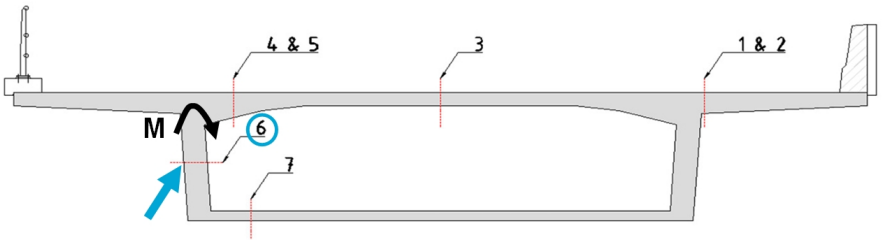

Figure 4.17: Check 6: Moment capacity of the box girder's webs. Adapted from [5]

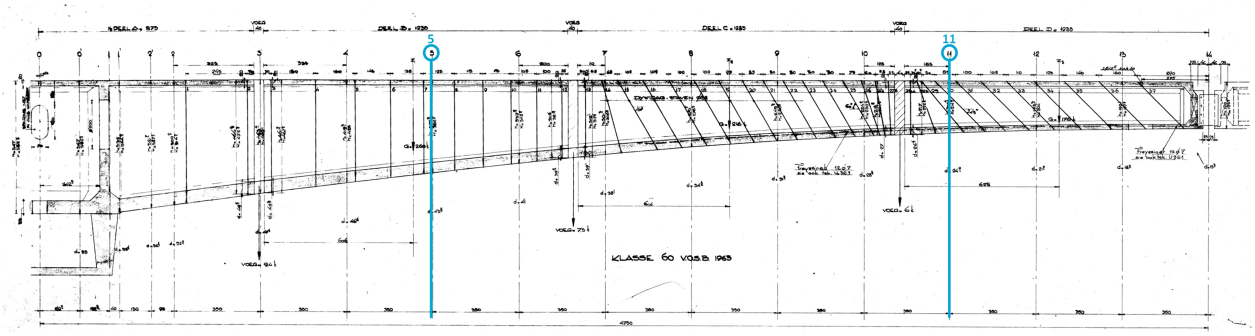

Figure 4.18: Check 6: Cross-sections 5 and 11 in the longitudinal section of the Zeelandbrug. Modified [NZC-78].

The diameter and center-to-center distance of the applied soft steel reinforcement vary across different cross-sections. Additionally, the center-to-center distance of the Dywidag bars changes along the longitudinal section of the structure. Iv-Infra predicts that cross-sections 5 and 11 could be critical [5]. This prediction is due to the relatively high center-to-center distance of the Dywidag bars in cross-section 5, and the low amount of soft steel reinforcement combined with the angle of the Dywidag bars in cross-section 11. Therefore, in this recalculation cross-sections 5 and 11 will be checked as well. The soft steel reinforcement applied in cross-sections 5 and 11 are given in Table 4.15. Regarding the prestressing, the Dywidag bars are also essential for enhancing the shear force capacity of the webs in longitudinal direction. According to Iv-Infra, approximately 50% of the Dywidag bars' capacity contribute to the moment capacity in the transverse direction, while the remaining 50% enhances the shear force capacity in the longitudinal direction of the webs [5].

Table 4.15: Reinforcement applied in the box girder's webs at cross-sections 5 and 11

	Reinforcement QR42
Cross-section 5	Ø22-400 + Ø19-400
Cross-section 11	Ø19-400 + Ø16-400

Applied bending moment
The outcomes of the Iv-Infra model based on the box girder segment type D were utilised [5]. For cross-sections 5 and 11, the web thickness is greater than the web thickness employed in the model. Consequently, the applied moment due to the Tandem System was slightly increased compared to the model's outcome. This outcome corresponds to the highest applied bending moment resulting from the Tandem System of Eurocode Load Model 1. This was achieved by repositioning the Tandem System on the bridge. Additionally, the applied bending moment was calculated by considering the cantilever's

self-weight, the pavement, and the uniformly distributed traffic load. The total applied bending moment in the box girder's webs was then determined by summing these contributions. At cross-sections 5 and 11, this results in a bending moment of 163 kNm/m [5].

Bending moment resistance
Subsequently, the bending moment resistances have been determined. The relevant strain, stress and free body diagram are shown in Figure 4.19.

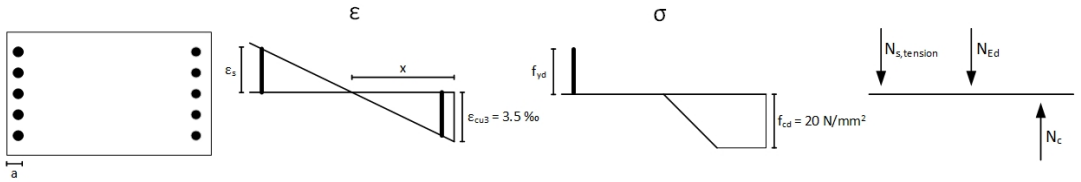

Figure 4.19: Strain and stress diagram with tension left and ϵ_c is 3.50 ‰ as moment of failure

As previously mentioned, by summing the horizontal forces and the moments, the height of the concrete compressive zone and the bending moment resistance can be calculated.

$$\sum H = 0$$
$$N_c - N_{s,tension} - N_{Ed} = 0$$
$$\tfrac{3}{4} \cdot b \cdot x \cdot f_{cd} - A_{s,tension} \cdot f_{yd} - N_{Ed} = 0$$
$$x = \tfrac{N_{Ed} + A_{s,tension} \cdot f_{yd}}{\frac{3}{4} \cdot b \cdot f_{cd}}$$

$$\sum M_{|center}$$
$$M_{Rd} = N_c \cdot (\tfrac{1}{2}h - \tfrac{7}{18}x) + N_{s,tension} \cdot (\tfrac{1}{2}h - a)$$

The abbreviations shown represent the following:
h is the height in [mm].
b is the width in [mm].
x is the height of the concrete compressive zone in [mm].
a is the length from the top surface of the tension zone to the center of gravity of the tensile reinforcement in [mm]. $a = h - d$
d is the effective depth of the reinforced concrete section, which is measured from the top surface of the compression zone to the center of gravity of the tensile reinforcement in [mm].
f_{cd} is the design value of the compressive strength of the concrete in [N/mm^2].
f_{yd} is the design yield strength of the reinforcement in [N/mm^2].
f_{pd} is the design tensile strength in [N/mm^2].
N_{Ed} is the design normal force due to transverse prestressing in [N]. $N_{Ed} = f_{pd} \cdot A_p$
A_p is the area of the prestressing tendons applied in [mm^2/m].
N_c is the design normal force of the concrete in [N].
$N_{s,tension}$ is the design normal force of the reinforcing steel under tension in [N].
$A_{s,tension}$ is the area of the reinforcement under tension in [mm^2].

For the calculation of the moment resistance, a width of 1 m is considered. From the material properties in section 2.3, the following are known:
Cross-section 5:
- $h = 380\ mm$
- $d = 340\ mm$
- $a = 380 - 340 = 40\ mm$
- $f_{cd} = 20\ N/mm^2$
- $f_{yd} = 300\ N/mm^2$
- $N_{Ed} = 0\ kN/m$
- $A_{s,tension} = \frac{\pi \cdot (22/2)^2 \cdot 1000}{400} + \frac{\pi \cdot (19/2)^2 \cdot 1000}{400} = 1659\ mm^2$

Cross-section 11:
- $h = 352\ mm$
- $d = 298\ mm$
- $a = 352 - 298 = 54\ mm$
- $f_{cd} = 20\ N/mm^2$
- $f_{yd} = 300\ N/mm^2$
- $N_{Ed} = f_{pd} \cdot A_p = 713 \cdot 285 = 202738\ N/m = 203\ kN/m$
- $f_{pd} = 713\ N/mm^2$
- $A_p = \frac{\pi \cdot (32/2)^2 \cdot 1000}{1000} \cdot 50\% \cdot sin(45) = 285\ mm^2$

It is possible to combine the prestressing tendon area with the tensioned reinforcement area. The Dywidag prestressing is applied as Ø32-1000. Since the Dywidag bars contribute only 50% to the moment capacity and are positioned at an angle of approximately 45 degrees, the effective prestressing area is 285 mm^2. To account for this in the reinforcement area, the prestressing has been converted to a reinforcement configuration of Ø32-2820.
- $A_{s,tension} = \frac{\pi \cdot (19/2)^2 \cdot 1000}{400} + \frac{\pi \cdot (16/2)^2 \cdot 1000}{400} + \frac{\pi \cdot (32/2)^2 \cdot 1000}{2820} = 1495\ mm^2$

Substitution of the values obtained into Equations 4.4 and 4.5 yields the bending moment resistance.

Unity check
The unity check (U.C.) to evaluate the bending moment capacity is calculated through Equation 4.6.

$$U.C. = \frac{M_{Ed}}{M_{Rd}}$$

Table 4.16 demonstrates the applied bending moment, the moment resistance and the unity check for the box girder's webs with tension on the outer side.

Table 4.16: Unity check moment capacity of box girder's webs (tension outer side)

	M_{Ed} [kNm/m]	$A_{s,tension}$ [mm2]	h [mm]	d [mm]	x [mm]	M_{Rd} [kNm/m]	$U.C.$
Cross-section 5	163	1659	380	340	33.18	162.81	1.00
Cross-section 11	163	1495	352	298	43.41	158.32	1.03

Conclusion
In this check, it was considered that the Dywidag bars have a lower design yield point f_{pd}. The design yield point f_{pd} of the Dywidag bars was assumed to be 713 N/mm^2, as specified by TNO [6]. Notably, the contribution of the Dywidag bars was only considered for cross-section 11, thereby influencing only this bending moment capacity. The results reveal a unity check value of 1 at cross-section 5, which can be attributed to the exclusion of the Dywidag bar contribution due to their substantial center-to-center spacing. Conversely, cross-section 11 has a unity check that slightly exceeds 1, despite having a closer spacing of the Dywidag bars. This means that the influence of the Dywidag bars' prestressing in cross-section 11 were taken into account. Nevertheless, cross-section 11 has less soft steel reinforcement and the contribution of the prestressing was restricted to 50% of their capacity, as the other 50% was allocated for the longitudinal shear force capacity.

4.3.2. Checks in longitudinal direction

After completing the checks in transverse direction to analyse potential critical structural elements, this assessment will proceed longitudinally. In these checks, the additional shear forces identified by the Finite Element Model (model with supports) will be incorporated due to a support settlement of 100 mm and a lower and upper bound of 5 and 200 mm.

Check 8: Moment capacity top and bottom slab (tension top slab)

In check number 8, the moment capacity of both the top and bottom slabs of the box girder are assessed in the longitudinal direction. The loads acting on the bridge could induce a moment that results in tension in the top slab and compression in the bottom slab. Figure 4.20 depicts the locations of this assessment along the longitudinal direction of the bridge. This evaluation is carried out at four cross-sections: adjacent to the support and at the construction joints between the segment types within a cantilever, as illustrated in Figure 4.21.

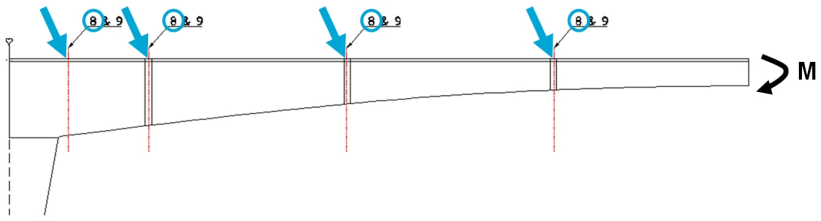

Figure 4.20: Check 8: Moment capacity of the box girder's top and bottom slab. Adapted from [5]

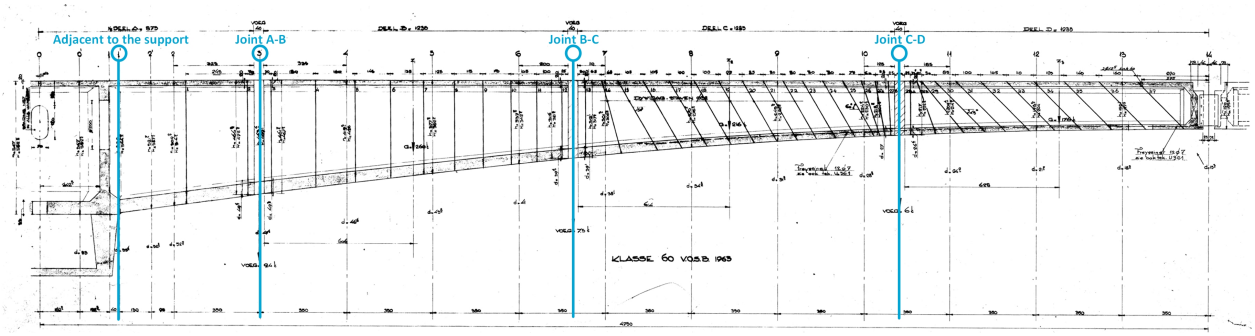

Figure 4.21: Check 8: Cross-sections in the longitudinal section of the Zeelandbrug. Modified [NZC-78].

Applied bending moment

The outcomes of the Iv-Infra model were utilised to find the maximum occurring bending moment [5]. The Iv-Infra model for the longitudinal direction consists of five T-frames of the Zeelandbrug. Within this model, various load cases were implemented incorporating different configurations of the uniformly distributed traffic load and the Tandem System of Eurocode Load Model 1. Ultimately, the applied bending moment is the cumulative result of the bending moments due to the self-weight, the barrier, the pavement, the Tandem System, the uniformly distributed traffic load and the braking force. Table 4.17 presents these total maximum bending moments that are applied at the construction joints and adjacent to the support.

Table 4.17: Total design bending moment [5]

	M_{Ed} [MNm]
Adjacent to the support	317
Joint A-B	269
Joint B-C	126
Joint C-D	38

It should be noted that the influence of torsion resulting from the eccentricity of the traffic loads has been neglected. According to Iv-Infra, this is omission is deemed acceptable since the traffic loads have a significantly small contribution compared to the permanent loads [5].

Operative forces
Figure 4.22 depicts a free body diagram illustrating the distribution of forces due to the applied moment resulting in tension in the top slab and compression in the bottom slab. Figure 4.22 shows an additional tension force in the top slab due to shear forces from the webs. This check aims to determine if the prestressing force in the top slab is adequate to resist the tension induced by the bending moment. Additionally, this check evaluates whether the compressive stress in the bottom slab, resulting from the bending moment, remains within acceptable limits.

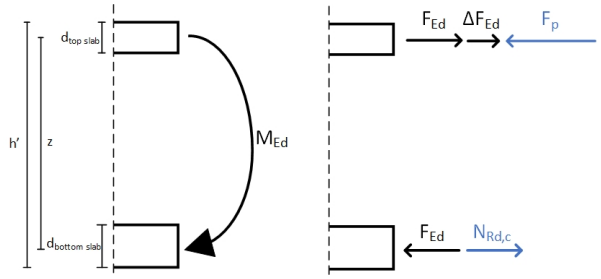

Figure 4.22: Free body diagram of the box girder's top and bottom slab

Top slab
To determine if the prestressing force in the top slab is sufficient to resist the tension induced by the bending moment, the normal force caused by the bending moment should first be calculated. This can be done using Equation 4.11.

$$F_{Ed} = M_{Ed}/z \tag{4.11}$$

where:
F_{Ed} is the design value of the normal force resulting from the applied bending moment in [MN].
M_{Ed} is the design value of the applied bending moment in [MNm].
z is the the effective arm between the line of action of the tension force and the line of action of the compressive force in [m]. $z = h' - (d_{top\ slab} + d_{bottom\ slab})/2$
h' is the height from the top of the top slab to the bottom of the bottom slab in [m].
$d_{top\ slab}$ is the thickness of the top slab in [m].
$d_{bottom\ slab}$ is the thickness of the bottom slab in [m].

The additional force due to shear forces from the webs can be calculated with Equation 4.12.

$$\Delta F_{Ed} = (V_{Ed} + V_{sett}) \cdot a_L/z \tag{4.12}$$

where:
ΔF_{Ed} is the additional force due to shear forces from the webs in [MN].
V_{Ed} is the design value of the occurring shear force in [MN].
V_{sett} is the shear force due to a settlement of a pier in [MN], see Tables 3.3 and 3.5.
a_L is the distance of the shift of the moment curve in [m]. $a_L/z = (\cot(\theta) - \cot(\alpha))/2$
θ is the angle between the concrete compressive strut and the beam axis perpendicular to the shear force in [deg].
α is the angle between shear reinforcement and the beam axis perpendicular to the shear force (measured positive) in [deg].

The prestressing force of a single tendon can be computed through Equation 4.13.

$$F_p = f_{pd,20\%} \cdot A_p \tag{4.13}$$

where:
F_p is the prestressing force of a single tendon in [N].
$f_{pd,20\%}$ is the design tensile strength with a prestress loss accounted for of 20% in [N/mm^2].
A_p is the area of the prestressing tendon applied in [mm^2].

The total prestressing force from all the tendons present in the box girder can be determined using Equation 4.14.

$$\sum F_p = n \cdot F_p \tag{4.14}$$

where:
$\sum F_p$ is the total prestressing force in [N].
F_p is the prestressing force of a single tendon in [N].
n is the number of prestressing tendons.

Based on the applied moment and the box girder's dimensions, the normal force resulting from the applied bending moment can be calculated. Additionally, the box girder's dimensions allow for the computation of the additional force due to shear forces from the webs, using a theta (θ) of 30 and 21.8 degrees.
With $\theta = 30°$:
- $\theta = 30° \rightarrow \cot(30°) = 1.73$
- $\alpha = 90° \rightarrow \cot(90°) = 0$
- $a_L/z = (1.73 - 0)/2 = 0.866$ −

With $\theta = 21.8°$:
- $\theta = 21.8° \rightarrow \cot(21.8°) = 2.50$
- $\alpha = 90° \rightarrow \cot(90°) = 0$
- $a_L/z = (2.50 - 0)/2 = 1.25$ −

Furthermore, based on the number of tendons present in the box girder, the total prestressing force can be calculated. The prestressing force of a single tendon can be determined using the material properties provided in section 2.3.
- $f_{pd,20\%} = 1231\ N/mm^2$
- $A_p = 12 \cdot \pi \cdot (Ø/2)^2 = 12 \cdot \pi \cdot (14/2)^2 = 462\ mm^2$
- $F_p = 1231 \cdot 462 = 568520\ N = 568.5\ kN$

Bottom slab
In addition to the tension in the top slab, the applied bending moment will induce compression in the bottom slab. It should be evaluated whether this compressive stress does not exceed the compressive strength of the concrete. To determine this, Equation 4.15 can be used to compute the concrete's compressive force resistance.

$$N_{Rd,c} = f_{cd} \cdot b' \cdot d_{bottom\ slab} \tag{4.15}$$

where:
$N_{Rd,c}$ is the design axial compressive force resistance of the concrete in [N].
f_{cd} is the design value of the compressive strength of the concrete in [N/mm^2].
b' is the width of the bottom slab in [mm].
$d_{bottom\ slab}$ is the thickness of the bottom slab in [mm].

With a compressive strength of 20 N/mm^2 for the concrete, the compressive resisting force from the concrete can be calculated based on the dimensions of the box girder.

Unity check
After performing the required calculations, the unity check can be presented for both the top and bottom slab.

Top slab

The unity check for the top slab can be calculated through Equation 4.16.

$$U.C. = \frac{(F_{Ed} + \Delta F_{Ed})}{F_p} \tag{4.16}$$

The box girder's dimensions and forces are outlined in Table 4.18, enabling the calculation of the unity check for the top slab across the various cross-sections considered. In this Table, θ is set to 30 degrees.

Table 4.18: Unity check bending moment top slab with $\theta = 30°$

	M_{Ed} [MNm]	h' [m]	$d_{top\ slab}$ [m]	$d_{bottom\ slab}$ [m]	z [m]	F_{Ed} [MN]	ΔF_{Ed} [MN]	n [number]	$\sum F_p$ [MN]	$U.C.$
Adjacent to the support	317	5.44	0.20	0.53	5.08	62.46	13.86	143	81.30	0.94
Joint A-B	269	4.69	0.20	0.50	4.34	61.98	12.47	123	69.93	1.06
Joint B-C	126	3.18	0.20	0.39	2.89	43.67	8.14	87	49.46	1.05
Joint C-D	38	2.22	0.20	0.27	1.99	19.14	4.33	45	25.58	0.92

Similarly, Table 4.19 provides the unity check for the top slab, where θ is set to 21.8 degrees.

Table 4.19: Unity check bending moment top slab with $\theta = 21.8°$

	M_{Ed} [MNm]	h' [m]	$d_{top\ slab}$ [m]	$d_{bottom\ slab}$ [m]	z [m]	F_{Ed} [MN]	ΔF_{Ed} [MN]	n [number]	$\sum F_p$ [MN]	$U.C.$
Adjacent to the support	317.00	5.44	0.20	0.53	5.08	62.46	20.00	143	81.30	1.01
Joint A-B	269.00	4.69	0.20	0.50	4.34	61.98	18.00	123	69.93	1.14
Joint B-C	126.00	3.18	0.20	0.39	2.89	43.67	11.75	87	49.46	1.12
Joint C-D	38.00	2.22	0.20	0.27	1.99	19.14	6.25	45	25.58	0.99

Table 4.20 presents an impact assessment evaluating the unity check for the bending moment capacity of the top slab across various cases. The default case, as previously calculated, assumes a θ of 30 degrees, no settlement, a Young's modulus of 30 GPa, and a prestress loss of 20%. Additional cases are analysed with either a θ of 21.8 degrees, settlements of 5 mm, 100 mm or 200 mm, a settlement of 100 mm combined with a Young's modulus of 20 GPa or 25 GPa, or a prestress loss of 15%. The percentage values represent deviations from the default case.

Table 4.20: Impact assessment: Unity check bending moment top slab with altering parameters

	U.C.	U.C. (θ=21.8°)	U.C. (100 mm)	U.C. (5 mm)	U.C. (200 mm)	U.C. (100 mm) (E=25 GPa)	U.C. (100 mm) (E=20 GPa)	U.C. ($f_{pd,15\%}$)
Adjacent to the support	0.94	1.01 (8.1%)	0.95 (1.0%)	0.94 (0.0%)	0.96 (1.9%)	0.95 (0.8%)	0.94 (0.6%)	0.88 (-5.9%)
Joint A-B	1.06	1.14 (7.4%)	1.08 (1.0%)	1.07 (0.0%)	1.09 (2.0%)	1.07 (0.8%)	1.07 (0.7%)	1.00 (-5.9%)
Joint B-C	1.05	1.12 (7.0%)	1.06 (1.4%)	1.05 (0.1%)	1.08 (2.8%)	1.06 (1.2%)	1.06 (1.0%)	0.99 (-5.9%)
Joint C-D	0.92	0.99 (8.2%)	0.95 (3.1%)	0.92 (0.2%)	0.97 (6.2%)	0.94 (2.6%)	0.94 (2.1%)	0.86 (-5.9%)

Bottom slab

Equation 4.17 yields the unity check values for the bottom slab, which are presented in Table 4.21 for the various cross-sections considered.

$$U.C. = \frac{F_{Ed}}{N_{Rd,c}} \tag{4.17}$$

Table 4.21: Unity check bending moment bottom slab

	M_{Ed} [MNm]	F_{Ed} [MN]	b' [mm]	$d_{bottom\ slab}$ [mm]	f_{cd} [N/mm^2]	$N_{Rd,c}$ [MN]	$U.C.$
Adjacent to the support	317	62.46	6412	530	20	67.97	0.92
Joint A-B	269	61.98	6524	500	20	65.24	0.95
Joint B-C	126	43.67	6720	390	20	52.42	0.83
Joint C-D	38	19.14	6850	270	20	36.99	0.52

Conclusion
In this section, calculations were conducted to evaluate the bending moment capacity of the box girder in longitudinal direction. The following were taken into account:

- For the bottom slab, the calculation took into account its actual width.
- For the top slab, the prestress loss was adjusted to 20%. This reflects a more accurate estimation of the longitudinal prestress loss. A prestress loss of 15% was also considered.
- For the top slab, a modified value of θ was taken into account.
- For the top slab, the additional tensile force has been considered due to the shear forces resulting from a support settlement. As settlement of the support, a lower and upper bound of 5 and 200 mm have been considered, as well as a settlement of 100 mm. A varying Young's modulus has been considered, where the modulus was adjusted to 20 and 25 GPa combined with a support settlement of 100 mm.

All in all, it is evident from the results that the concrete compressive strength of the bottom slab sufficiently withstands the compressive stresses induced by the applied bending moment. On the other hand, the unity check values for the top slab indicate that the prestressing force is often insufficient in withstanding the tensile forces induced by the bending moment across most cross-sections considered. It is visible that reducing the value of θ increases the force in the top slab due to shear forces from the webs, which in turn results in higher unity checks. Similarly, accounting for the additional shear force due to the settlement of a support also increases the force in the top slab. Considering a support settlement of 100 mm, it is evident that variations in the Young's modulus do not produce significant effects. Lastly, a lower percentage of prestress loss correlates with a higher prestressing force present in the top slab and hence lower unity checks.

Check 9: Shear force capacity webs
Lastly, check number 9 assesses the shear force capacity of the webs in longitudinal direction. Figure 4.23 demonstrates how the loads applied on the bridge will generate shear forces in the webs. Figure 4.24 specifies the locations where this assessment is conducted along the longitudinal span of the bridge. Similar to check 8, this evaluation is performed at the same four cross-sections: adjacent to the support and at the construction joints between the segment types within a cantilever.

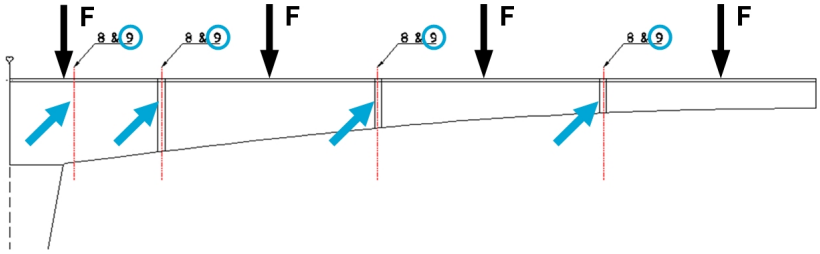

Figure 4.23: Check 9: Shear force capacity of the box girder's webs. Adapted from [5]

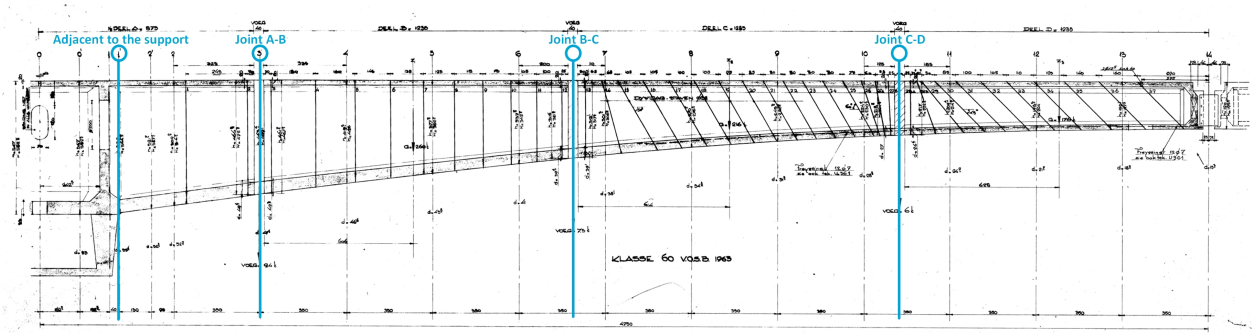

Figure 4.24: Check 9: Cross-sections in the longitudinal section of the Zeelandbrug. Modified [NZC-78].

Applied shear force
The results from the Iv-Infra model were used to determine the highest shear force experienced in the web [5]. The model considers various load cases, including different setups of the uniformly distributed traffic load and the Tandem System from Eurocode Load Model 1. The total shear force applied includes contributions from the self-weight, the barriers, the pavement, the Tandem System, the uniformly distributed traffic load, and the braking force. The column with V_{Ed} in Table 4.22 presents the highest shear forces found at the construction joints and adjacent to the support [5].

As a result of torsion, tension/compression couples develop in the webs, adding to the applied shear force. Iv-Infra has quantified the torsional contribution resulting from traffic eccentricity using Equation 4.18 [5]. Iv-Infra found for $\Delta V_{Ed;TS}$ a value of 345 kN and for $\Delta V_{Ed:UDL}$ a value of 11.4 kN/m [5]. Based on the effective length over which the uniformly distributed load acts, the additional shear force in the web due to torsion can be calculated.

$$\Delta V_{Ed} = \Delta V_{Ed;TS} + \Delta V_{Ed;UDL} \cdot L_{eff} \tag{4.18}$$

where:
ΔV_{Ed} is the total shear force induced by torsion due to traffic eccentricity in [kN].
$\Delta V_{Ed;TS}$ is the shear force induced by torsion due to the eccentricity from the Tandem System in [kN].
$\Delta V_{Ed;UDL}$ is the shear force induced by torsion due to the eccentricity from the uniformly distributed traffic load in [kN/m].
L_{eff} is the effective length over which the uniformly distributed load acts in [m].

Finally, the applied shear force per web is calculated by dividing the total applied shear force by two, then adding the torsional shear force and half of the shear force due to a pier's settlement. In the absence of settlements, the results are presented in Table 4.22.

$$V_{Ed,tot} = \Delta V_{Ed} + (V_{Ed} + V_{sett})/2 \tag{4.19}$$

where:
$V_{Ed,tot}$ is the design value of the total occurring shear force per web in [MN].
ΔV_{Ed} is the total shear force induced by torsion due to traffic eccentricity in [MN].
V_{Ed} is the design value of the occurring shear force in [MN].
V_{sett} is the shear force due to a settlement of a pier in [MN], see Tables 3.3 and 3.5.

Table 4.22: Total design shear force [5]

	V_{Ed} [MN]	L_{eff} [m]	ΔV_{Ed} [MN]	V_{sett} [MN]	$V_{Ed,tot}$ per web [MN]
Adjacent to the support	16.0	47.5	0.89	0	8.89
Joint A-B	14.4	47.5	0.89	0	8.09
Joint B-C	9.4	25.2	0.63	0	5.33
Joint C-D	5.0	12.35	0.49	0	2.99

Shear force resistance
The shear force resistance is governed by the minimum value between the total shear resistance, which includes contributions from the reinforcement components, and the shear force resistance limited by the crushing of the concrete compressive strut. The shear force resistance will be calculated per web.

Total shear force resistance
The total shear force resistance includes the combined effects of prestressing, reinforcement and the strength of concrete, along with any additional contribution from forces in the case of an inclined chord. The total shear force resistance can be calculated with Equation 4.20.

$$V_{Rd} = V_{Rd,s} + V_{ccd} + V_{td} + V_{Rd,c} \tag{4.20}$$

where:
V_{Rd} is the design value of the total shear force which can be sustained by the concrete member in [N].
$V_{Rd,s}$ is the design value of the shear force which can be sustained by the yielding shear reinforcement in [N].
V_{ccd} is the design value of the force in the compression area, in the case of an inclined compression chord in [N].
V_{td} is the design value of the shear component of the force in the tensile reinforcement in the case of an inclined tensile chord in [N].
$V_{Rd,c}$ is the design shear resistance of the concrete member without shear reinforcement in [N].

Contribution prestressing
According to NEN-EN 1992-1-1:2005, the contribution of the shear reinforcement to the total shear force resistance can be computed through Equation 4.21. This equation holds true for concrete members with inclined shear reinforcement.

$$V_{Rd,s} = A_{sw}/s \cdot z \cdot f_{ywd} \cdot \cot(\theta) \cdot +\cot(\alpha)) \cdot \sin(\alpha) \tag{4.21}$$

where:
$V_{Rd,s}$ is the design value of the shear force which can be sustained by the yielding shear reinforcement in [N].
A_{sw} is the cross-sectional area of the shear reinforcement in [mm^2].
s is the spacing of the stirrups in [mm].
z is the the inner lever arm between the line of action of the tension force and the line of action of the compressive force in [mm].
f_{ywd} is the design yield strength of the shear reinforcement in [N/mm^2].

θ is the angle between the concrete compressive strut and the beam axis perpendicular to the shear force in [deg].
α is the angle between shear reinforcement and the beam axis perpendicular to the shear force (measured positive) in [deg].

Contribution soft steel reinforcement
The soft steel reinforcement will not be taken into account in the shear force resistance of the webs in longitudinal direction. Namely, the soft steel reinforcement is already accounted for in the bending moment capacity of the webs in the transverse direction. Because it is difficult to quantify the contribution of the soft steel reinforcement to each capacity, the soft steel reinforcement is excluded from the shear force resistance [5]. This exclusion only has an effect when the shear force resistance is smaller than the shear force resistance limited by the crushing of the concrete compressive strut.

Contribution concrete
Similar to previous calculations, the contribution of concrete to the shear force resistance can be determined using the formula provided by RBK 1.2.1 (see Equation 4.9). However, TU Delft has shown in 2019 that for greater structural heights the scale effect in this formula is underestimated, resulting in an overly favourably calculation of the concrete contribution. Therefore, TNO recommends calculating the contribution of the concrete to the shear force resistance using the formula described by TU Delft (see Equation 4.22) [6].

$$V_{Rd,c} = \frac{1}{\gamma_c} \cdot k_{di} \cdot f_{ck}^{(1/3)} \cdot b_w \cdot z \tag{4.22}$$

where:
$V_{Rd,c}$ is the design shear resistance of the concrete member without shear reinforcement in [N].
γ_c is the partial factor for concrete. $\gamma_c = 1.5$ $-$
k_{di} is the factor accounting for properties of the reinforcement and concrete member.
$k_{di} = 0.7 \cdot (\frac{100 \cdot \rho_l \cdot d_{dg}}{d})^{1/3}$
ρ_l is the flexural reinforcement ratio. $\rho_l = \frac{A_{sL}}{b_w \cdot d} \leq 0.02$ $-$.
d_{dg} is the shear crack roughness parameter.
$d_{dg} = 16 + D_{grain} \leq 40\ mm$ for $f_{ck} \leq 60\ N/mm^2$
D_{grain} is the maximum grain size in [mm].
d is the effective depth to the main flexural reinforcement in [mm].
f_{ck} is the characteristic cylinder compressive strength of the concrete in [N/mm^2].
b_w is the smallest width of the cross-section in the tensile area in [mm].
z is the the inner lever arm between the line of action of the tension force and the line of action of the compressive force in [mm].

Contribution inclined chords
Equation 4.23 provides the calculation for the shear component V_{ccd} of the force in the compression area when dealing with an inclined chord. The division by two is applied because the shear resistance is computed per web. The shear component V_{td} of the force in the tensile reinforcement is considered to be zero, since the tensile chord is not inclined.

$$V_{ccd} = F_{Ed} \cdot dy/dx\ /2 \tag{4.23}$$

where:
V_{ccd} is the design value of the force in the compression area, in the case of an inclined compression chord in [N].
F_{Ed} is the design value of the normal force resulting from the applied bending moment in [N].
dy/dx is the inclination of the chords.

Shear force resistance limited by crushing of the concrete compressive strut
The maximum shear force resistance constrained by the crushing of the concrete compressive strut should also be determined. This can be computed using a formula from NEN-EN 1992-1-1:2005, specifically designed for concrete members with inclined shear reinforcement. The formula is provided in Equation 4.24.

$$V_{Rd,max} = \alpha_{cw} \cdot b_w \cdot z \cdot \upsilon_1 \cdot f_{cd} \cdot (cot(\theta) + cot(\alpha)) \ / \ (1 + cot^2(\theta)) \tag{4.24}$$

where:
$V_{Rd,max}$ is the design value of the maximum shear force which can be sustained by the concrete member, limited by crushing of the compression struts in [N].
α_{cw} is the coefficient taking account of the state of the stress in the compression chord.
b_w is the smallest width of the cross-section in the tensile area in [mm].
z is the the inner lever arm between the line of action of the tension force and the line of action of the compressive force in [mm].
υ_1 is the strength reduction factor for concrete cracked in shear. $\upsilon_1 = 0.6 \cdot (1 - f_{ck})/250$
f_{cd} is the design value of the compressive strength of the concrete in [N/mm^2].
θ is the angle between the concrete compressive strut and the beam axis perpendicular to the shear force in [deg].
α is the angle between shear reinforcement and the beam axis perpendicular to the shear force (measured positive) in [deg].

Computation of the shear force resistance
Now that the methods have been outlined, the shear force resistances can be computed. From the material properties in section 2.3, the following are known:
- $A_{sw} = \pi \cdot (Ø/2)^2 = \pi \cdot (32/2)^2 = 804.25\ mm^2$
- $f_{ywd} = 713\ N/mm^2$
- $A_p = 12 \cdot \pi \cdot (Ø/2)^2 = 12 \cdot \pi \cdot (7/2)^2 = 461.81\ mm^2$
- $\alpha = 90°$
- $\alpha_{cw} = 1$
- $D_{grain} = 32\ mm$

With $\theta = 30°$ and C30/37:
- $f_{ck} = 30\ N/mm^2$
- $f_{cd} = 20\ N/mm^2$
- $\upsilon_1 = 0.6 \cdot (1 - f_{ck})/250 = 0.6 \cdot (1 - 30)/250 = 0.528\ -$

With $\theta = 21.8°$ and C40/50:
- $f_{ck} = 40\ N/mm^2$
- $f_{cd} = 26.67\ N/mm^2$
- $\upsilon_1 = 0.6 \cdot (1 - f_{ck})/250 = 0.6 \cdot (1 - 40)/250 = 0.504\ -$

Additionally, Table 4.23 provides an overview of the variable values corresponding to the different components contributing to the total shear resistance.

Table 4.23: Variables of the components contributing to the total shear force resistance

	$V_{Rd,s}$				V_{ccd}		$V_{Rd,c}$				
	s [mm]	z [mm]	α [-]	$cot(\alpha)$ [-]	F_{Ed} [MN]	dy/dx [-]	b_w [mm]	d [mm]	k [-]	n [number]	ρ_l [-]
Adjacent to the support	1800	5075	90	0.00	62.46	0.133	410	5075	1.20	143	0.02
Joint A-B	1800	4340	90	0.00	61.98	0.128	405	4340	1.21	123	0.02
Joint B-C	1000	2885	90	0.00	43.67	0.103	380	2885	1.26	87	0.02
Joint C-D	750	1985	70	0.36	19.14	0.044	360	1985	1.32	45	0.02

Unity check
To evaluate the shear force capacity of the webs in the longitudinal direction, Equation 4.25 can be used. This equation calculates the unity check of the shear force capacity per web. The applied shear force was equal to the applied shear force per web combined with the contribution from the torsional shear force due to traffic eccentricity. The shear force resistance is determined by the minimum value between the total resistance involving reinforcement components and the resistance limited by the crushing of the concrete compressive strut.

$$U.C. = \frac{V_{Ed,tot}}{\min(V_{Rd}; V_{Rd,max})} \tag{4.25}$$

In Table 4.24 the results are displayed for a θ of 30 degrees and a concrete strength of C30/37.

Table 4.24: Unity check shear force capacity webs (per web) with $\theta = 30°$ and C30/37

	$V_{Ed,tot}$ [MN]	$V_{Rd,s}$ [MN]	V_{ccd} [MN]	V_{td} [MN]	$V_{Rd,c}$ [MN]	V_{Rd} [MN]	$V_{Rd,max}$ [MN]	$U.C.$
Adjacent to the support	8.89	2.80	4.15	0	0.76	7.71	9.51	1.15
Joint A-B	8.09	2.39	3.97	0	0.67	7.03	8.04	1.15
Joint B-C	5.33	2.87	2.25	0	0.48	5.60	5.01	1.06
Joint C-D	2.99	2.99	0.42	0	0.36	3.77	3.95	0.79

A reduction in unity checks is possible by assuming a smaller value of θ (θ=21.8°), and subsequently assuming $V_{Rd,c} = 0$. Furthermore, a concrete strength class of C40/50 is considered, as suggested by TNO [6]. Table 4.25 presents the corresponding results.

Table 4.25: Unity check shear force capacity webs (per web) with $\theta = 21.8°$ and C40/50

	$V_{Ed,tot}$ [MN]	$V_{Rd,s}$ [MN]	V_{ccd} [MN]	V_{td} [MN]	$V_{Rd,c}$ [MN]	V_{Rd} [MN]	$V_{Rd,max}$ [MN]	$U.C.$
Adjacent to the support	8.89	4.04	4.15	0	0	8.20	9.64	1.08
Joint A-B	8.09	3.46	3.97	0	0	7.42	8.15	1.09
Joint B-C	5.33	4.14	2.25	0	0	6.39	5.08	1.05
Joint C-D	2.99	4.08	0.42	0	0	4.51	3.79	0.79

Table 4.26 presents an impact assessment evaluating the unity check for the shear force capacity of the webs across various cases. Again, the default case uses a θ of 30 degrees, no settlement, a Young's modulus of 30 GPa, and a prestress loss of 20%. Additional cases are examined which have either a θ of 21.8 degrees, settlements of 5 mm, 100 mm or 200 mm, a settlement of 100 mm combined with a Young's modulus of 20 GPa or 25 GPa, or a prestress loss of 15%. Deviations from the default case are indicated with percentages.

Table 4.26: Impact assessment: Unity check shear force capacity webs (per web) with altering parameters

	U.C.	U.C. (θ=21.8°) (C40/50)	U.C. (100 mm)	U.C. (5 mm)	U.C. (200 mm)	U.C. (100 mm) (E=25 GPa)	U.C. (100 mm) (E=20 GPa)
Adjacent to the support	1.15	1.08 (-5.9%)	1.21 (4.7%)	1.16 (0.2%)	1.26 (9.5%)	1.20 (4.0%)	1.19 (3.2%)
Joint A-B	1.15	1.09 (-5.2%)	1.21 (5.2%)	1.15 (0.3%)	1.27 (10.4%)	1.20 (4.4%)	1.19 (3.5%)
Joint B-C	1.06	1.05 (-1.3%)	1.15 (7.9%)	1.07 (0.4%)	1.23 (15.8%)	1.13 (6.7%)	1.12 (5.4%)
Joint C-D	0.79	0.79 (-0.7%)	0.91 (14.1%)	0.80 (0.7%)	1.02 (28.3%)	0.89 (11.9%)	0.87 (9.6%)

Conclusion

For the shear force capacity of the webs in the longitudinal direction, the following have been taken into account:

- The shear force resistance was calculated per web.
- The scale effect was considered, reducing the contribution of the concrete to the total shear force resistance.
- A different value was taken into account for the θ (θ=21.8°) and the concrete strength class (C40/50).
- The additional shear force has been considered resulting from a 5, 100 and 200 mm support settlement. A Young's modulus of 20 and 25 GPa have also been considered combined with a support settlement of 100 mm.

In conclusion, the results indicate that the unity checks exceed 1 for the cross-sections adjacent to the support and at the construction joint between segment types A and B, as well as B and C. A lower value of θ and an increased concrete strength class slightly reduce the unity checks. It has, however, been observed from check 8 that a lower value of θ increases the unity checks for the bending moment capacity of the top slab. This is attributed to a gentler cracking slope leading to higher tensile forces. These tensile forces add to the total tensile force under the applied bending moments. The additional shear force resulting from a support settlement significantly impacts the total shear force within the webs, thereby increasing the unity checks. As already observed, a lower modulus of elasticity results in a slight reduction in shear forces due to the settlement of a support, consequently leading to lower unity checks.

4.3.3. Discussion

This subsection discusses the reliability of the Finite Element Model and interprets the results.

Reliability

To better understand the outcomes of the Finite Element Model, there is looked at the moment and shear force diagram of a balanced cantilever bridge as a beam with fixed supports at the piers locations. Then, Figures 4.25, 4.26 and 4.27 display the expected moment and shear force diagrams due to self-weight, settlement and their combination, respectively. As is visible, the results of the Finite Element Model correspond to these diagrams. Due to the symmetry of the cantilevers, the shear force at the midspan joints resulting from self-weight is zero. A support settlement induces a uniform shear force across the entire adjacent cantilever spans. These shear forces due to self-weight and settlement can be superimposed.

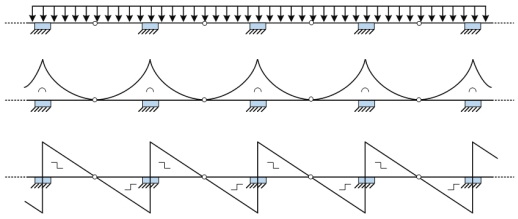

Figure 4.25: Expected moment and shear force diagram due to self-weight

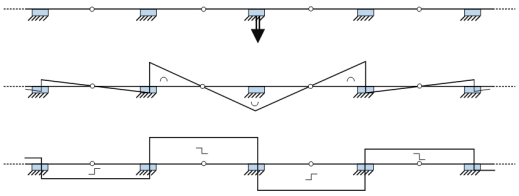

Figure 4.26: Expected moment and shear force diagram due to settlement

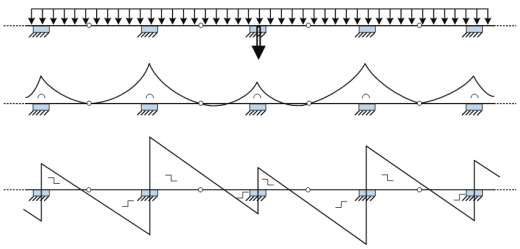

Figure 4.27: Expected moment and shear force diagram due to both self-weight and settlement

Various modelling assumptions were made in the Finite Element Model. One important modelling assumption was to model the material behaviour as linear elastic isotropic and to perform structural linear static analyses. As demonstrated in Tables 3.3, 3.4 and 3.7, a proportional load-deformation relationship is evident. With the concrete modelled linearly elastic, this relationship implies that the load is directly proportional to the applied deformation; hence, doubling the deformation results in a doubled load. Consequently, linear interpolation and extrapolation can be used to determine the shear force in the cantilever for any given settlement.

Since the concrete was modelled as linear elastic isotropic, both nonlinear and linear analyses yield identical responses. Nonlinear analysis is generally more accurate for large deformations because it takes

into account both material and geometric nonlinearities. Regarding the material behaviour, nonlinear materials do not exhibit a direct proportionality between stress and strain. Instead, complex behaviours can be modelled such as concrete cracking under tensile stresses and crushing under compressive stresses. Regarding the geometry, nonlinear analysis considers changes in the geometry that affect the structural stiffness and the internal force distribution. This includes the generation of additional moments due to the deformed shape of the structure, which linear analyses do not capture. Furthermore, the concrete was assumed to be isotropic, meaning it has identical mechanical properties in all directions. This includes properties such as the Young's modulus and Poisson's ratio.

The exact difference in the structural response when applying either a linear or nonlinear model is unknown. However, it can be speculated what impact a nonlinear model would have. A linear elastic model, which assumed the stress in the concrete to be directly proportional to the strain it experiences, is valid for situations where the concrete remains within its elastic range. This means that the stresses induced by the settlements do not cause permanent deformation such as cracking or crushing. Hence, for small settlements, the shear forces in the cantilevers can be described very accurately. For larger settlements, and the higher deformations they induce, the concrete may begin to behave nonlinearly and crack. At this point the linear model does not accurately describe this behaviour as it assumes that the concrete does not crack. Therefore, the linear model might estimate the concrete to be stiffer and overestimate the shear force that is induced by a support settlement. Hence, the linear model is conservative. Nevertheless, the linear model does provide a good indication of the magnitude of shear forces that can be expected in the bridge as a result of varying magnitudes of settlement.

In addition to the modelling approach, the Young's modulus was set to 30 GPa. This value was chosen under the assumption that the concrete remains uncracked due to the reinforcement and prestressing. As is visible in Tables 3.5 and 3.6, a reduction in Young's modulus would result in lower shear forces in the cantilevers. Lastly, the translational stiffness of the shear force dowels was derived from detailed Finite Element Model simulations under vertical loading. It is possible that the stiffness of the dowels varies between certain cantilevers. If the stiffness of the dowels is higher than initially calculated, it would result in increased internal forces in the concrete surrounding the dowels.

Interpretation of the results
The results obtained from the Finite Element Model and subsequent calculations provide significant insights into the structural behaviour of the Zeelandbrug under combined traffic loading and settlement conditions.

As illustrated in Tables 4.20 and 4.26, the contribution of shear forces due to a support settlement increases near the midspan joints. This is because the shear forces and moments resulting from the bridge's self-weight decrease in the vicinity of the midspan joints, as shown in Figure 4.25. The two shear force dowels located in the midspan joints between the cantilevers have a combined capacity of 1.3 MN. According to the FEM results, the induced shear force only exceeds this capacity for scenario 1f (support settlement of 200 mm). However, even at lower settlements, the effects could be critical. Namely, the settlement is more likely to cause additional shear forces that, due to high load concentrations around the dowels, may lead to the failure of the concrete and the Dywidag bars around the dowels.

It has been observed that when a pier of the Zeelandbrug experiences settlement, several issues may arise, particularly under high traffic loads on the cantilever. Settlement of a support leads to an increase in shear forces within the cantilever that mirrors the adjacent cantilever. This results in increased tensile forces in the top slab of the box girder. If these tensile forces exceed the prestressing force, tension will develop in the top slab of the box girder. Additionally, the increased shear force in the webs of the bridge could exceed their capacity. The question that now arises is: what happens if the moment or shear force capacity gets exceeded? As previously observed, exceeding the moment capacity results in tension in the top slab of the box girder, leading to gradual cracking over time. In contrast, exceeding the shear force capacity in the webs leads to sudden and brittle cracking, which can cause an abrupt failure of the webs.

As noted earlier, Tables 4.20 and 4.26 present the effects of altering various parameters on the unity check across different cases. From these Tables, it can be observed that a support settlement has a

smaller impact on the unity checks of the moment capacity of the top slab compared to its influence on the unity check of the shear force capacity of the webs. Modifying the Young's modulus in the Finite Element Model to assess the additional shear force has a relatively small impact. This is due to the fact that, for both the top slab and the webs, the shear force resulting from support settlement comprises only a small portion of the total shear force. At the joints where the moment capacity is exceeded in the top slab in longitudinal direction, the loss of prestress significantly affects their performance. Initially, a 20% prestress loss has been assumed in the recalculations for the longitudinal prestressing. Applying a longitudinal prestress loss of 15% would result in a reduction of nearly 6% in the unity check for the moment capacity of the top slab. Specifically, if the prestress loss were 15% rather than 20%, the top slab at the examined locations would meet the required moment capacity.

For the webs, the shear force capacity was most critical adjacent to the support and at joint A-B in the longitudinal direction. At these locations the unity check appears to be significantly reduced due to a higher concrete compressive strength and a reduction in θ (the angle between the concrete compressive strut and the beam axis perpendicular to the shear force). Reducing θ increases the compressive force in the concrete strut, thereby increasing the shear resistance provided by the reinforcement. However, this adjustment also reduces the shear resistance limited by the compressive strength of the concrete strut, which may become governing in assessing the shear resistance. As a result, merely reducing θ does not necessarily lead to lower unity checks. If the concrete compressive strength is increased, the capacity of the compressive strut to resist crushing improves, making the shear resistance of the reinforcement governing and the reduction of θ effective in lowering the unity check.

The FEM results underscore the necessity of strategically choosing the supports of the Zeelandbrug to monitor for settlements. It is evident that while the settlement of a support significantly impacts the adjacent cantilever spans, its effects on more distant spans are minimal. For instance, the FEM results indicate that a 100 mm settlement of a support can induce a shear force of 845.2 kN in the midspan joint of the adjacent cantilever, whereas the shear force at the midspan joint in the next cantilever span is only 8.68 kN. This highlights the localised nature of settlement effects, which necessitates precise position of monitoring to accurately capture these changes.

From this analysis, several key points have emerged. Firstly, it is important to determine if pier settlement of the Zeelandbrug is occurring and to quantify its extent. Additionally, understanding the concrete compressive strength and the degree of prestress loss is important for evaluating the long-term structural health of the bridge. Finally, given the localised impact of settlement, monitoring should be applied strategically to effectively measure and monitor these effects.

4.3.4. Conclusion

Overall, the recalculation has proven valuable insights into the current condition of the Zeelandbrug. It can be concluded that the settlement of a support induces additional shear forces, with the most significant contributions observed near the midspan joints. These settlement-induced shear forces add to the existing shear forces generated by the bridge's self-weight and traffic loads, thereby elevating the risk of surpassing the bridge's shear and moment capacity.

Critical structural elements

Through the structural recalculation of the Zeelandbrug, it was found that the moment capacity of the box girder's top slab in the transverse direction is sufficient. Similarly, the compression in the box girder's bottom slab as a result of the longitudinal moment does not exceed the bottom slab's resistance. However, the recalculation did identify the following structural elements of the Zeelandbug's superstructure to be critical. Structural elements have been defined as critical when their resistance is exceeded by the applied loading.

In transverse direction:

- The moment and shear force capacity of the cantilever of the box girder.
- The shear force capacity of the top slab of the box girder.
- The moment capacity of the webs when tension occurs on the outer side of the webs.

In longitudinal direction:

- As a result of the longitudinal moment; tension in the top slab of the box girder.
- The shear force capacity of the box girder's webs.

Since no new information or insights were obtained, recalculation of the coupling elements was deemed unnecessary. However, based on the available information and previous calculations of Iv-Infra and TNO, the coupling elements are identified as critical and are listed below [5, 6].

Coupling elements:

- Shear force dowels
- Shock absorbers
- Hinges

4.4. Identified uncertainties

To assess the safety of a structure, it is important to identify the uncertainties in the structure's behaviour. Understanding these uncertainties is important as it clarifies the gaps in knowledge within the current calculations, enables more thorough assessments, and thereby improves decision-making processes related to the structure. Through the recalculation process of the Zeelandbrug, uncertainties in the bridge's performance have been identified. The uncertainties can be viewed from two perspectives: the uncertainties regarding the applied loading and those regarding the material resistance.

4.4.1. Material resistance

The uncertainties identified related to the material resistance will be listed for each identified critical structural element. In general, it was observed while developing the Finite Element Model that the value of the concrete's Young's modulus is uncertain.

Top slab of the box girder

In transverse direction, the cantilever of the top slab was identified as critical for the bending moment and shear forces, along with the shear forces at the section extending from the midspan towards the web of the box girder.

- What is the prestress loss of the transverse prestressing?
- What is the condition of the top slab? (visual inspection of the top surface is hindered by the pavement)
- Is there corrosion of the reinforcement?
- The occurrence of shear failure due to its unpredictability

In longitudinal direction, the box girder's top slab was identified as critical for the bending moment with tension in the top slab.

- What is the prestress loss of the longitudinal prestressing?

Webs of the box girder

In transverse direction, the box girder's webs were identified as critical for the bending moment.

- What amount of capacity of the Dywidag bars can be attributed to the moment capacity in the transverse direction?

In longitudinal direction: the box girder's webs were identified as critical for the shear forces.

- What amount of capacity of the Dywidag bars can be attributed to the shear force capacity in the longitudinal direction?
- What is the actual concrete compressive strength?
- The occurrence of shear failure due to its unpredictability

Coupling elements

In the longitudinal direction, the shear force dowels were identified as critical for managing shear forces, along with the shock absorbers and hinges for handling normal forces.

- What is the actual load on the shear force dowels?
- To what extent is the freedom of rotation of the hinges prevented due to corrosion?
- What is the efficiency of the shock absorbers?

4.4.2. Applied loading

From an alternative viewpoint, assessing the structural safety of a bridge also requires a thorough understanding of the uncertainties related to the applied loading when the structure is in use. There is considerable knowledge regarding the traffic that utilises the Zeelandbrug, which in turns informs the traffic loads applied to it. This includes the number of passenger cars, light trucks and heavy trucks per year. Additionally, a regulatory maximum weight limit of 50 tons for vehicles was established in 2016 [16]. Nevertheless, some uncertainties remain concerning the loads applied to the bridge. For instance, with the Westerscheldetunnel becoming toll-free, an increase in traffic intensity on the bridge is anticipated, although the exact extent of this increase is unclear [4]. Moreover, as previously discussed, the extent of differential settlements that the Zeelandbrug experiences is unknown. As a result, the impact that these potential settlements have on the load effects within the bridge's structure is also unknown.

5

Structural Health Monitoring

This chapter begins with section 5.1, which lists the important physical parameters of the Zeelandbrug suitable for monitoring. Following this, section 5.2 identifies two types of failures of the bridge and outlines the corresponding monitoring strategy. An introduction to Structural Health Monitoring is provided in section 5.3. Then, in section 5.4, a brief literature review is conducted on monitoring technologies that have been applied to bridges constructed using the balanced cantilever method. Subsequently, section 5.5 discusses the technologies recommended for monitoring the physical parameters of the Zeelandbrug. The final monitoring plan is presented in section 5.6. Lastly, section 5.7 addresses additional studies and maintenance activities recommended for the Zeelandbrug.

5.1. Physical parameters

In the previous chapter, the uncertainties associated with the assessment of each structural element and their failure modes were identified. Based on these findings, the physical parameters suited for monitoring are listed in Table 5.1. Monitoring these parameters is expected to reduce the identified uncertainties and enhance the accuracy of the structural assessment, thereby improving the overall safety of the Zeelandbrug. For the failure modes in the longitudinal direction, the physical parameters have been listed in order of importance, from most to least important. This is based on the results from the impact assessment in subsection 4.3.2, which examined the effects of modifying these physical parameters on the unity checks for the bending moment capacity and shear force capacity in the longitudinal direction.

Table 5.1: Physical parameters

Location	**Failure mode**	**Physical parameter**
In transverse direction: cantilever of top slab (Loc. B of cantilever)	Bending moment capacity	Transverse prestress loss
In transverse direction: cantilever of top slab (Loc. A of cantilever, near the joints)	Shear force capacity	
In transverse direction: top slab at the section from midspan to the web of the box girder (Loc. B of top slab)	Shear force capacity	
In longitudinal direction: top of the top slab (Joint A-B and joint B-C)	Bending moment capacity	1. Longitudinal prestress loss
		2. Support settlement
		3. Young's modulus
In transverse direction: webs (Outer side of webs, cross-sections 5 and 11)	Bending moment capacity	Concrete cracking related parameter
In longitudinal direction: webs (Adjacent to support, joint A-B and joint B-C)	Shear force capacity	1. Concrete compressive strength
		2. Support settlement
		3. Young's modulus

A physical parameter not demonstrated in Table 5.1 that relates to all locations is the weight of the vehicles. Namely, it is important to have a good understanding of the actual weight of the vehicles

travelling over the Zeelandbrug in order to accurately determine the loads experienced by the bridge. Regarding the first physical parameter listed in Table 5.1, all assessments conducted in the transverse direction for the top slab account for a prestress loss of 15%. However, this value represents an estimate, and a more precise determination of the prestress loss would improve the accuracy of the calculations. Furthermore, the impact assessment on the bending moment capacity of the top slab in longitudinal direction revealed that the longitudinal prestress loss has a significant impact. Specifically, if the prestress loss were 15% rather than 20%, the top slab at the examined locations would meet the required moment capacity. Support settlement also affects the moment capacity of the top slab in longitudinal direction, though to a lesser extent, with the greatest contribution observed near the midspan joint. In longitudinal direction, for both the top slab's moment capacity and the web's shear force capacity, the Young's modulus would improve the accuracy of the Finite Element Model. According to the impact assessment, a bigger impact on the shear force capacity of the webs in longitudinal direction, however, is the selection of the concrete compressive strength and the angle (θ) between the concrete compressive strut and the beam axis perpendicular to the shear force. Lastly, the associated physical parameter to the web's bending moment capacity in transverse direction is a concrete cracking related parameter. This parameter can be monitored to detect the formation or growth of concrete cracks.

5.2. Global and local failure

Through the structural assessment and the Finite Element Analysis, two types of failures can be specified, with each requiring a different monitoring strategy:

1. Global failure (high consequence, low probability) - Strategy I
2. Local failure (low consequence, high probability) - Strategy II

These types of failures and strategies will be described each.

Global failure

If a global failure of the Zeelandbrug would happen, this can be characterised as a high consequence, low probability event. Specifically, should such a failure occur, it may result in the collapse of a significant portion of the bridge, potentially an entire span. The consequence of such a collapse would be high, affecting nearby people, the economy, society, and the environment. The probability of such an extensive failure is relatively low. In the context of a global failure, the dominant load on the bridge is its self-weight. This is because, on a global scale, the traffic loads are minor in comparison to the self-weight of the bridge. The monitoring strategy (strategy I) for addressing global failure primarily involves using data collected during monitoring campaigns to refine and update the Finite Element Model and recalculations of the bridge. These enhancements provide more accurate predictions of the load effects and the overall bearing capacity of the bridge. Consequently, monitoring serves as a tool for obtaining more precise information, thereby enabling better assessment of the bridge on a global scale.

From the structural assessment in chapter 4, it follows that global failure may result from the failure of the box girder's top slab which is subjected to a bending moment in the longitudinal direction causing tension in the top slab. Similarly, the shear failure of the box girder's webs in longitudinal direction could also be categorised as a potential global failure. From Table 5.1 it follows that the associated physical parameters are the prestress loss, the concrete compressive strength, the support settlements and the Young's modulus, as well as the weight of the vehicles.

Local failure

If a local failure of the Zeelandbrug would happend, this can be characterised as a low consequence, high probability event. In such instances, it is expected that only a small portion of the bridge would be affected, such as the crumbling of a corner of a cantilever in the transverse direction. While the consequence of such a failure is quite small, the probability of its occurrence is relatively high. On a local level, the dominant load on the bridge is the traffic load. When examining specific areas of the bridge, the self-weight is minimal compared to the substantial load imposed by passing vehicles, such as heavy trucks. The most effective strategy (strategy II) for addressing local failures is to implement a monitoring system designed to detect early signs of structural damages. This approach allows for timely warnings and could enable preventive measures, thereby mitigating the risk of localised damages

escalating into localised failures.

The structural assessment in chapter 4 reveals that potential local failure modes could be failure induced by the bending moment within the cantilever of the top slab. Additionally, local failure may arise from shear force failures within the cantilever of the top slab, or at the section extending from the midspan towards the web of the box girder. Another categorised local failure relates to the box girder's webs, which may fail in the transverse direction due to bending moments. Because of this exceeding bending moment capacity, crack formation or growth can occur on the outer side of the webs. Hence, the main associated physical parameter is a concrete cracking related parameter. While strategy II is very effective in addressing local failures, not all local failures are easily detectable or accessible. Consequently, the first strategy can also be used to obtain data from monitoring technologies concerning physical parameters, such as the transverse prestress loss and the weight of the vehicles, to update the recalculations. This approach can help determine locations for applying monitoring technologies and improve decision-making about these local failure modes. However, this topic will not be explored in further detail.

5.3. Introduction to Structural Health Monitoring

Structural Health Monitoring (SHM) is the process of implementing a damage-detection strategy [17]. Farrar and Worden define damage in structural and mechanical systems as "intentional or unintentional changes to the material and/or geometric properties of these systems, including changes to the boundary conditions and system connectivity, which adversely affect the current or future performance of these systems" [18, p. xxvi]. Hence, this definition of damage encompasses the concept that damage is identified by comparing two states of a system, with one state typically assumed to represent the initial, often undamaged, state [17]. The process of Structural Health Monitoring can be split into four general stages [18]:

1. Operational evaluation. This evaluation establishes the limitations of what will be monitored and how the monitoring will be implemented.
2. Data acquisition. This stage requires the selection of the types of sensors to be used, determining the locations for the sensors, deciding on the number of sensors to use, and selecting the data acquisition hardware.
3. Feature selection. In this selection data features are identified that enable one to distinguish between a structure's undamaged and damaged states.
4. Statistical modelling for feature discrimination. This stage of Structural Health Monitoring involves developing statistical models to discriminate between features of undamaged and damaged structures.

This study briefly addresses the initial two stages: the operational evaluation and the data acquisition. The important physical parameters and failure modes of the Zeelandbrug have already been identified. Subsequently, a brief literature review will be conducted on monitoring technologies previously implemented on bridges constructed using the balanced cantilever method. Then, as part of the operational evaluation, limitations will be identified of the Zeelandbrug regarding the application of monitoring technologies. For the data acquisition, the type of sensors that could be used will be listed, their locations will be determined if necessary, and the utilisation of the collected data will be considered.

5.4. Brief literature review

The balanced cantilever method is one of the most commonly used techniques for constructing large-span concrete bridges. Over the past decades, balanced cantilever prestressed bridges have become widely utilised in bridge construction. Numerous studies in literature have documented cases of these bridges being monitored to gather essential data on their structural behaviour over time. There is looked at various concrete bridges where monitoring has been applied to understand what monitoring strategies have already been employed in practice and its relevance for the Zeelandbrug.

Residual prestress

A paper by Abdel-Jaber and Glisic has evaluated strain-based methods to indirectly monitor the prestressing force in prestressed concrete structures [19]. According to this research, long-term strain

changes can be effectively monitored if sensors are installed in structures during their construction, either by attaching them to the prestressing strands or embedding them within the concrete [19]. The strain at the prestressing strand's center of gravity can then be determined by assuming a linear strain distribution [19]. As reported by Abdel-Jaber and Glisic, strain-based methods appear to be the most promising for calculating the prestressing force when the structures are equipped with embedded strain gauges during construction [19]. This is recognised as a limitation for the Zeelandbrug, as there were no strain gauges embedded in the concrete, and historical data on prestress loss is unavailable. Therefore, the use of alternative methods for measuring residual prestress should be considered. A paper by Agredo Chávez et al. provides a comprehensive review of the testing methods applied over the years to prestressed concrete bridges for evaluating the residual prestress force [20]. Three of these techniques were implemented on a 66-year-old balanced cantilever box girder bridge (the Kalix Bridge in Sweden) [20]. These methods are the saw-cut method, the strand cutting method and the deflection-based method. In a research conducted by Bagge et al., the saw-cut method was further developed and carried out on a 55-year-old multi-span continuous concrete girder bridge (located in Kiruna in Sweden) [20]. The saw-cut method and strand cutting method have now been recognised as potentially effective approaches for assessing the residual prestress in the Zeelandbrug.

The saw-cut method is a non-destructive approach. This technique estimates the prestress force by applying saw cuts that isolate a concrete block from the surrounding applied forces, allowing the measurement of strain changes in the region adjacent to the cuts [20]. The concrete block is considered fully isolated once significant strain changes within the block are no longer detected during the progression of saw cuts in the concrete cover adjacent to the prestressed reinforcement [20]. The prestress force is then calculated based on the strain observed on the fully isolated concrete surface. In this calculation, the factors influencing the strain are considered. These are the prestress force and its eccentricity, the dead load of the member, secondary moments from restraining forces, and any externally applied loads [20]. A recommendation by Agredo Chávez et al. is that for older bridges with low concrete cover, the distance between the cuts should be minimised to ensure more effective isolation of the concrete block [20]. Additionally, Bagge et al. recommend to repair the saw cuts on the concrete surface to prevent unnecessary exposure of the internal components [21].

The strand cutting technique is a destructive method used to evaluate residual stresses in prestressed strands. In this approach, a strain gauge is installed on an exposed prestressed bar. When the prestressed bar is cut, the strain in the wires is measured by sensors oriented along their longitudinal axis [20]. The stress is then determined by applying Hooke's law to the measured strain following the relaxation of the bar [20]. In the experiment conducting the strand cutting method conducted by Agredo Chávez et al., temperature was continuously monitored throughout the whole test to account for thermal effects [20]. This allowed the detection of thermal strains induced by the cutting process, ensuring that only strain measurements were considered after all thermal effects had been normalised [20]. The study emphasises that careful consideration is required when applying the strand cutting method for in-service evaluations, particularly when the prestressing system is approaching the tendon's ultimate tensile strength, as this could increase the risk of tendon breakage [20].

Concrete compressive strength and Young's modulus

The Second Stichtse Bridge in the Netherlands is a balanced cantilever structure constructed using high-strength concrete and implemented with monitoring technologies. The research by Lantsoght et al. studies the high-strength concrete's long-term material and structural behaviour in this cantilever bridge [22]. Part of the monitoring plan for the bridge was the measurement of creep and shrinkage, as well as the concrete compressive strength and splitting tensile strength over time. These assessments were conducted using pre-prepared concrete specimens. The moisture and temperature were measured as well. No additional concrete specimens were prepared for the Zeelandbrug. Hence, other methods should be employed to assess the compressive concrete strength and Young's modulus.

Non-destructive approaches which could be used to assess the compressive concrete strength and Young's modulus are the rebound hammer and/or the ultrasonic pulse velocity test. The rebound hammer test provides a rapid and convenient assessment of the concrete compressive strength [23]. This test measures the energy of a specialised hammer's rebound to estimate the concrete strength [24]. Due to

significant scatter in the data, it is advisable to conduct at least ten measurements [24]. The ultrasonic pulse velocity test is another in-situ, non-destructive test. This test calculates the time required for an ultrasonic pulse to travel through the concrete member in km/sec [25]. This gives information about the Young's modulus, the density and the overall condition of the concrete element. However, the rebound hammer test and ultrasonic pulse velocity test have been reported in literature to not be very reliable nor accurate for assessing concrete properties [25, 26]. Consequently, it is proposed to drill concrete cores from the Zeelandbrug to test the concrete compressive strength, Young's modulus, and splitting tensile strength.

Settlement
The deflections of the Second Stichtse Bridge superstructure were measured periodically by a surveyor [22]. For the Second Stichtse Bridge it was found that the first support is undergoing a settlement which directly influences the midspan deflection [22]. This study has highlighted the significant impact of settlements on the shear forces within the Zeelandbrug's superstructure. Therefore, it is recommended that the settlements that the Zeelandbrug may have experienced be investigated. The study by Lantsoght et al. demonstrates that periodic measurements by a surveyor could effectively track the settlements that are currently occurring [22]. It is important to note that in the FEM of the Zeelandbrug, the settlement of a support exhibits very localised effects. Therefore, if supports are selected for settlement monitoring, careful consideration should be given to the selection of the specific supports to be monitored. Furthermore, satellite data could be used to analyse the settlements that have occurred over time of the Zeelandbrug. Specifically, InSAR data from Sentinel-1 could be used for this purpose. A preliminary investigation was conducted to explore the applicability of satellite data in assessing the settlement of the Zeelandbrug. The findings indicate that the spatial resolution of the data is low. Measurement points are located either on the bridge or on the water's surface due to the relatively small width of the Zeelandbrug. Upon filtering out data points associated with the water, it became evident that obtaining reliable and significant measurements of the bridge's settlement is challenging.

Concrete cracking
In a paper from Richard et al., two similar balanced cantilever bridges have been monitored and evaluated on their shear crack propagation in the webs of the box girder sections [27]. Preliminary investigations suggested that the cracking was caused by insufficient shear reinforcement in the webs [27]. The sensors used to measure the displacements were Linear Variable Differential Transformers (LVDTs). The LVDTs were attached perpendicular to the cracks to measure the displacement across them. Temperature gauges were also installed on the concrete surface of the webs to measure the surface temperature [27]. The monitoring results have shown that the post-tensioned tendons that were used to strengthen the structure has so far been successful [27]. This case demonstrates that LVDTs can effectively measure displacements of the concrete and the growth of concrete cracks. Additionally, monitoring temperature variations is necessary to determine how variations in temperature contribute to the displacement across the cracks. To date, visual inspections of the Zeelandbrug have not revealed any observable cracks [5, 6]. Consequently, there are no specific cracks requiring growth measurement. A method that can be used to detect possible crack formation in the webs of the Zeelandbrug's box girders is the acoustic emission technique. This technique allows for the identification of structural discontinuities and flaws without the need for a point-by-point search over the entire surface of the structure [28]. Bagherifaez et al. conducted a study that successfully applied acoustic emission monitoring to multicell box girder specimens under laboratory-induced torsion loading, which led to the development and detection of torsional cracks [28]. Even though acoustic emission sensors are a good option for detecting concrete cracking, this technique is very costly and impractical to apply to all 52 spans of the Zeelandbrug.

Limitations
A part of the operational evaluation involves establishing the limitations of what can be monitored and how the monitoring technologies can be implemented. As observed in the brief literature review, several limitations are evident in the monitoring of the Zeelandbrug. Notably, strain gauges were not embedded in the concrete during construction, nor were additional concrete specimens prepared for later testing. Furthermore, historical parameters such as settlements and prestress loss cannot be monitored retrospectively. Additional limitations identified include the inability to monitor the contribution of the

Dywidag bars in the webs to the shear force capacity in the longitudinal direction and to the moment capacity in the transverse direction. It is also acknowledged that the sensors for monitoring should be strategically placed to avoid interference with traffic flow on the bridge. Further limitations on the types of monitoring systems that can be employed come from variable weather conditions affecting the bridge and the bridge's physical size.

5.5. Recommended monitoring technologies

In this section, monitoring technologies that are proposed to be implemented on the Zeelandbrug are discussed under either strategy I or II. As previously mentioned, the data collected about the physical parameters in strategy I can be used to update the FEM and/or the recalculations, whereas the data collected about the physical parameters in strategy II can be used to detect local damage.

5.5.1. Strategy I

First, it is acknowledged that the uncertainties regarding the prestress loss significantly impact the calculated capacities in the structural assessment of the Zeelandbrug. The brief literature review highlighted that monitoring prestress loss could be challenging without embedded strain gauges. Two methods are proposed for measuring the residual prestress in the strands; the saw-cut method and the strand cutting method. The first method is at first glance preferred as it is non-destructive. Nevertheless, further investigation is required to assess the feasibility of applying these methods to the Zeelandbrug, as further discussed in section 5.7. In addition, it is recommended to initiate measurements to determine whether settlements of the Zeelandbrug's supports are currently occurring. As observed in the research by Lantsoght et al., settlement measurements can be conducted periodically by a surveyor [22]. Furthermore, the feasibility of using satellite data to obtain information on potential settlements that have occurred over time should be investigated (see section 5.7). Utilising the results from the Finite Element Model and the estimated settlements that may have occurred over time, one can reference the tables generated from the FEM analysis to determine the additional shear forces in the bridge's cantilever. This approach enables a more precise structural assessment of the Zeelandbrug, ultimately leading to more informed decision-making regarding its structural safety.

By drilling concrete cores from the Zeelandbrug, the compressive strength, Young's modulus and splitting tensile strength of the concrete can be evaluated. The concrete strength should be tested for both the prestressed concrete and the in-situ concrete used in the construction joints. Currently, it is assumed that the concrete strength in the construction joints is equivalent to that of the prestressed concrete. However, due to varying environmental conditions at the construction site, the in-situ concrete may exhibit lower strength. In the original design, the concrete strength was found to be corresponding to C30/37. However, TNO suggests that the concrete strength could potentially correspond to C40/50 [6]. Measurements should indicate whether this is the case or not. If the concrete strength is found to be higher than initially estimated, this would indicate an increased residual capacity. Consequently, recalculations should be revised to incorporate this new strength assessment. The Finite Element Model currently estimates the Young's modulus to be 30 GPa, based on a rough approximation. Testing the concrete's Young's modulus would provide a more accurate value, thereby enhancing the precision of the model and its subsequent predictions.

Besides reducing uncertainties in the material resistance, detailed knowledge of the traffic loading on the Zeelandbrug is also necessary for a more accurate assessment of the structural elements. Weigh-In-Motion (WIM) sensors could be utilised for this purpose. Available WIM sensors include piezoelectric sensors, bending plate sensors, and fiber optic sensors [29]. For instance, piezoelectric sensors could be employed. These sensors operate by converting mechanical energy into electrical energy [30]. Following data acquisition from the piezoelectric sensors, an algorithm for weight determination is used to estimate the static weight of the vehicles driving over the bridge [31]. If the capacity of a structural element is found to be insufficient, a re-evaluation can be performed using the actual weights of the vehicles that travel over the bridge.

5.5.2. Strategy II

For the monitoring of the webs in the Zeelandbrug's box girders, various sensor options can be employed to detect the formation of cracks in the concrete. It is important to identify the specific locations where cracks are likely to develop, thereby determining the precise points for the implementation of the sensors. The recalculations indicate that the tension on the outer side of the webs is critical at cross-sections 5 and 11 of the bridge. Nevertheless, monitoring all 52 spans of the Zeelandbrug for concrete cracking is challenging. Therefore, it is recommended to further study the most suitable monitoring technique for this purpose, see section 5.7. The optimal solution would be the implementation of passive sensors, which allow for continuous monitoring of the concrete without the need for manual testing.

5.6. Monitoring plan

Figures 5.1 and 5.2 demonstrate monitoring strategies I and II that together form the final monitoring plan for the Zeelandbrug.

5.6.1. Strategy I

For strategy I, as previously discussed, in-situ measurements are suggested to assess the concrete compressive strength, Young's modulus and the residual prestressing force. Furthermore, Weigh-In-Motion (WIM) sensors could monitor the weights of the vehicles on the bridge and regular surveys could check for any settlement of the supports. The data collected from these monitoring technologies about these physical parameters are important for updating the Finite Element Model and the recalculations used in the structural assessment of the bridge. Specifically, the recalculations should yield a unity check value below 1, confirming that the structural elements can safely carry the loads. If the unity check exceeds 1, the use of these structural elements should be re-evaluated. This re-evaluation may involve developing a nonlinear Finite Element Model to improve the accuracy of the structural assessment or conduct recalculations using the actual weight of the vehicles found by the WIM sensors. Based on the model's outputs and recalculations, decision-making processes can be initiated. During this process, predictions can be made about the expected lifespan of the structural elements. If the structural elements still do not suffice, a global warning could be issued if deemed necessary.

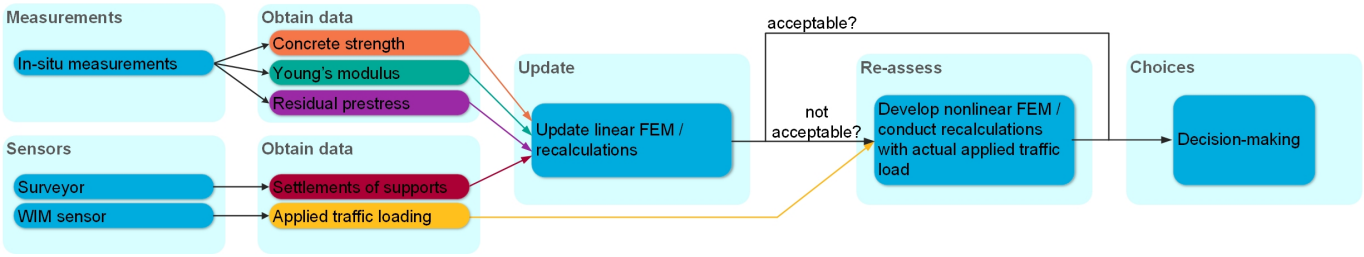

Figure 5.1: Monitoring plan: strategy I

5.6.2. Strategy II

For strategy II, passive sensors can be used to identify early signs of concrete cracking and provide an early warning if the cracking exceeds a predetermined threshold. This approach enhances decision-making and could lead to timely repair of the concrete, thereby mitigating the risk of local damage progressing to a local failure.

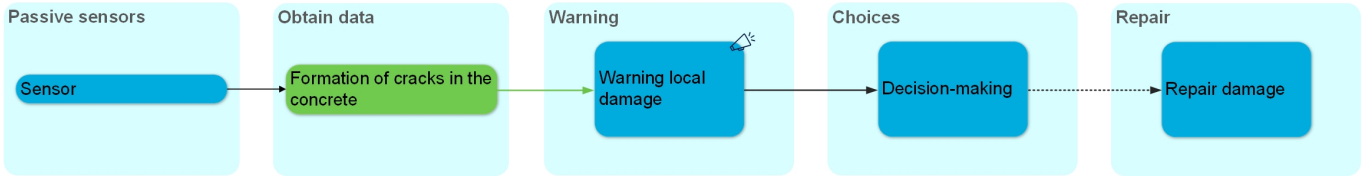

Figure 5.2: Monitoring plan: strategy II

5.7. Other recommended activities

In addition to the implementation of monitoring technologies, other activities are also recommended. These are the performance of additional studies and maintenance activities.

5.7.1. Studies

As previously discussed, important uncertainties in the structural assessment of the Zeelandbrug include the extent of prestress loss and support settlements. To address these uncertainties, it is recommended that additional studies be conducted to evaluate the prestress loss and settlements that may have occurred over time. As previously discussed, possible methods to assess the residual prestress of the prestressing strands include the saw-cut method and the strand cutting method. It is advisable to investigate the feasibility of these techniques, particularly the saw-cut method, as it is non-destructive, while also determining whether the destructive strand cutting method can be safely applied to a bridge in service. Another method that could be investigated to assess the residual prestress loss is the application of smart aggregates in the concrete. A method to evaluate the potential support settlements of the Zeelandbrug that may have occurred over time is to analyse satellite data, such as InSAR data from Sentinel-1. Alternatively, other approaches that could be explored to estimate prestress loss and support settlement include studying bridges of similar design and construction on comparable soil profiles, where more extensive data on prestress loss and settlement over time are available. Such comparisons could then provide estimates for these parameters in the Zeelandbrug. Another recommended study is to investigate the most suitable monitoring technique for detecting potential concrete crack formation. Given that the Zeelandbrug has 52 spans, careful consideration should be given to both the choice of monitoring technique and the location of its application.

Furthermore, this research has identified a knowledge gap concerning the actual load on the shear force dowels, particularly in relation to the behaviour of the surrounding concrete under load concentration near the dowels. It is therefore recommended that the magnitude of this load be studied in greater detail. Lastly, a subject that has not received enough attention is the expected increase in traffic intensity on the Zeelandbrug when the Westerscheldetunnel becomes toll-free [4]. The previously discussed implementation of sensors that measure the weight of the vehicles on the Zeelandbrug coupled with a study to project future traffic growth, would provide a more accurate assessment of the loading conditions.

5.7.2. Maintenance

Some recommendations are provided for the maintenance activities on the Zeelandbrug. Since visual inspection of the top surface is hindered by the pavement, it is advisable to inspect the underlying concrete of the top slab for cracks and corrosion of the reinforcement when replacing the pavement. The results of the recalculations indicate that certain locations of the top slab are prone to cracking due to the exceeding moment capacities. Transverse moments can induce cracking at location B along the longitudinal section of the bridge (see subsection 4.3.1, which contains check 1: Moment capacity cantilever). Critical locations where tension occurs at the top of the top slab due to longitudinal moments have been identified at construction joints A-B and B-C. Hence, during the replacement of the pavement, these locations should be prioritised for crack inspection in the concrete.

As part of the ongoing maintenance on the Zeelandbrug, several shock absorbers are being replaced in the bridge over time [6]. Furthermore, a visual inspection conducted by TNO revealed corrosion products in the hinges between the cantilevers of the bridge [6]. Therefore, the presence of corrosion and its implications on the functionality of the hinges could be examined. By addressing these issues at an early stage, the durability of the bridge can be maintained and its service life expanded. This is the benefit of early intervention.

6

Conclusion and recommendations

This chapter presents the main conclusions of this research in section 6.1 and concludes with several recommendations in section 6.2.

6.1. Conclusion

This study aimed to improve the safety of the Zeelandbrug by gaining a better understanding of the bridge's structural behaviour. The Zeelandbrug serves as an important connection between Noord-Beveland and Schouwen-Duiveland. After the construction of the bridge was completed in 1965, the bridge has been in operation for almost 60 years. Over this period, the current condition of the Zeelandbrug's load-bearing capacity has become uncertain. This research focused on assessing the structural elements of the Zeelandbrug and exploring monitoring strategies to reduce the uncertainties identified during this structural assessment. The findings of this research make it possible to return to the main research question.

What monitoring strategies could be applied to improve the safety of the Zeelandbrug?

By answering the five sub-questions formulated at the start of this research, the main research question will be addressed.

How can a physical model contribute to the understanding of the Zeelandbrug's behaviour, and in which detail level does the model need to be?

An initial uncertainty identified before the start of the structural assessment was the expected load effects on the Zeelandbrug due to differential settlement. A physical model helped to understand how the settlement of a support affects the magnitude of shear forces within the bridge's cantilever. To study this effect, a Finite Element Model with the bridge's cantilevers modelled as one-dimensional beam elements was found adequate.

What is known about the current status of the bearing capacity of the Zeelandbrug?

The recalculations have provided valuable insights into the current status of the Zeelandbrug's bearing capacity. The recalculations identified the following structural elements of the Zeelandbrug's superstructure where the applied loading exceeds their resistance. In the transverse direction, the moment and shear force capacities of the cantilever of the box girder, as well as the shear force capacity of the top slab of the box girder. Furthermore, in transverse direction, the moment capacity of the webs with tension on their outer sides. In the longitudinal direction, the tensile force in the top slab resulting from longitudinal moments and the shear force capacity of the box girder's webs.

What are important uncertainties involved in determining the safety of the Zeelandbrug's structure?

Multiple uncertainties have been identified in the structural assessment, with the most important ones discussed herein. Notably, shear forces may be introduced in the bridge's superstructure as a result of the settlement of a support. However, the extent of settlements of the Zeelandbrug is unknown, posing a challenge in assessing their actual impact. Another uncertainty is the loss of prestress that has accumulated over time in the transverse and longitudinal prestressing. This significantly complicates the evaluation of the bridge's structural elements. Additional uncertainties include the condition of the top slab, which is difficult to assess due to the overlaying pavement, the compressive strength and Young's modulus of the concrete, and the magnitude of the traffic loading applied to the bridge.

What are the critical failure modes of the Zeelandbrug and its associated physical parameters?

Two types of possible failures have been identified: a global and a local failure. Each requires a different monitoring strategy. Corresponding failure modes to a global failure are the shear failure of the box girder's webs in longitudinal direction and the exceeded tensile force in the box girder's top slab due to the bending moment in the longitudinal direction. The associated physical parameters to these failure modes are the prestress loss, the concrete compressive strength, the support settlements and the Young's modulus, as well as the weight of the vehicles. To address the risk of global failure, the monitoring strategy (strategy I) should focus on utilising data from monitoring technologies to improve and update the Finite Element Model of the bridge. This updated model could then give more accurate predictions on the bridge's overall bearing capacity. The corresponding failure modes to a local failure are the shear force failures in transverse direction within the cantilever of the top slab, or at the section extending from the midspan towards the web of the box girder. Additionally, local failure could be induced by the bending moment within the cantilever of the top slab in transverse direction. Another corresponding failure mode relates to the box girder's webs, which may fail in the transverse direction due to bending moments. These may cause cracks to form on the outer surface of the webs. Therefore, the primary physical parameter of interest is a concrete cracking related parameter which could be monitored to detect the formation and progression of concrete cracks. The most effective strategy (strategy II) for mitigating local failures is thus the implementation of monitoring technologies designed to detect early signs of structural damage. This approach allows for timely warnings and interventions.

What kind of technologies can be used to monitor the physical parameters and reduce the identified uncertainties?

As part of strategy I, in-situ measurements can be performed to assess the concrete compressive strength, Young's modulus and the residual prestressing force. The weight of the vehicles that travel over the Zeelandbrug can be monitored with Weigh-In-Motion (WIM) sensors. Additionally, regular surveys can be performed to assess potential support settlements of the Zeelandbrug. As part of strategy II, monitoring technologies can be used to detect the formation of cracks in the concrete.

All in all, the main research question: "What monitoring strategies could be applied to improve the safety of the Zeelandbrug?" can be answered. Two monitoring strategies were defined. The monitoring technologies that could be implemented for each strategy on the Zeelandbrug have been mentioned above. For mitigating a global failure, strategy I should be applied. As noted earlier, strategy I focuses on collecting data from monitoring technologies to update the Finite Element Model and recalculations for the structural assessment of the bridge. The updates of the model and recalculations should confirm that the structural elements can support the loads in a safe manner. If not, the structural elements should be re-evaluated. This re-evaluation may include the development of a nonlinear Finite Element Model to achieve more accurate structural evaluations or recalculations that incorporate the actual vehicle weights recorded by the WIM sensors. Based on the model's outputs and recalculations, the subsequent decision-making process could include evaluating the expected lifespan of the structural elements. Should the structural elements still prove to have insufficient capacity, issuing a global warning could be considered if deemed necessary. In contrast, strategy II should be applied for mitigating a local failure. In strategy II, the data from the monitoring technologies can directly issue a local warning if a certain threshold is exceeded. Then, a decision could be made regarding the repair of the local damage.

6.2. Recommendations

In light of the ongoing structural assessment of the Zeelandbrug, several recommendations are proposed. Foremost, it is suggested to investigate the prestress loss and support settlements that may have occurred over the bridge's lifespan. This research has indicated that a better prediction of these parameters would significantly enhance the accuracy of the Zeelandbrug's structural assessment. Recommended approaches for a further investigation in assessing the residual prestress include the saw-cut method and the strand cutting method. To evaluate potential support settlements of the Zeelandbrug, a further study of satellite data analysis is recommended. Careful consideration should be given to the choice and application of monitoring techniques for detecting potential concrete crack formation. If the capacity of the structural elements is found to be insufficient, it is advisable to evaluate the concrete structure of the Zeelandbrug under the actual applied traffic loads to the bridge. Moreover, developing a nonlinear Finite Element Model is recommended to improve the model's accuracy and better predict the bridge's behaviour. Regarding the maintenance of the Zeelandbrug, it is recommended to inspect the concrete for cracks and corrosion of the reinforcement during the replacement of the pavement.

References

[1] V. Stoop. The Zeelandbrug, 2024.

[2] Provincie Zeeland. Zeelandbrug, . URL https://www.zeeland.nl/onderwerpen/verkeer-en-openbaar-vervoer/zeelandbrug.

[3] Provincie Zeeland. Proeftuin Zeelandbrug, . URL https://www.zeeland.nl/onderwerpen/verkeer-en-openbaar-vervoer/zeelandbrug/proeftuin-zeelandbrug#:~:text=De%20Zeelandbrug%20is%20een%20hele,n%20vierduizend%20keer%20per%20jaar.

[4] Provincie Zeeland. Westerscheldetunnel, 2023. URL https://www.zeeland.nl/onderwerpen/verkeer-en-openbaar-vervoer/westerscheldetunnel.

[5] J. van Cappellen. *Beoordeling constructieve veiligheid betonconstructie Zeelandbrug. (Assessment of the structural safety of the concrete structure Zeelandbrug)*. 1st edition, 2017.

[6] H.G. Burggraaf and H. Borsje. *Advies Zeelandbrug*. 2023.

[7] Van Hattum en Blankevoort. Zeelandbrug, 2021. URL https://magazine.vhbinfra.nl/1-1/zeelandbrug/.

[8] Google Maps. Zeeland, 2023. URL https://maps.app.goo.gl/zA6irx6mFcfBa2588.

[9] V. Stoop. Panoramic view of the Zeelandbrug, 2024.

[10] H. T. Hoving, A. C. Krijn, and J. H. van Loenen. Brug over de oosterschelde. *Cement XVI*, (11): 685–693, 1964.

[11] J. Burcksen and R. Herblot. Elementen trotseren elementen. URL https://www.youtube.com/watch?v=JqEiyveCZNI&ab_channel=RobKerker.

[12] H. T. Hoving, A. C. Krijn, and J. H. van Loenen. Brug over de oosterschelde. *Cement XVI*, (12): 760–764, 1964.

[13] A. Lahri and V. Garg. Effect of differential settlement on frame forces-a parametric study. *International Journal of Research in Engineering and Technology*, 4(9):453–464, 2015.

[14] Delmeco Projecten. Werksteiger voor de Zeelandbrug. URL https://projecten.delmeco.nl/nl/referenties/project:werksteiger-voor-de-zeelandbrug.htm.

[15] J. Walraven and C. Braam. *Prestressed concrete*. 2019. Reader TUDelft CIE3150/4160.

[16] R. Bosboom. PZC. Om Zeelandbrug te sparen moet zwaar verkeer mogelijk gaan omrijden, 2022. URL https://www.pzc.nl/zeeuws-nieuws/om-zeelandbrug-te-sparen-moet-zwaar-verkeer-mogelijk-gaan-omrijden~a15c03d0/.

[17] C. R. Farrar, S. W. Doebling, and D. A. Nix. Vibration-based structural damage identification. *Philosophical Transactions: Mathematical, Physical and Engineering Sciences*, 359(1778):131–149, 2001. ISSN 1364503X. URL http://www.jstor.org/stable/3066397.

[18] C. R. Farrar and K. Worden. *Structural Health Monitoring A Machine Learning Perspective*. 01 2013. ISBN 978-1-119-99433-6. doi: 10.1002/9781118443118.

[19] H. Abdel-Jaber and B. Glisic. Monitoring of prestressing forces in prestressed concrete structures—an overview. *Structural Control and Health Monitoring*, 26(8):e2374, 2019. doi: https://doi.org/10.1002/stc.2374. URL https://onlinelibrary.wiley.com/doi/abs/10.1002/stc.2374.

[20] A. Agredo Chávez, J. Gonzalez-Libreros, C. Wang, L. Capacci, F. Biondini, L. Elfgren, and G. Sas. Assessment of residual prestress in existing concrete bridges: The kalix bridge. *Engineering Structures*, 311:118194, 2024. ISSN 0141-0296. doi: https://doi.org/10.1016/j.engstruct.2024.118194. URL https://www.sciencedirect.com/science/article/pii/S0141029624007569.

[21] N. Bagge, J. Nilimaa, and L. Elfgren. In-situ methods to determine residual prestress forces in concrete bridges. *Engineering Structures*, 135:41–52, 2017. ISSN 0141-0296. doi: https://doi.org/10.1016/j.engstruct.2016.12.059. URL https://www.sciencedirect.com/science/article/pii/S0141029616317503.

[22] E. O. L. Lantsoght, C. van der Veen, A. de Boer, and H. van der Ham. Long-term material and structural behavior of high-strength concrete cantilever bridge: Results of 20 years monitoring. *Structural Concrete*, 19(4):1079–1091, 2018. doi: https://doi.org/10.1002/suco.201700214. URL https://onlinelibrary.wiley.com/doi/abs/10.1002/suco.201700214.

[23] A. Brencich, R. Bovolenta, V. Ghiggi, D. Pera, and P. Redaelli. Rebound hammer test: An investigation into its reliability in applications on concrete structures. *Advances in Materials Science and Engineering*, 2020(1):6450183, 2020. doi: https://doi.org/10.1155/2020/6450183. URL https://onlinelibrary.wiley.com/doi/abs/10.1155/2020/6450183.

[24] G. Mishra. Rebound Hammer Test - Purpose, Principle, Procedure, Advantages and Disadvantages, 2023. URL https://theconstructor.org/concrete/rebound-hammer-test-concrete-ndt/2837/.

[25] K. Komloš, S. Popovics, T. Nürnbergerová, B. Babál, and J.S. Popovics. Ultrasonic pulse velocity test of concrete properties as specified in various standards. *Cement and Concrete Composites*, 18(5):357–364, 1996. ISSN 0958-9465. doi: https://doi.org/10.1016/0958-9465(96)00026-1. URL https://www.sciencedirect.com/science/article/pii/0958946596000261.

[26] G.H. Wilgenburg. Non-destructive material evaluation of a reinforced concrete viaduct: a practical methodology. 2024. URL https://repository.tudelft.nl/record/uuid:5cd2d5be-0472-4814-a334-73ac95ae0de2.

[27] M. Richard, J. Gerard, and S. Håkan. Monitoring and evaluation of shear crack initiation and propagation in webs of concrete box-girder sections. 11 2006.

[28] M. Bagherifaez, A. Behnia, A.A. Majeed, and C. Hwa Kian. Acoustic emission monitoring of multicell reinforced concrete box girders subjected to torsion. *The Scientific World Journal*, 2014(1):567619, 2014. doi: https://doi.org/10.1155/2014/567619. URL https://onlinelibrary.wiley.com/doi/abs/10.1155/2014/567619.

[29] G. Yannis and C. Antoniou. Integration of weigh-in-motion technologies in road infrastructure management. *ITE Journal*, 75(1):39–43, 2005.

[30] S. Bairagi, S. U. Islam, M. Shahadat, D. M. Mulvihill, and W. Ali. Mechanical energy harvesting and self-powered electronic applications of textile-based piezoelectric nanogenerators: A systematic review. *Nano Energy*, 111:108414, 2023. ISSN 2211-2855. doi: https://doi.org/10.1016/j.nanoen.2023.108414. URL https://www.sciencedirect.com/science/article/pii/S2211285523002513.

[31] X. Chen, L. Guo, J. Yu, J. Li, and R. Liu. Evaluating innovative sensors and techniques for measuring traffic loads. In *2008 IEEE International Conference on Networking, Sensing and Control*, pages 1074–1079, 2008. doi: 10.1109/ICNSC.2008.4525376.

A

Applied bending moment cantilever

The cantilever of the box girder will experience bending moments in the transverse direction due to both permanent and variable loads. Figure A.1 illustrates the traffic loads according to Eurocode Load Model 1 (LM1) and Load Model 2 (LM2) applied to the cantilever. Additionally, Figure A.2 shows the load from the Maintenance Platform (MP) on the cantilever. It is conservatively assumed that the entire load of the Maintenance Platform is applied to the outer wheel. In this Appendix, the calculation of the bending moments due to the applied loads is shown in detail for location A of the cantilever (see Figure A.3). Due to the load distribution near the joints only being possible in one direction, these areas have been assessed separately.

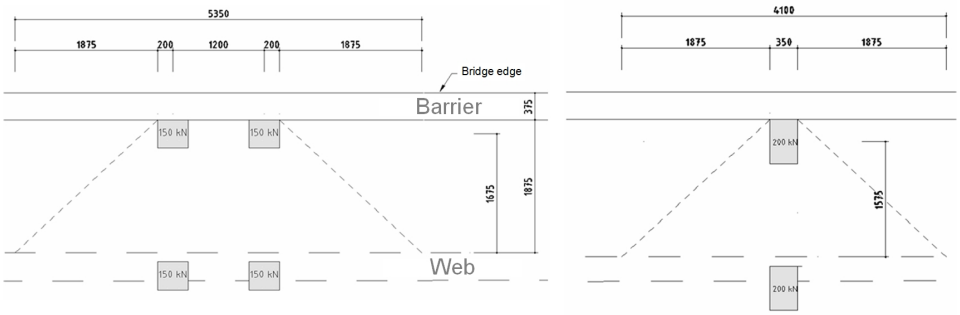

Figure A.1: Top view of the traffic loads on the cantilever with LM1 (left) and LM2 (right). Adapted from [5]

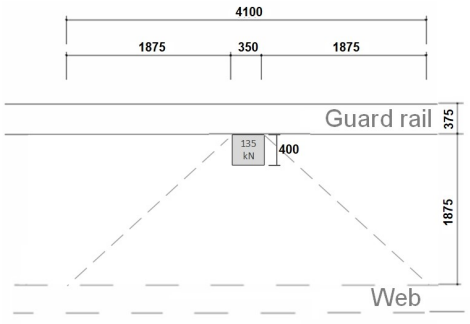

Figure A.2: Top view of the load of the maintenance platform on the cantilever. Adapted from [5]

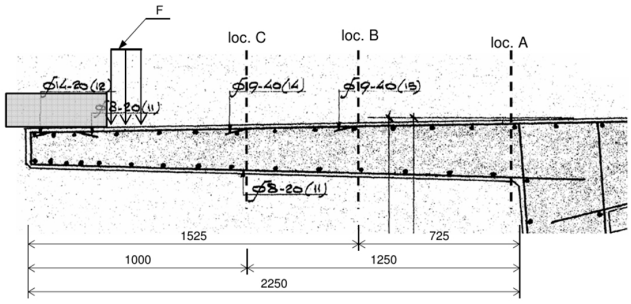

Figure A.3: Location A in the box girder's cantilever [5]

The total bending moment applied at location A of the cantilever is then calculated as follows.

Location A:

M	=	q		x	arm				
Self weight cantilever	=	14.5	kN/m	x	1.125	=	16	kNm/m	
Weight pavement	=	3.588 x 1.876	kN/m	x	0.938	=	6	kNm/m	
Weight barrier	=	9.88	kN/m	x	2.250	=	22	kNm/m	
UDL	=	9 x 1.875	kN/m	x	0.938	=	16	kNm/m	

General:

M	=	F		x	arm	/	distribution			
LM1	=	300	kN	x	1.675	/	5.35	=	94	kNm/m
LM2	=	200	kN	x	1.575	/	4.1	=	77	kNm/m
MP	=	135	kN	x	1.675	/	4.1	=	55	kNm/m
								Mmax =	94	kNm/m

M_{Ed}	=	(cantilever	+	pavement	+	barrier)	x γ_F	+	(UDL	+	max(TS;MP))	x γ_F		
	=	(16	+	6	+	22)	x 1.15	+	(16	+	94)	x 1.25		
	=	188	kNm/m											

Near the joints

M	=	F		x	arm	/	distribution			
LM1	=	300	kN	x	1.675	/	3.475	=	145	kNm/m
LM2	=	200	kN	x	1.575	/	2.225	=	142	kNm/m
MP	=	135	kN	x	1.675	/	2.225	=	102	kNm/m
								Mmax =	145	kNm/m

M_{Ed}	=	(cantilever	+	pavement	+	barrier)	x γ_F	+	(UDL	+	max(TS;MP))	x γ_F		
	=	(16	+	6	+	22)	x 1.15	+	(16	+	145)	x 1.25		
	=	252	kNm/m											

B

Geometry of the modelled segments

In this Appendix, the geometry of the modelled segments is described. First, the general geometric properties of a single cantilever span of the Zeelandbrug are outlined. Table B.1 presents the general geometry of one cantilever, including the x, y, and z coordinates for each segment, the segment length and height-to-length ratio. Each segment's element geometry is based on the corresponding cross-section. To determine the cross-sectional area and the moments of inertia about the y and z axes, each cross-section was modelled in AutoCAD (see Figures B.1 to B.16). The geometric properties of each cross-section are summarised in Tables B.2 to B.17.

General geometry of one cantilever span

Total length of a cantilever's concrete structure:	46.875	m
Total length of an expansion joint:	1.25	m
Total length of one cantilever:	47.5	m
Total length of one span:	95	m

Table B.1: Geometry of the segments for one cantilever

Segment	Based on cross-section	x1 [m]	y1 [m]	z1 [m]	x2 [m]	y2 [m]	z2 [m]	length [m]	h'/length [-]
Segment 1	0	0	0	0.00	2.85	0	0.00	2.85	1.19
Segment 2	2'	2.85	0	0.00	7.25	0	0.38	4.42	1.45
Segment 3	3	7.25	0	0.38	10.75	0	0.63	3.51	1.34
Segment 4	4	10.75	0	0.63	14.25	0	0.87	3.51	1.21
Segment 5	5	14.25	0	0.87	17.75	0	1.10	3.51	1.09
Segment 6	6	17.75	0	1.10	21.25	0	1.31	3.51	0.87
Segment 7	7	21.25	0	1.31	24.75	0	1.50	3.51	0.79
Segment 8	8	24.75	0	1.50	28.25	0	1.66	3.50	0.79
Segment 9	9	28.25	0	1.66	31.75	0	1.80	3.50	0.71
Segment 10	10	31.75	0	1.80	35.25	0	1.91	3.50	0.66
Segment 11	11	35.25	0	1.91	38.75	0	2.00	3.50	0.61
Segment 12	12	38.75	0	2.00	42.25	0	2.07	3.50	0.58
Segment 13	13	42.25	0	2.07	46.875	0	2.12	4.63	0.43

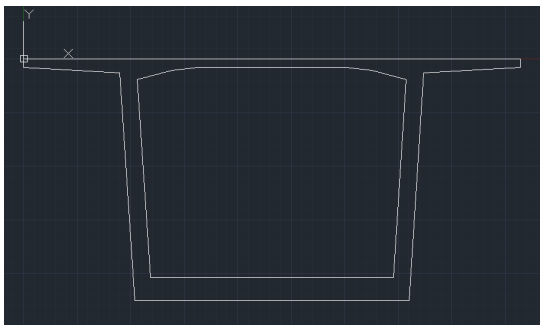

Figure B.1: Cross-section 0

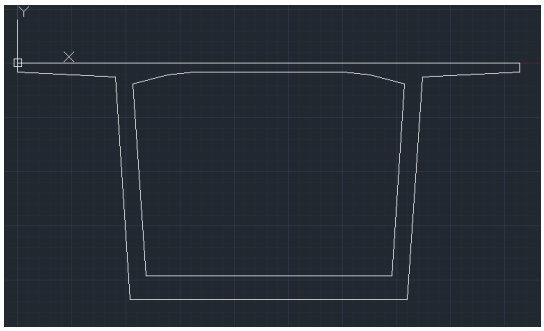

Figure B.2: Cross-section 1'

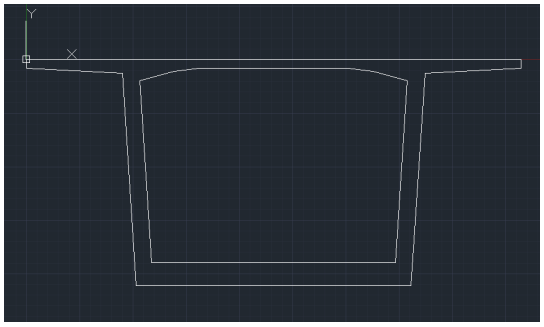

Figure B.3: Cross-section 2'

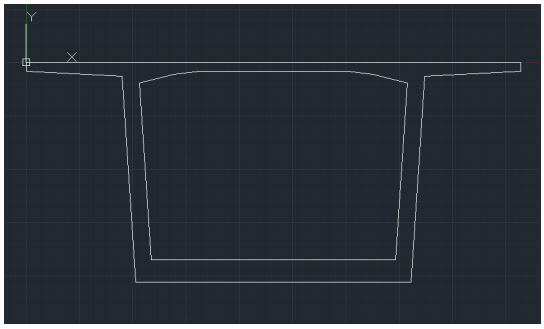

Figure B.4: Cross-section 2

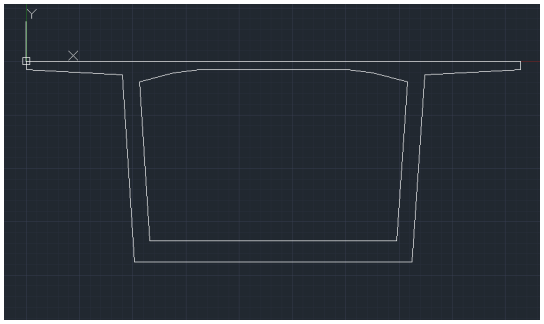

Figure B.5: Cross-section 3

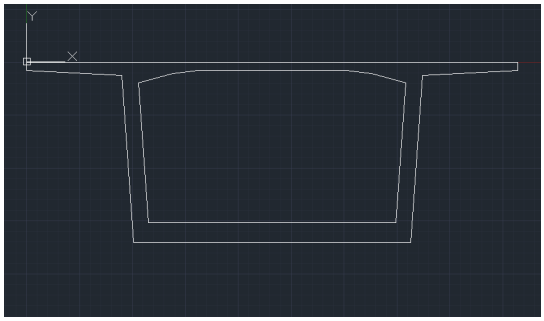

Figure B.6: Cross-section 4

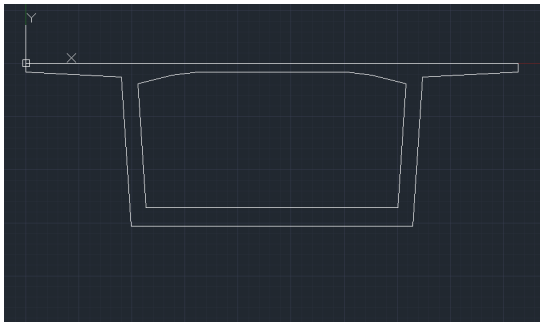

Figure B.7: Cross-section 5

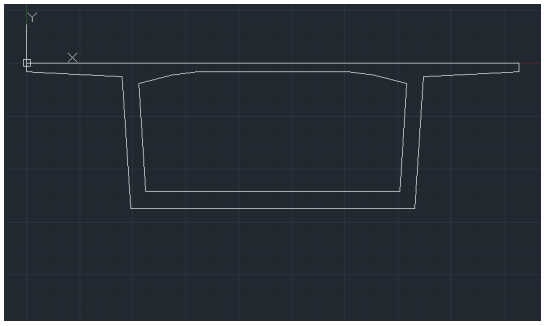

Figure B.8: Cross-section 6

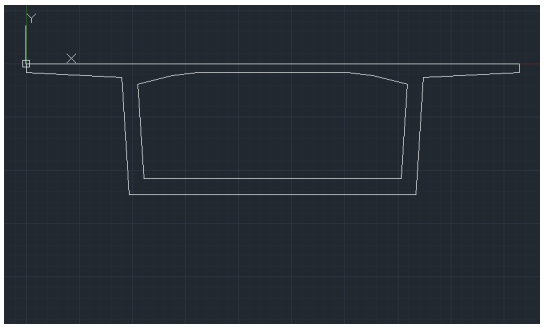

Figure B.9: Cross-section 7

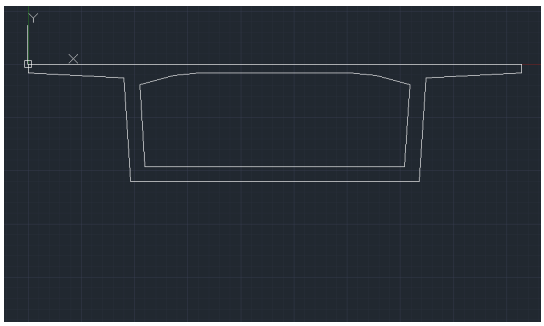

Figure B.10: Cross-section 8

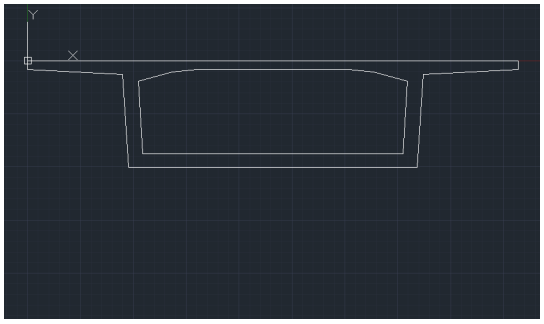

Figure B.11: Cross-section 9

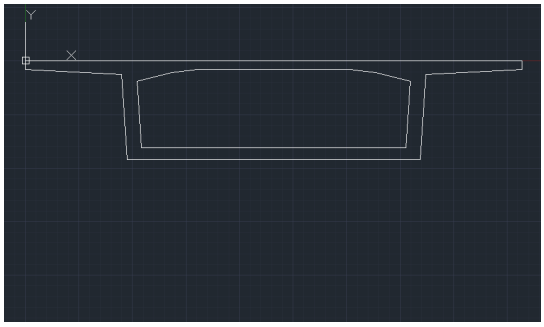

Figure B.12: Cross-section 10

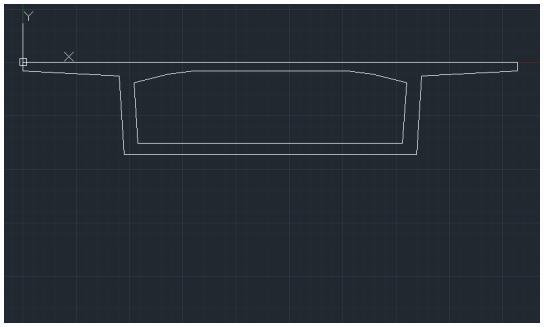

Figure B.13: Cross-section 11

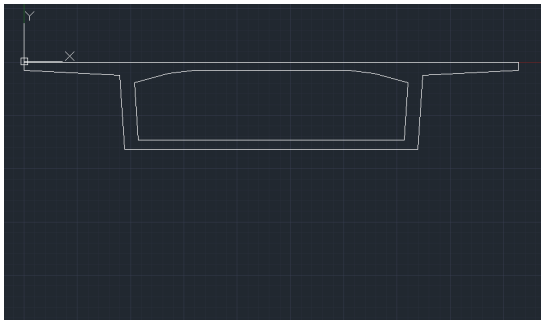

Figure B.14: Cross-section 12

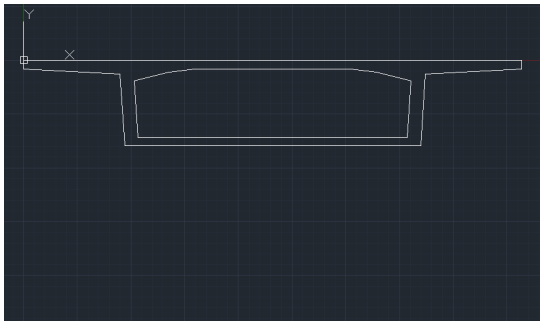

Figure B.15: Cross-section 13

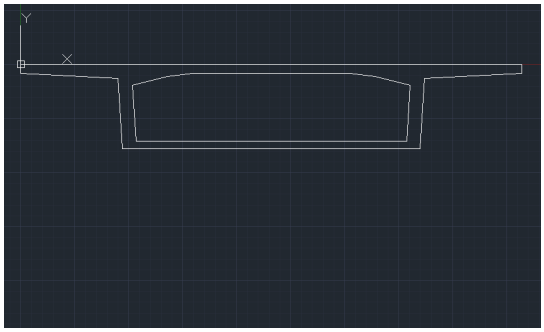

Figure B.16: Cross-section 14

Cross-section 0			
h'	5625 mm	A	10.233 m^2
b'	6412 mm	I_y	51.025 m^4
w	410 mm	I_z	85.293 m^4
d	530 mm	I_t	63.232 m^4

Table B.2: Cross-section 0: geometric properties

Cross-section 1'			
h'	5445 mm	A	10.107 m^2
b'	6412 mm	I_y	47.377 m^4
w	410 mm	I_z	83.853 m^4
d	534 mm	I_t	59.756 m^4

Table B.3: Cross-section 1': geometric properties

Cross-section 2'			
h'	5272 mm	A	9.954 m^2
b'	6446 mm	I_y	43.873 m^4
w	410 mm	I_z	82.729 m^4
d	528 mm	I_t	56.643 m^4

Table B.4: Cross-section 2': geometric properties

Cross-section 2			
h'	5147 mm	A	9.830 m^2
b'	6464 mm	I_y	41.380 m^4
w	410 mm	I_z	81.807 m^4
d	522 mm	I_t	54.354 m^4

Table B.5: Cross-section 2: geometric properties

Cross-section 3			
h'	4691 mm	A	9.287 m^2
b'	6524 mm	I_y	32.812 m^4
w	404 mm	I_z	77.795 m^4
d	494 mm	I_t	45.974 m^4

Table B.6: Cross-section 3: geometric properties

Cross-section 4			
h'	4260 mm	A	8.752 m^2
b'	6552 mm	I_y	25.722 m^4
w	398 mm	I_z	73.669 m^4
d	466 mm	I_t	38.331 m^4

Table B.7: Cross-section 4: geometric properties

Cross-section 5			
h'	3827 mm	A	8.257 m^2
b'	6640 mm	I_y	19.721 m^4
w	392 mm	I_z	70.119 m^4
d	438 mm	I_t	31.422 m^4

Table B.8: Cross-section 5: geometric properties

Cross-section 6			
h'	3427 mm	A	7.774 m^2
b'	6692 mm	I_y	14.945 m^4
w	386 mm	I_z	66.490 m^4
d	410 mm	I_t	23.358 m^4

Table B.9: Cross-section 6: geometric properties

Cross-section 7			
h'	3068 mm	A	7.319 m^2
b'	6740 mm	I_y	11.282 m^4
w	380 mm	I_z	63.151 m^4
d	381 mm	I_t	20.324 m^4

Table B.10: Cross-section 7: geometric properties

Cross-section 8			
h'	2762 mm	A	6.882 m^2
b'	6782 mm	I_y	8.568 m^4
w	374 mm	I_z	60.126 m^4
d	348 mm	I_t	16.334 m^4

Table B.11: Cross-section 8: geometric properties

Cross-section 9			
h'	2503 mm	A	6.467 m^2
b'	6816 mm	I_y	6.560 m^4
w	368 mm	I_z	57.391 m^4
d	313 mm	I_t	13.184 m^4

Table B.12: Cross-section 9: geometric properties

Cross-section 10			
h'	2304 mm	A	6.120 m^2
b'	6842 mm	I_y	5.200 m^4
w	362 mm	I_z	55.167 m^4
d	282 mm	I_t	10.921 m^4

Table B.13: Cross-section 10: geometric properties

Cross-section 11			
h'	2142 mm	A	5.774 m^2
b'	6864 mm	I_y	4.175 m^4
w	352 mm	I_z	53.052 m^4
d	249 mm	I_t	9.130 m^4

Table B.14: Cross-section 11: geometric properties

Cross-section 12			
h'	2040 mm	A	5.477 m^2
b'	6880 mm	I_y	3.518 m^4
w	342 mm	I_z	51.405 m^4
d	217 mm	I_t	7.944 m^4

Table B.15: Cross-section 12: geometric properties

Cross-section 13			
h'	1976 mm	A	5.204 m^2
b'	6886 mm	I_y	3.046 m^4
w	332 mm	I_z	50.001 m^4
d	185 mm	I_t	7.054 m^4

Table B.16: Cross-section 13: geometric properties

Cross-section 14			
h'	1953 mm	A	5.189 m^2
b'	6886 mm	I_y	2.962 m^4
w	332 mm	I_z	49.832 m^4
d	185 mm	I_t	6.885 m^4

Table B.17: Cross-section 14: geometric properties

C

Torsional moment of inertia

Figure C.1 shows a cross-section of the membrane in the Prandtl membrane analogy to derive the torsional moment of inertia for a single-cell box girder.

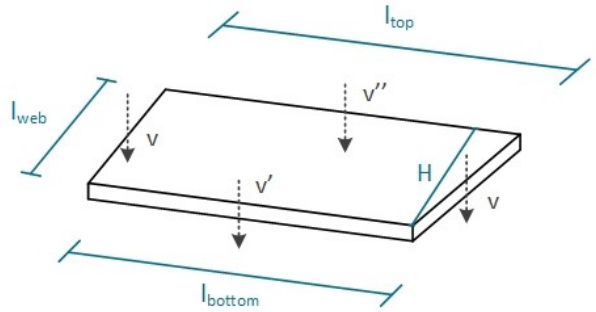

(a) Cross-section of membrane with transverse forces

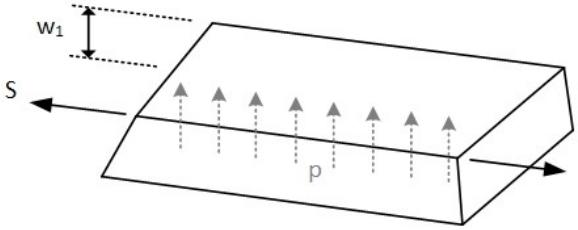

(b) Membrane

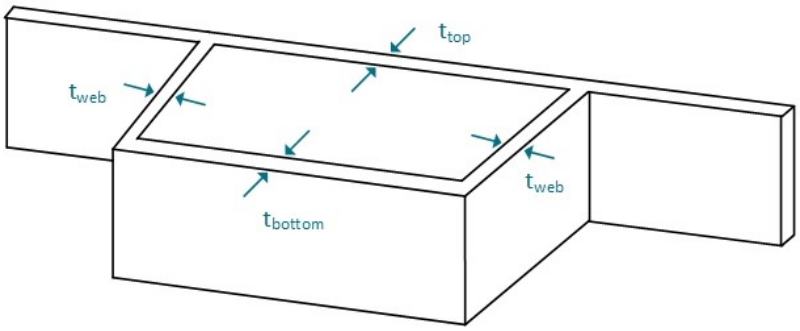

(c) Section of the box girder

Figure C.1: Prandtl membrane analogy

The transverse forces v, v' and v'' of the members are described by their displacement w_1, the member's thickness t and the shear flow S:
$v = \frac{w_1}{t_{web}} \cdot S \qquad ; \qquad v' = \frac{w_1}{t_{bottom}} \cdot S \qquad ; \qquad v'' = \frac{w_1}{t_{top}} \cdot S$

The four transverse forces of the members need to be in equilibrium with the shear stress distribution p. The area is a trapezium and can be calculated with $\frac{1}{2} \cdot (l_{bottom} + l_{top}) \cdot H$. The vertical equilibrium gives:
$v \cdot l_{web} + v' \cdot l_{bottom} + v \cdot l_{web} + v'' \cdot l_{top} = p \cdot \frac{1}{2} \cdot (l_{bottom} + l_{top}) \cdot H$

Substitution of the transverse forces provides:
$\frac{w_1}{t_{web}} \cdot l_{web} \cdot S + \frac{w_1}{t_{bottom}} \cdot l_{bottom} \cdot S + \frac{w_1}{t_{web}} \cdot l_{web} \cdot S + \frac{w_1}{t_{top}} \cdot l_{top} \cdot S = p \cdot \frac{1}{2} \cdot (l_{bottom} + l_{top}) \cdot H$
$w_1 \cdot [\frac{2}{t_{web}} \cdot l_{web} \cdot S + \frac{1}{t_{bottom}} \cdot l_{bottom} \cdot S + \frac{1}{t_{top}} \cdot l_{top} \cdot S] = p \cdot \frac{1}{2} \cdot (l_{bottom} + l_{top}) \cdot H$
$w_1 = \frac{\frac{1}{2} \cdot p \cdot (l_{bottom} + l_{top}) \cdot H}{\frac{2}{t_{web}} \cdot l_{web} \cdot S + \frac{1}{t_{bottom}} \cdot l_{bottom} \cdot S + \frac{1}{t_{top}} \cdot l_{top} \cdot S}$

In this case, the translation to the φ-bubble can be made by the introduction of $p = 2 \cdot \theta$ and $S = \frac{1}{G}$. Here, θ is the angle of twist and G is the shear modulus. This substitution delivers:
$\varphi_1 = \frac{2 \cdot \theta \cdot G \cdot \frac{1}{2} \cdot (l_{bottom} + l_{top}) \cdot H}{\frac{l_{web}}{t_{web}} + \frac{l_{bottom}}{t_{bottom}} + \frac{l_{web}}{t_{web}} + \frac{l_{top}}{t_{top}}}$

The torsional moment of inertia is twice the volume of the φ-bubble:
$M_t = 2 \cdot \varphi_1 \cdot \frac{1}{2} \cdot (l_{bottom} + l_{top}) \cdot H$
$M_t = \frac{4 \cdot \theta \cdot G \cdot (\frac{1}{2} \cdot (l_{bottom} + l_{top}) \cdot H)^2}{\frac{l_{web}}{t_{web}} + \frac{l_{bottom}}{t_{bottom}} + \frac{l_{web}}{t_{web}} + \frac{l_{top}}{t_{top}}}$

Lastly, the torsional moment of inertia equals $I_t = \frac{M_t}{\theta \cdot G}$. This results in the following torsional moment of inertia:
$I_t = \frac{4 \cdot (\frac{1}{2} \cdot (l_{bottom} + l_{top}) \cdot H)^2}{\frac{l_{web}}{t_{web}} + \frac{l_{bottom}}{t_{bottom}} + \frac{l_{web}}{t_{web}} + \frac{l_{top}}{t_{top}}}$
$I_t = \frac{4 \cdot A_0^2}{\sum \frac{l}{t}}$

This last equation is used to calculate the torsional moments of inertia of the cross-sections.